University of Alberta

Electrohydrodynamic Deformation of Water Drops in Oil with an Electric Field

by

Yu Lu

A thesis submitted to the Faculty of Graduate Studies and Research in partial fulfillment of the requirements for the degree of Master of Science

Department of Mechanical Engineering

Edmonton, Alberta

Spring 2002

National Library of Canada
Acquisitions and Bibliographic Services
395 Wellington Street
Ottawa ON K1A 0N4
Canada

Bibliothèque nationale du Canada
Acquisitions et services bibliographiques
395, rue Wellington
Ottawa ON K1A 0N4
Canada

Your file Votre référence

Our file Notre référence

The author has granted a non-exclusive licence allowing the National Library of Canada to reproduce, loan, distribute or sell copies of this thesis in microform, paper or electronic formats.

The author retains ownership of the copyright in this thesis. Neither the thesis nor substantial extracts from it may be printed or otherwise reproduced without the author's permission.

L'auteur a accordé une licence non exclusive permettant à la Bibliothèque nationale du Canada de reproduire, prêter, distribuer ou vendre des copies de cette thèse sous la forme de microfiche/film, de reproduction sur papier ou sur format électronique.

L'auteur conserve la propriété du droit d'auteur qui protège cette thèse. Ni la thèse ni des extraits substantiels de celle-ci ne doivent être imprimés ou autrement reproduits sans son autorisation.

0-612-69732-0

Canada

University of Alberta

Library Release Form

Name of Author: Yu Lu

Title of Thesis: Electrohydrodynamic Deformation of Water Drops in Oil with an Electric Field

Degree: Master of Science

Year this Degree Granted: 2002

Permission is hereby granted to the University of Alberta Library to reproduce single copies of this thesis and to lend or sell such copies for private, scholarly or scientific research purposes only.

The author reserves all other publication and other rights in association with the copyright in the thesis, and except as herein before provided, neither the thesis nor any substantial portion thereof may be printed or otherwise reproduced in any material form whatever without the author's prior written permission.

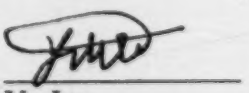

Yu Lu
146 Rowhouse
Michener Park
Edmonton, Alberta
Canada T6H 4M4

Date: Jan 7, 2002

University of Alberta

Faculty of Graduate Studies and Research

The undersigned certify that they have read, and recommend to the Faculty of Graduate Studies and Research for acceptance, a thesis entitled ELECTROHYDRODYNAMIC DEFORMATION OF WATER DROPS IN OIL WITH AN ELECTRIC FIELD submitted by YU LU in partial fulfillment of the requirements for the degree of Master of Science

Dr. Douglas Dale (Supervisor)

Dr. Jacob Masliyah (Co-supervisor)

Dr. Anthony Yeung (Co-supervisor)

Dr. Daniel Kwok

Date: Jan 4, 2002

Abstract

The objective of this study is to acquire a better understanding of the demulsification of water-in-oil emulsions using electric fields. An experimental study is conducted on the deformation behaviors of single water drops and water drop pairs in hydrocarbon media (model oils as well as diluted bitumen) under applied electric fields. For visualization, sequences of high speed video images which capture the coalescence of water drop pairs under applied fields are also shown.

For a single water drop under an electric field, the deformation in the limit of very low electric field was found to be in accordance with Taylor's leaky dielectric theory. At higher electric fields, however, the deformation of a single drop was found to be larger than that predicted by Taylor. Similar conclusions were drawn for both model oil systems and diluted bitumen systems. For a water drop pair, the drops' deformations are largest when the two drops are in close proximity. The drop deformation behavior will deviate noticeably from the single drop's behavior when the edge-to-edge separation distance is less than one radius of the undeformed drop. Weber number appears to be a reasonable parameter for predicting drop deformations.

Acknowledgements

I thank my adviser, Dr. Jacob H. Masliyah, for his insight and advice during the course of the thesis. I am very grateful for his encouragement and patience throughout this project. I feel very lucky to have had the opportunity to be supervised by him, to be associated with him.

I thank Dr. Tony Yeung, my co-supervisor, for his guidance and for suffering through the many drafts of this thesis. Without his support, this thesis could not be completed.

I thank Dr. Douglas Dale and Dr. Dongqing Li (now a professor at University of Toronto) for their guidance, support and help as supervisors.

I also thank my colleagues, Dr. Emily Zholkovskiy, Dr. Guoxing Gu, Dr. Joe Zhou, Dr. Weixing Wang and Mr. Wei Li, for their valuable discussion and friendship.

I thank Mr. Alberta Yeun, Mr. Terry Nord, Mr. Bob Scott and Mr. Walter Boddez for their assistance in the experimental work.

Financial support for this research was provided by the Natural Sciences and Engineering Research Council of Canada (NSERC).

I thank my wife Ling Duan for her unconditional love, encouragement and support. I also thank my parents, ZhengHuo Lu and ChunYing Wang, who sacrificed their lives for my younger brother Ming and me. For all that they have done for me and the love that they have given me, I dedicate this thesis to Ling, ZhengHuo and ChunYing.

TABLE OF CONTENTS

Chapter 1 Introduction 1

1.1 Bitumen Froth Treatment 1

1.1.1 Oil Sands in Alberta 1

1.1.2 Froth Treatment in Bitumen Recovery Process 2

1.2 Water-in-Oil Emulsions 3

1.2.1 Definition of Water-in-Oil Emulsions 3

1.2.2 Stability of Water-in-Oil Emulsions 3

1.2.3 Necessity for Emulsion Breaking 5

1.2.4 Demulsification Methods 6

1.3 Motivation and Objectives 8

1.3.1 Thesis Motivation 8

1.3.2 Research Objectives 9

Chapter 2 16

Literature Review on Drop Deformation and Coalescence in an Electric Field

2.1 Deformation of a Single Drop in an Electric Field 16

2.1.1 Deformation of a Single Drop in Systems without Surfactants 16

2.1.2 Deformation of a Single Drop in Systems with Nonionic Surfactants 25

2.2 Deformation of a Drop Pair in an Electric Field 28

2.3 Coalescence of a Drop Pair in an Electric Field 30

Chapter 3 Interfacial Tension Measurements 44

3.1 Materials 44

3.2 Interfacial Tension Measurements 45

3.2.1 Ring Method 46

3.2.1.1 Apparatus 46

3.2.1.2 Principle of Ring Method 46

3.2.1.3 Experimental Procedure 48

3.2.2 Axisymmetric drop shape analysis method 49
3.2.2.1 Apparatus 49
3.2.2.2 Principle of ADSA Method 50
3.2.2.3 Experimental Procedures 51
3.3 Results of Interfacial Tension Measurements 52

Chapter 4 66
Experimental Protocol for the Measurement of Drop Deformation and Coalescence in an Electric Field
4.1 Introduction 66
4.2 Experimental Set-up and Procedures 67
4.2.1 Single Drop System 67
4.2.1.1 Experimental Set-up 67
4.2.1.2 Experimental Procedures 69
4.2.2 Drop Pair System 71
4.2.2.1 Experimental Set-up 71
4.2.2.2 Experimental Procedures 71
4.2.3 Drop Coalescence 72
4.2.3.1 Experimental Set-up 72
4.2.3.2 Experimental Procedures 74
4.3 Drop Deformation Measurements 76
4.3.1 Single Drops 76
4.3.2 Drop Pair 76
4.4 Drop Coalescence Process 77

Chapter 5 Results and Discussion 92
5.1 Single Drop Deformation 92
5.1.1 Model Systems 94
5.1.1.1 Model Systems without Surfactant 94
5.1.1.2 Model Systems with Surfactants 97
5.1.2 Diluted Bitumen Systems 98
5.1.2.1 Effect of Aging 99

5.1.2.2 Effect of Bitumen Concentration 100
5.2 Drop Pair Deformation 101
5.2.1 Model System 101
5.2.2 Diluted Bitumen Systems 102
5.3 Coalescence between Two Drops 104

Chapter 6 Summary, Conclusions and Recommendations 135
6.1 Review of Problem and Objectives 135
6.2 Conclusions/Summary of Experimental Results 136
6.2.1 Study of Deformation Behavior of Single Water Drops 136
6.2.2 Study of Deformation Behavior of Water Drop Pairs 137
6.2.3 Study of the Coalescence of Water Drops 137
6.3 Recommendations for Future Work 138

References 140

Appendix I Raw Data for the Figures Included in the Thesis 143

Appendix II Calculation of Maxwell Stress Tensor 193

Appendix III 202
Attractive Force Between Two Equal Sized Water Drops in a Uniform Electric Field

Appendix IV Physical Properties of Organic Compounds 207

LIST OF TABLES

Table 2.1. Comparison of experimental and calculated deformations for different systems (reproduced from [Torza et al. 1971]) 33

Table 2.2. Electric field enhancement factor Ω with regard to the initial separation distance of two rigid spheres (reproduced from [Davis, 1964]) 34

Table 3.1. Physical properties of various oils used 54

Table 3.2. Parameters set in the setup menu of process tensiometer K12 55

Table 3.3. Surface and interfacial tension of various systems measured with ring method 56

Table 3.4. Surface and interfacial tension of various systems measured with ADSA method 57

Table 4.1. MotionScope PCI8000S frame storage and recording time 78

Table 4.2. Aging time, frame rate and shuttle speed of the systems tested for drop coalescence 79

Table 5.1. Comparison of calculated and experimental values for water drops in different continuous phases 106

LIST OF FIGURES

Figure 1.1. Simplified flowsheet of Syncrude froth treatment plant 6 [Tipman and Shaw, 1993] 11

Figure 1.2. Two micro size water droplets held by micropipettes in a diluted bitumen solution [Yeung et al., 1999] 12

Figure 1.3. Depiction of emulsion stabilization mechanisms related to electrostatic repulsion, Marangoni-Gibbs effect [McLean et al., 1998] 13

Figure 1.4. Depiction of emulsion stabilization mechanisms related to mechanically rigid film [McLean et al., 1998] 14

Figure 1.5 Deflating an emulsion drop using micropipette [Yeung et al., 1999] 15

Figure 2.1. Definition of the degree of drop deformation 35

Figure 2.2. Sequence of photographs of prolate and oblate drops as the horizontally electric field increases (reproduced from [Vizika & Saville, 1992]) 36

Figure 2.3. Schematic representation of a water drop suspended in oil under an applied electric field 37

Figure 2.4. Computational results for degree of deformation in the case of very large R at the limit of creeping flow. [Feng & Scott, 1996] 38

Figure 2.5. Comparison of experimental results with Taylor's theory in the presence of surfactant PS-b-PMMA. (reproduced from [Ha & Yang, 1995]) 39

Figure 2.6. Schematic representation of the electric field enhancement between two rigid spheres in a uniform electric field 40

Figure 2.7. Tangential component of the electrical stress along the drop surface of one drop when two drops are placed in an electric field. [Baygents et al., 1998] 41

Figure 2.8. Drop deformation and translation as a function of the initial separation distance h/a and time t; $R = 5$, $S = 4$, $M = 1$, and $We = 1$ [Baygents et al., 1998] 42

Figure 2.9. Circulation pattern according to the leaky dielectric model for water drop pairs in a uniform electric field 43

Figure 3.1. (a) Scheme of K12 measuring unit 58
(b) Photograph of K12 Processor Tensiometer 59

Figure 3.2. Measured force including lifted volume in the ring method 60

Figure 3.3. Schematic diagram of interfacial tension measurements using ADSA method 61

Figure 3.4. A digital image of water drop in decyl alcohol for interfacial tension measurement using ADSA method 62

Figure 3.5. Examples of optical distortions in digital images 63

Figure 3.6. Time dependence of the interfacial tension of diluted bitumen solution over water 64

Figure 3.7. Equilibrium interfacial tension of toluene over water with different concentration of sodium naphthenate (aqueous) added to water 65

Figure 4.1. (a) Block diagram of experimental set-up for single drop system 80
(b) Photograph of experimental set-up for single drop system 81

Figure 4.2. (a) Photograph of glass test cell 82
(b) Dimension of glass test cell 82

Figure 4.3. Photograph of microscope 83

Figure 4.4. The process of making the outer surface of the capillary hydrophobic 84

Figure 4.5. Schematic diagram of the difference between a drop pair system and a single drop system experimental set-up 85

Figure 4.6. Photograph of micromanipulator 86

Figure 4.7. Block diagram of experimental set-up for drop coalescence record 87

Figure 4.8. Water drop in 0.5% vol. diluted bitumen solution in 1.5 kV/cm electric field being applied horizontally 88

Figure 4.9. Displacement of the entire water drops in addition to the deformation when an electric field is applied 89

Figure 4.10. (a) Water drops in 1.5% vol diluted bitumen solution when applying 2.4 kV/cm electric field horizontally 90
(b) Water drops in decyl alcohol when applying 1.0 kV/cm electric field horizontally 91

Figure 5.1. Degree of deformation as a function of Weber number for a single water drop in decyl alcohol 107

Figure 5.2. Degree of deformation as a function of Weber number for a single water drop in diethyl phthalate 108

Figure 5.3. Degree of deformation as a function of Weber number for a single water drop in cycloheptanone 109

Figure 5.4. Degree of deformation as a function of Weber number for a single water drop in alpha-ionone 110

Figure 5.5. Degree of deformation as a function of Weber number for a single water drop in cyclohexyl acetate 111

Figure 5.6. Degree of deformation as a function of Weber number for a single water drop in ethyl benzoate 112

Figure 5.7. Degree of deformation as a function of Weber number for a single water drop in 2-ethyl-1, 3-hexanediol 113

Figure 5.8. Degree of deformation as a function of Weber number for a single water drop in various organic compounds 114

Figure 5.9. Degree of deformation as a function of Weber number for a single water drop in toluene (with and without surfactants added) 115

Figure 5.10. Degree of deformation as a function of Weber number for a single water drop in decyl alcohol with surfactant added 116

Figure 5.11. Deformation of a single water drop in toluene solution (0.5% vol. bitumen added) at two different aging times 117

Figure 5.12. Deformation of a single water drop in toluene solution (1.0% vol. bitumen added) at two different aging times 118

Figure 5.13. Deformatoin of a single water drop in toluene solution (1.5% vol. bitumen added) at two different aging times 119

Figure 5.14. Deformation of a single water drop in toluene solution (2.0% vol. bitumen added) at two different aging times 120

Figure 5.15. Deformation of a single water drop in toluene solution for different volume percent of bitumen added (no aging time) 121

Figure 5.16. Deformation of a single water drop in toluene solution for different volume percent of bitumen added (30 minutes aging time) 122

Figure 5.17. Degree of deformation as a function of distance for a water drop pair in decyl alcohol with no aging time 123

Figure 5.18. Degree of deformation as a function of Weber number for a water drop pair in decyl alcohol with no aging time 124

Figure 5.19. Degree of deformation as a function of distance with different Weber numbers for a water drop pair aged 30 minutes in toluene solution (0.5% vol. bitumen added) 125

Figure 5.20. Degree of deformation as a funciton of weber number for a water drop pair aged 30 minutes in toluene solution (0.5% vol. bitumen added) 126

Figure 5.21. Degree of deformation as a function of distance with different Weber numbers for a water drop pair aged 30 minutes in toluene solution (1.5% vol. bitumen added) 127

Figure 5.22. Degree of deformation as a function of Weber number for a water drop pair aged 30 minutes in toluene solution (1.5% vol. bitumen added) 128

Figure 5.23 Coalescence process of a water drop pair in 2-ethyl-1, 3-hexanediol under an electric field (E = 0.515 kV/cm) 129

Figure 5.24 Coalescence process of a water drop pair in decyl alcohol under an electric field (E = 1.031 kV/cm) 130

Figure 5.25 Coalescence process of a water drop pair in heptane-toluene (1:1) solution (1.5% vol. bitumen added) under an electric field (E = 3.350 kV/cm) 131

Figure 5.26 Coalescence process of a water drop pair in toluene solution (0.3% vol. bitumen added) under an electric field (E = 3.093 kV/cm) 133

Figure 5.27. Depiction of water drops coalescence in hydrocarbon medium under an electric field 134

Nomenclature

a	drop length that is parallel to the direction of the electric field, (m), as shown in Figure 2.1
b	drop length that is perpendicular to the direction of the electric field, (m), as shown in Figure 2.1
C	empirical correction factor, as defined in equation (3.4)
Ca	Capillary number, dimensionless, as defined in equation (5.1 c)
D	degree of deformation of the drop, as defined in Figure 2.1
D_s	surface diffusivity of surfactants, (m^2/s)
E_0	electric field strength, (V/m)
E_A	electric field at the inside surface of the drop, (V/m), as shown in Figure 2.6
E_s	Gibbs elasticity, (m^2/mol), as defined in equation (2.16)
f	volume fraction of the dispersed phase in emulsion, as shown in equation (1.1)
F	pulling force when ring detaches from the interface, (N)
F_a	attractive force between two equal size drops in an electric field, (N), as defined in equation (2.18)
g	gravitational acceleration, (m/s^2)
m	calculated deformation factor, as shown in equation (2.10)
m^*	experimental deformation factor, as defined in Table 2.1
M	dynamic viscosity ratio of the drop phase to the continuous phase, as defined in equation (2.8)
P_e	surface Peclet number, as defined in equation (2.14)
ΔP	pressure difference across the water-oil interface, (Pa), as shown in equation (3.5)
ΔP_0	pressure difference across the water-oil interface at a reference elevation, (Pa), as shown in equation (3.6)
r	radius of the ring cross-section, (m)
r_0	undeformed drop radius, (m), as shown in Figure 2.1

R electrical conductivity ratio of the drop phase to the continuous phase, as shown in equation (2.6)

R_1 first principal radius of curvature, (m), as shown in equation (3.5)

R_2 second principal radius of curvature, (m), as shown in equation (3.5)

Re Renolds number, dimensionless, as defined in equation (5.1 b)

R_{in} inner radius of the ring, (m)

R_m mean radius of the ring, (m)

R_{out} outer radius of the ring, (m)

S dielectric constant ratio of the drop phase to the continuous phase, as shown in equation (2.7)

u_c characteristic velocity, (m/s), as defined in equation (2.15)

U maximum surface velocity, (m/s), as defined in equation (5.2)

V volume of lifted liquid, (m^3), as shown in Figure 3.2

We Weber number, dimensionless, as defined in equation (2.12)

W_{ring} weight of the ring, (N)

x_0 initial edge-to-edge separation distance, (m), as shown in Figure 2.6

x_c center-to-center drop separation distance, (m)

Z height measured from the reference elevation, (m), as shown in equation (3.6)

Latin letters

Γ surface concentration of the surfactants, (mol/m^2)

Ω enhancement factor of the electric field, as defined in equation (2.17)

Greek letters

ε_0 permittivity of vacuum, (C/m·V)

ε_e dielectric constant of the continuous phase

ε_i dielectric constant of the drop phase

ϕ_e electrical potential in the continuous phase, (V)

ϕ_i electrical potential in the drop phase, (V)

β discriminating function, as defined in equation (2.5)

γ interfacial tension between the drop phase and the continuous phase, (N/m)

γ_{0-} interfacial tension in the absence of surfactants, (N/m), as shown in equation (2.16)

μ_e dynamic viscosity of the continuous phase, (Pa·s)

μ_{emu} dynamic viscosity of emulsion, as shown in equation (1.1), (Pa·s)

μ_i dynamic viscosity of the drop phase, (Pa·s)

μ_{oil} dynamic viscosity of clean oil, as shown in equation (1.1), (Pa·s)

θ angle between the electric field vector and the radial vector from the center of the drop to its surface, as shown in Figure 2.3(a)

ρ density of drop phase, (kg/m^3)

ρ_c surface charge density, (C/m^2), as defined in equation (2.13)

$\Delta\rho$ density difference between the heavy and light phase, (kg/m^3)

σ_e electrical conductivity of the continuous phase, (S/m)

σ_i electrical conductivity of the drop phase, (S/m)

Subscripts

e continuous phase

i drop phase

Chapter 1

Introduction

1.1 Bitumen Froth Treatment

1.1.1 Oil Sands in Alberta

In North America, the reserves of conventional petroleum are declining while there is a growing demand for oil consumption. This gap can be filled by increased production from heavy oil resources such as oil sands. It is expected that the oil sands industry will play an increasingly important role in the overall energy resources. For example, the production of synthetic crude oil from surface mining by Syncrude and Suncor is about 330,000 barrels per day, which is equivalent to approximately 15% of Canada's oil demand.

Oil sands is also known as tar sands or bituminous sands. As the largest known deposit in the world, the Athabasca deposit contains more hydrocarbons than all of the oil fields in Saudi Arabia combined. The total estimate of bitumen in place in Alberta is 1.3 trillion barrels and that in the Athabasca region alone is 830 billions barrels [Outrim and Evans, 1977]. Typical oil sands is made of quartz sands, water, fine clays and bitumen. The oil sand ore typically contains 16 wt% of bitumen and connate water. A rich ore contains more than 11% bitumen by weight. There are also various amounts of salts present in the water. For example, the sodium ion concentration can range from 30 to 300 mg in every kilogram of oil sands [Masliyah, 2000].

Oil sands from the Athabasca deposit is water-wet, while some deposits in other locations (e.g., Utah, Alabama, California) are considered oil-wet. It is this unique

characteristic of the Athabasca deposit that allows the extraction of bitumen using water-based processes, as described in the following section.

1.1.2 Froth Treatment in Bitumen Recovery Process

Bitumen from water-wet oil sands can be extracted using the Clark Hot Water Extraction (CHWE) process[Masliyah, 2000]. In this process, mined oil sands is first slurried with hot water. It is then transported to the extraction plant through hydrotransport pipelines, during which time the bitumen is liberated from the sand grains and is aerated. Upon arrival at the extraction plant, the slurry is diluted with more water and is fed into a primary separation vessel (PSV). The aerated bitumen floats to the top of the vessel and forms a bitumen froth.

The froth is a bicontinuous mixture of bitumen and water. The froth mixture is first de-aerated using steam. The composition of the de-aerated froth contains about 60% bitumen, 30% water and 10% solids by weight. Figure 1.1 shows a Syncrude froth treatment process. First, the de-aerated bitumen is diluted with heated naphtha. Naphtha is used to lower the bitumen froth viscosity to facilitate solids and water separation in the subsequent processes. The diluted bitumen is divided into two streams: one stream is sent to an inclined plate settler (IPS) and the other is fed to scroll centrifuges. The overflow that leaves the IPS is the diluted bitumen product. The underflow from the IPS is combined with another stream of diluted bitumen from the froth tank and sent to scroll centrifuges to remove the coarse solids. The rejected stream from the scroll centrifuge is directed to a naphtha recovery unit (NRU) to recover the naphtha for reuse. To remove the remaining water and fine solids, the hydrocarbon phase, i.e., product from the scroll centrifuge is sent to another set of centrifuges (disc centrifuges) that operate at about 2500 g. Despite all these efforts, the diluted bitumen product from the disc centrifuges still contains about 2 to 3% emulsified water and 0.5% fine solids. The water is dispersed in the hydrocarbon phase in the form of 1-5 μm size water droplets, which do not

coalescence. As the water droplets contain salts, removal of the water droplets becomes necessary to avoid corrosion in the upgrade equipment.

1.2 Water-in-Oil Emulsions

1.2.1 Definition of Water-in-Oil Emulsions

An emulsion is a heterogeneous mixture of two immiscible liquids, with one of the liquids dispersed in the form of droplets in the other. There are two types of emulsions: water-in-oil (W/O) and oil-in-water (O/W). Most emulsions formed in the petroleum industry are W/O emulsion.

1.2.2 Stability of Water-in-Oil Emulsions

Emulsions are thermodynamically unstable systems. However, if the droplets in an emulsion can remain dispersed over long durations, the emulsion is considered "stable". Emulsions formed in diluted bitumen are very stable: water droplets have been observed to remain dispersed even after centrifugation at high speeds [Yarranton, 1997]. Yeung et al. (1999) applied micropipette techniques to examine the stability of individual water droplet in diluted bitumen. It was found that two water droplets could remain as separate entities after being forced to contact for 5 minutes. Figure 1.2 shows the resistance of the water droplets to coalescence in the diluted bitumen.

Three basic conditions are necessary to form a stable emulsion, namely, two immiscible liquids, stabilizing agents and mechanical agitation. In the petroleum industry, crude oil and water are immiscible. There are also numerous natural stabilizing agents present in bitumen, e.g., asphaltenes, resinous substances and oil-soluble organic acids (such as naphthenic acid). These are surface-active compounds that spontaneously

accumulate at the interface, increasing the interfacial viscosity and decreasing the interfacial tension. Stabilizing agents will form interfacial films around the water droplets and prevent their coalescence. In addition, during the processing of oil sands, mechanical agitation is very common (e.g., flow through pipings and pumps and pressure drops across valves). As a consequence of these factors, small water drops are often created in the diluted bitumen and result in very stable water-in-oil emulsions.

Emulsion are stabilized by any or all of the following three mechanisms: electrical double layer repulsion, Marangoni-Gibbs effect and mechanically rigid films.

The first mechanism that can be responsible for emulsion stability is electric double layer repulsion. It is illustrated in Figure 1.3 (a). Counter ions are attracted to the surface and co-ions are repelled. When two charged surfaces approach each other, the electric double layers overlap and co-ions will create electrostatic repulsive forces between the droplets. Thus, emulsion droplets would be stabilized. However, for W/O emulsions, there are virtually no ions due to their low solubilities in oil. Thus, double layer repulsion is effectively zero when the continuous phase is non-aqueous.

Marangoni-Gibbs effect is another mechanism that may contribute to emulsion stability. When two water droplets are in close proximity, there is a thin gap of the continuous liquid between the particles. As shown in Figure 1.3 (b), the continuous phase drains out from this gap region as the two droplets approached to each other. As a result, the adsorbed surfactants are dragged to the edge of this region, creating depletion of surfactants in the center part of this gap. Because of the concentration gradient of surfactants along the interface, a diffusion flux is generated to compensate for the depletion of surfactants in the center part, i.e., opposite to the direction of drainage flow. This effect slows down the drainage process and may be responsible for the prevention of droplet coalescence.

The third mechanism that accounts for emulsion stability is the adsorbed film formed around the droplets. Asphaltenes and other surfactants can form a viscous interfacial film which provides a mechanical barrier to coalescence. Figure 1.4 is a depiction of this emulsion stabilization mechanism. The flocculation of asphaltenic aggregate materials form a viscous and mechanically rigid film around the water drop. The presence of the interfacial film is also demonstrated by Yeung et al. (1999). They used a micropipette to deflate a water droplet in diluted bitumen and revealed the protective layer as the droplet area is reduced, as shown in Figure 1.5. In flow situations, when two water droplets collide, this film will prevent the surfaces of the water droplets from contacting each other, thus preventing coalescence.

1.2.3 Necessity for Emulsion Breaking

Water-in-oil emulsions are highly undesirable in the oil sands industry for several reasons: first, emulsions will increase pumping and transportation costs. One reason for this is the additional water volume that must be carried. Another reason is that oil with stable emulsions are always more viscous than the oil itself. The viscosity of an emulsion can be estimated by the following equation [Bradley, 1987]

$$\mu_{emu} / \mu_{oil} = 1 + 2.5f + 14.1f^2 \qquad (1.1)$$

where μ_{emu} is the viscosity of the emulsion, μ_{oil} is the viscosity of clean oil and f is the volume fraction of the dispersed phase. For example, if the volume fraction of water is 3%, the viscosity of the oil will increase by about 9%.

Second, the salts that are dissolved in the water droplets can cause corrosion problems in downstream equipment. For example, the chlorides contained in the water droplets could pose serious corrosion problems while contacting the hot metal processing

facilities in the downstream bitumen upgrading operations. From a refinery's perspective, basic sediment and water, as well as salt content are the main criteria in determining the quality of a particular type of crude oil.

To reduce pumping costs, achieve desired product quality and minimize corrosion to equipments, it is imperative that W/O emulsions be effectively broken (demulsified) before bitumen is sent to upgrading.

1.2.4 Demulsification Methods

When two water droplets come in contact during demulsification, a thin liquid film forms between them. Rupture of this film causes coalescence and results in the increase of water droplet size. As the water droplets grow large enough, they will settle out and be separated from the oil. Any method that contributes to the coalescence of the droplets will therefore be beneficial to the breaking of an emulsion.

A stable emulsion exists only when stabilizing agents are present. Therefore, undesirable emulsions could be broken by eliminating the stabilizing agents or nullifying their effects. Demulsifiers are widely used to assist in destabilizing emulsions. For example, asphaltenes adsorbed at the interface can be replaced or be made oil-wet to disperse in the oil by some demulsifiers, thus promoting rupture of the interfacial film. This weakening of the protective film makes the coalescence of water droplets easier. Chemical demulsifiers are commonly used because of their low cost, easy of addition and reduction of settling time requirements. However, bottle and field tests need to be done to select the best demulsifier and its optimum dosage.

A variety of physical methods could increase the collision rate of dispersed droplets and facilitate the coalescence process. Heating, agitation and centrifugation are three commonly used mechanical methods. Heating could reduce the viscosities of the

oil continuous phase. In this way, the water drop settling rate increases. Therefore, heating assists in the process of gravity separation. Also, the solubility of the stabilizing agents (e.g., asphaltenes) may increase in the oil phase because of the rise in temperature. There will be less stabilizing agents adsorbed to the interface, thus promoting coalescence. A factor that needs to be considered is the fuel cost to provide the thermal energy.

Agitation helps the process of coalescence by increasing the rate of collision of the water droplets. It is believed that agitation can help the coalescence of water droplets if the Reynolds number is between 50,000 to 100,000 [Bradley, 1987]. However, the agitation method needs to be designed carefully to prevent further emulsification through excessive shearing. Centrifugation is also used because of the density difference of water and oil. The negative aspect of centrifugation method is the high operating cost, high maintenance cost and low processing capacity.

Apart from the aforementioned physical and chemical means of demulsification, electrical methods are also used in breaking water-in-oil emulsions. When the water drops are subjected to an electric field, polarization charges are induced on the water droplets. Thus, coulombic attraction can bring the water droplets together. The enhanced electric field between two droplets may also cause the rupture of the adsorbed film and leads to coalescence of water droplets. However, electrical methods have their own limitation. If there is excess water, say, greater than 6%, it could cause electric short circuiting across the emulsion medium.

1.3 Motivation and Objectives

1.3.1 Thesis Motivation

As mentioned earlier, in the bitumen recovery process, a stable water-in-oil emulsion is present in the diluted bitumen product. For many reasons, it is desirable to break the emulsion and remove the water prior to bitumen upgrading. Centrifuges are now commonly used for demulsification purpose in the oil sands industry. However, because of its high operational and maintenance cost, it is desirable to find an alternative method to demulsify the water droplets.

Among the demulsification methods, a cost-effective method needs to be selected to break the emulsion and achieve the required quality of diluted bitumen prior to its upgrading. The fact that W/O emulsions are electrically nonconductive, or at least have very low electric conductivity, makes the application of electric fields a possible alternative.

Unfortunately, even though application of electric fields is widely used to improve drop coalescence [Waterman, 1965; Ptasinski & Kerkhof, 1992], no significant work has been carried out to improve the understanding of the coalescence mechanism. Most efforts are focused on the design of electrical coalescers since Cottrell's work in 1906. It is believed that a fundamental understanding of the electrical coalescence process is lacking because of the complexities of the hydrodynamic and electrical phenomena involved. Although it is well known that electric fields can aid in the coalescence process, the manner which it influences coalescence remains unclear.

It is necessary to study the process of coalescence due to electrical field and find factors that affect the coalescence of water drops in oil. In particular, one needs to understand what happens when two water droplets are close to each other as an electric

field is applied. If a clearer understanding of the process could be obtained, it is then possible to develop better electrical coalescers for industrial applications.

1.3.2 Research Objectives

To improve the understanding of demulsification by electric fields, it is helpful to study the effects of electric field on a single and a double water droplets in a hydrocarbon medium. In particular, the deformation of water droplet(s) in an applied electric field, especially that of water drop pairs, will provide basic insights into the behavior of two water droplets as they approach each other during the demulsification process. Furthermore, although the coalescence of two water drops is clearly of interest, there are very few reported studies. It will also be helpful to learn more about the electrical coalescence mechanism by studying the coalescence process of two water droplets. In addition, further research is needed to elucidate the role of surfactants in the deformation and coalescence process of water drops.

Accordingly, this research project can be divided into three stages which are tackled sequentially: the study of the deformation of a single water drop in oil under an electric field; the study of the deformation of a water drop pair in oil under an electric field; and the study of the coalescence process of a water drop pair in an electric field.

Consequently, the objectives of this thesis are:

1. To measure the degree of deformation of a single water drop in different hydrocarbons under an electric field and to examine the effect of time and surfactant.

2. To measure the degree of deformation of water drop pairs in hydrocarbons under an electric field.

3. To record video images of the coalescence process of water droplets in hydrocarbon systems under an electric field to gain better understanding on the coalescence process.

The thesis is composed of the following six chapters. Chapter 1 provides a general background to the research topic. Also, in this chapter, the industrial motivation for the research is described and the main objectives of this thesis are identified. Chapter 2 presents a literature review on the experimental and theoretical studies of the deformation of a single droplet and drop pairs. The coalescence due to an electric field is reviewed as well. Chapter 3 focuses on interfacial tension measurements using the ring method and drop profile analysis. Interfacial tension values will be needed in defining the electrical Weber number, which is an important parameter describing drop deformation in electric fields. Chapter 4 reports on the experimental approach of this thesis, including the experimental setup and procedures. Measurement of deformation is tackled in this chapter. Chapter 5 focuses on the experimental results and discussion. Chapter 6 summarizes the most important results and conclusions of the thesis. Some possible industrial implications and future work in this area are also suggested.

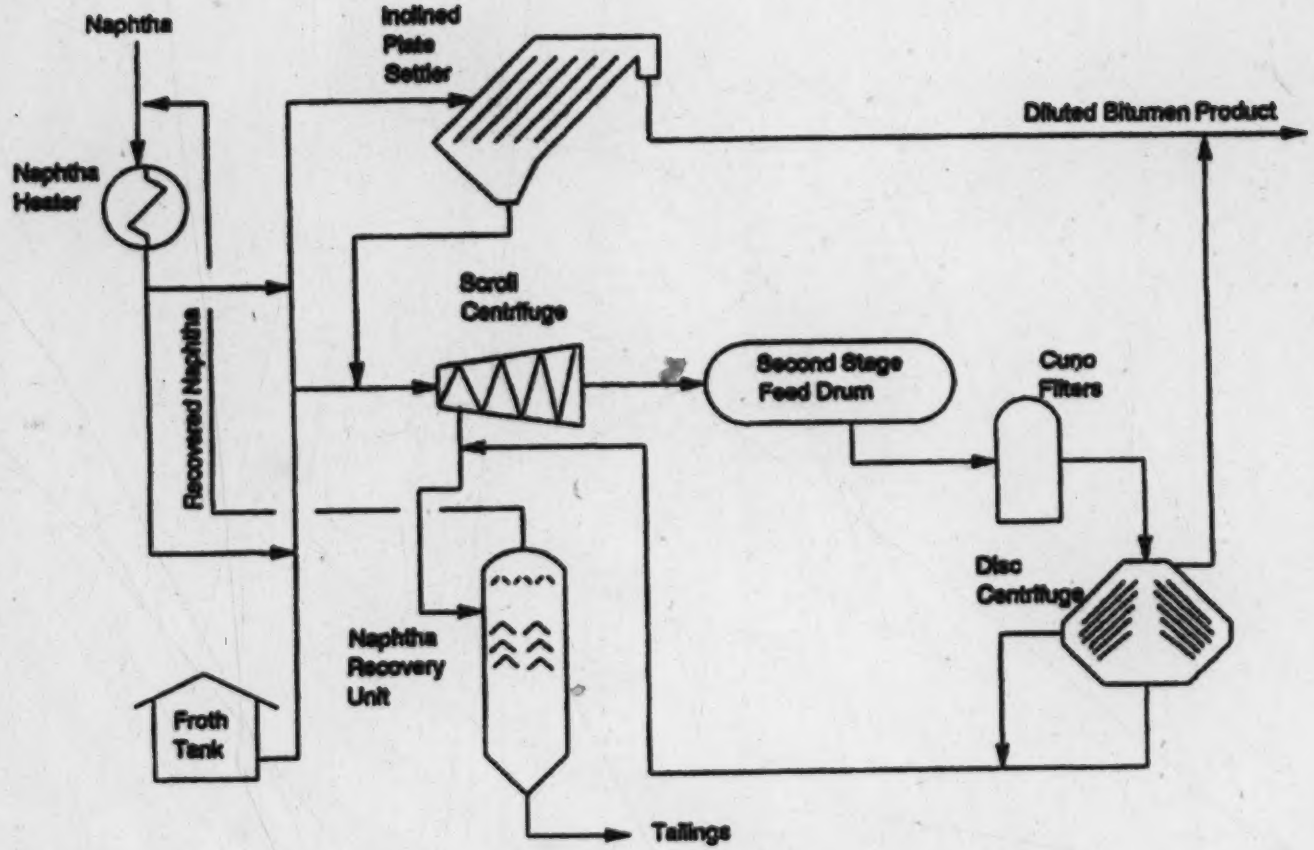

Figure 1.1 Simplified flowsheet of Syncrude froth treatment plant 6 [Tipman and Shaw, 1993]

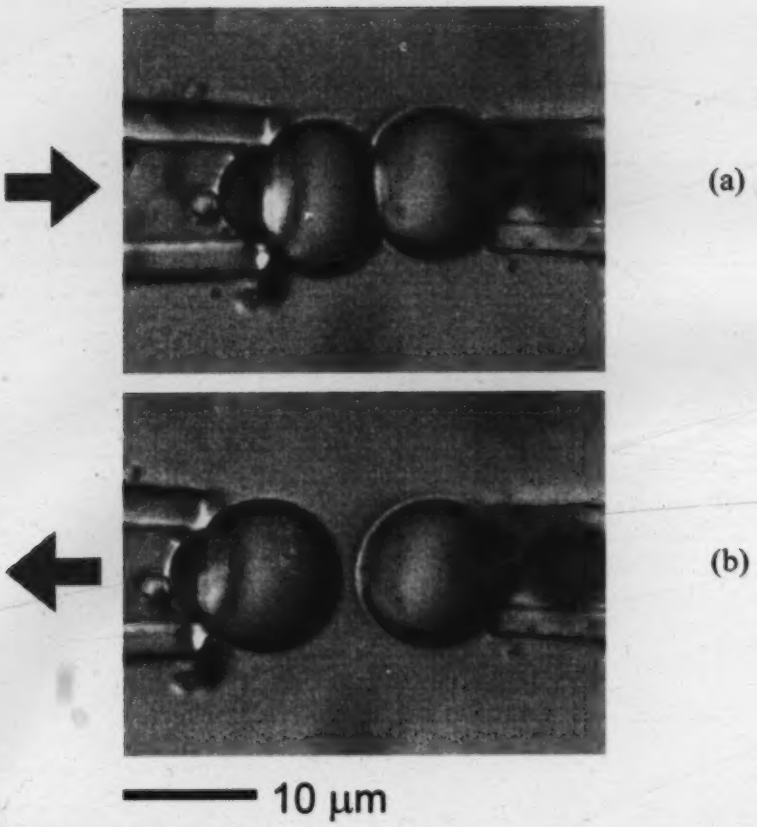

Figure 1.2 Two micro size water droplets held by micropipettes in a diluted bitumen solution [Yeung, et al., 1999]
(a) The water droplets are forced to be in contact with each other
(b) The two water droplets are allowed to be separated

(a) Electrical Double Layer Repulsion

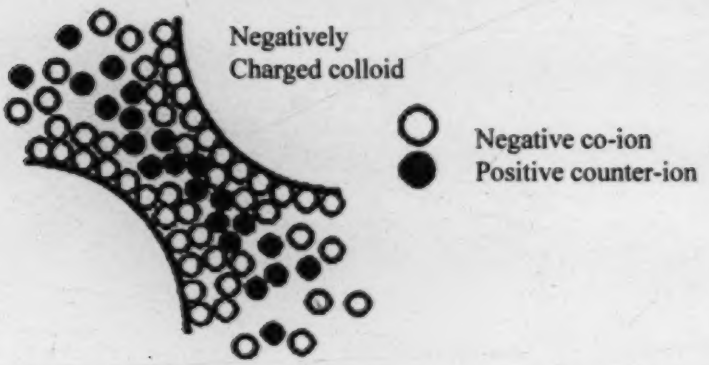

(b)Marangoni-Gibbs Effect

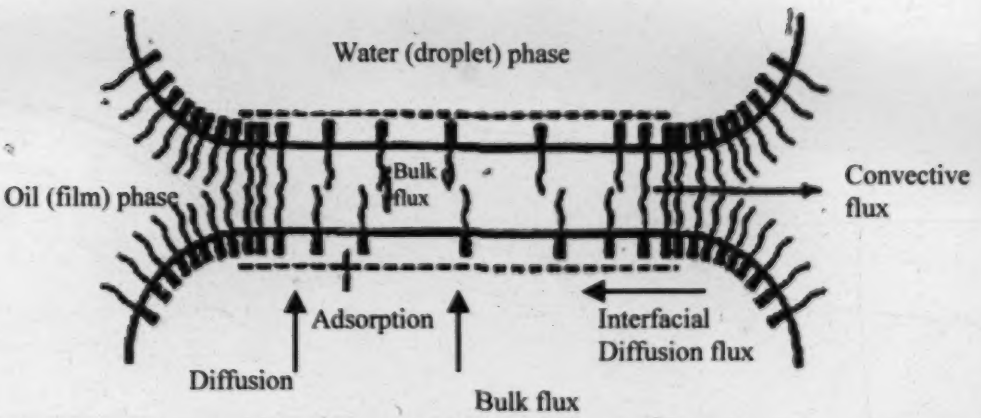

Figure 1.3 Depiction of emulsion stabilization mechanisms related to electrostatic repulsion, Marangoni-Gibbs effect [McLean et al., 1998]
(a) Electrical double layer repulsion
(b) Marangoni-Gibbs effect

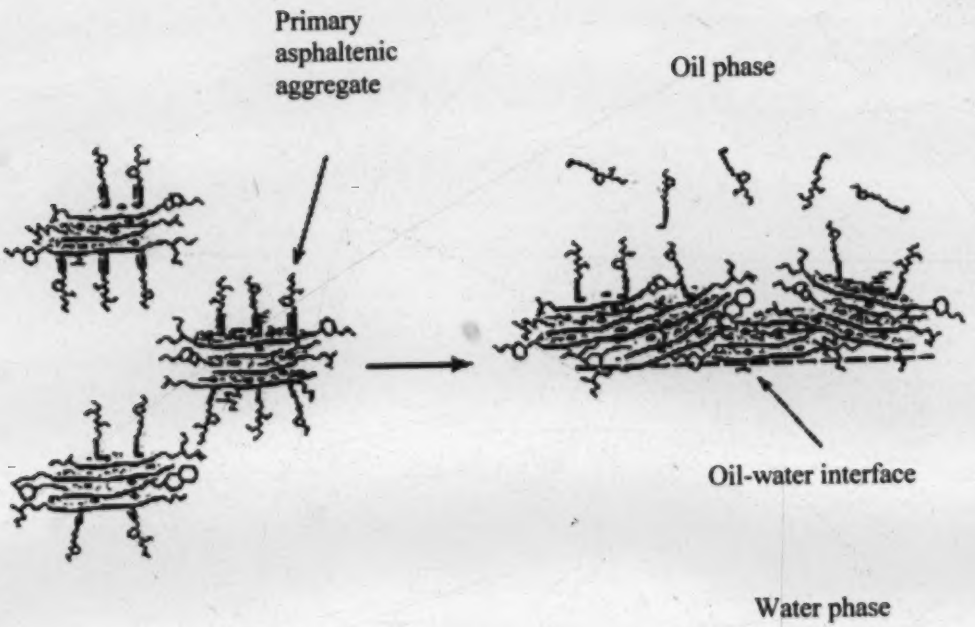

Figure 1.4 Depiction of emulsion stabilization mechanisms related to mechanically rigid film [McLean et al., 1998]

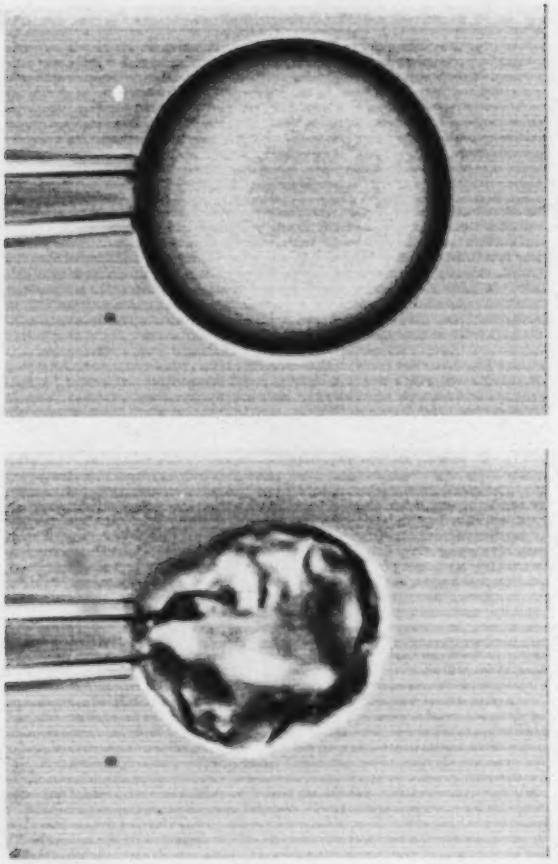

Figure 1.5 Deflating an emulsion drop using micropipette [Yeung et al., 1999]

Chapter 2

Literature Review on Drop Deformation and Coalescence in an Electric Field

The field of electrohydrodynamics (EHD) deals with fluid motion driven by an external electric field. It is a cross discipline that studies the combined effects of electric fields and the flow of fluids, as it involves both the effect of the fluid motion on the electric field and the electric field's influence on fluid motion. A variety of industrial applications (e.g., enhanced coalescence of drops, enhanced heat and mass transfer, electrical spraying and ink jet printing) rely heavily on a thorough understanding of the interactions between the flow and electric fields. The study of fluid interfaces, especially with regard to drop deformations, constitutes an important aspect of EHD.

In the following, a literature review will be given on the deformation of a single liquid drop and a liquid drop pair, as well as the study of the coalescence of two liquid drops in an electric field. Main findings and existing problems in the literature will be summarized to highlight the motivation for the present thesis .

2.1 Deformation of a Single Drop in an Electric Field

2.1.1 Deformation of a Single Drop in Systems without Surfactants

When a free drop is suspended in another immiscible non-conductive fluid, the drop deforms as an electric field is applied. Many theoretical and experimental studies on drop deformation were conducted in the past. The deformation and breakup of raindrops in air during rainstorms was first studied more than a century ago. Starting from 1880's to the 1960's, the deformation of fluid drops was investigated within the classical framework of electrohydrostatics. These studies were mainly focused on the

behavior of a perfect dielectric drop in a perfect dielectric. It was assumed that there was no current passing through the drop phase and the surrounding continuous phase. This, in turn, implied that no *free* charge was present in the bulk phase or at the fluid interface. The following system of governing equations is used to describe the electric field of a perfect dielectric drop in a perfect dielectric:

Governing equations:

$$\nabla^2 \phi_i = 0 \qquad \text{drop phase} \qquad (2.1\text{ a})$$

$$\nabla^2 \phi_e = 0 \qquad \text{continuous phase} \qquad (2.1\text{ b})$$

Boundary conditions:

$$\phi_e = \phi_i \qquad \text{drop interface} \qquad (2.1\text{ c})$$

$$\varepsilon_e \frac{\partial \phi_e}{\partial n} = \varepsilon_i \frac{\partial \phi_i}{\partial n} \qquad \text{drop interface} \qquad (2.1\text{ d})$$

$$-\nabla \phi_e = E_0 \qquad \text{far from the drop} \qquad (2.1\text{ e})$$

ϕ_i is finite $\qquad$ at drop center $\qquad$ (2.1 f)

The external continuous phase is denoted by e and the internal drop phase is denoted by i. Here, ϕ_i is the electric potential in the drop phase, ϕ_e is the electric potential in the continuous phase, ε_i is the dielectric constant of the drop phase, ε_e is the dielectric constant of the continuous phase, and E_0 is the applied electric field strength. As there is no free charge in the bulk phase, electric fields are described by the Laplace equation inside and outside the drop. The boundary conditions adopted are: (2.1 c), continuity of the electrical potential at the interface; (2.1 d), continuity of the electric displacement at the interface; (2.1 e), the electric field is uniform far from the drop; and (2.1 f), the electrical potential is finite at the center of the drop. The boundary condition (2.1 d) is valid because there is no free charge present at the fluid interface as would be the case for a perfect dielectric suspended in another perfect dielectric.

Due to the discontinuity of the electric field at the fluid interface, local electrical stresses will be induced. Because the electrical stresses act normal to the interface, they can be mechanically balanced by changes in the curvature of the drop surface. The fluids can remain motionless at steady state. Therefore, for a perfect dielectric drop suspended in another perfect dielectric medium under an electric field, the drop is always elongated to a prolate spheroid with its major axis in the direction of the electric field. More details regarding the electrical stresses and why a drop is deformed to a prolate spheroid could be found in Appendix II. Using equations (2.1 a-f), Allan & Mason (1962) derived the following expression for the drop deformation:

$$D = \frac{9}{16} \frac{\left(\frac{\varepsilon_i}{\varepsilon_e} - 1\right)^2}{\left(\frac{\varepsilon_i}{\varepsilon_e} + 2\right)^2} \frac{\varepsilon_0 \varepsilon_e}{\gamma} r_0 E_0^2 \qquad (2.2)$$

where ε_0 is the permittivity in vacuum, γ is the interfacial tension between the drop phase and the continuous phase, r_0 is the radius of the undeformed drop, and E_0 is the uniform electric field strength.

The degree of drop deformation D is defined as

$$D = \frac{a-b}{a+b} \qquad (2.3)$$

while a and b are the drop axes that are parallel and perpendicular to the direction of the electric field, respectively, as shown in Figure 2.1.

From equation (2.2), it can be noted that D is always greater than zero, independent of the properties of the dispersed and continuous phases. However, Allan & Mason (1962) observed that a suspended drop in an electric field can maintain a spherical shape or can even be changed to an oblate spheroid. They tested 13 pairs of liquids for

deformation behavior. The liquid systems were oil drops in another immiscible oil, as well as water drops in oil. It was evident that the occurrence of oblate spheroids could not be explained by electrohydrostatic theories alone.

To account for the phenomena of drop deformation into the shape of oblate spheroids, which was contrary to the existing theories at the time, Taylor (1966) proposed that the immiscible fluids could not be considered as perfect dielectrics. Instead, the fluids should be treated as "leaky dielectrics" which allow for the flow of a small electrical current within the system under an applied electric field. This is due to the finite electrical conductivity of the system, however small it may be. Taylor (1966) stated that, "however small the conductivity of either fluid the charge associated with steady currents must accumulate at the interface till the steady state is established." The fact that free charges accumulate at the drop interface leads to an interaction between the electric field and the charges built up at the interface. In the case of a leaky dielectric drop suspended in a leaky dielectric medium, the electric force is no longer normal to the drop interface (except at the two pole points), thus inducing tangential electrical stresses. These tangential stresses at the interface could only be balanced by a viscous shear stress. The hydrodynamic stresses give rise to steady fluid circulations inside and outside the drop. It is because of the interaction of the electric field and the induced fluid flow that makes oblate deformation possible.

The following set of governing equations was used by Taylor (1966) to describe the system of a leaky dielectric drop suspended in a leaky dielectric medium:

Governing equations:

$$\nabla^2 \phi_i = 0 \qquad \text{internal phase} \qquad (2.4\text{ a})$$

$$\nabla^2 \phi_e = 0 \qquad \text{external phase} \qquad (2.4\text{ b})$$

Boundary conditions:

$$\phi_e = \phi_i \qquad \text{drop interface} \qquad (2.4\text{ c})$$

$$\sigma_e \frac{\partial \phi_e}{\partial n} = \sigma_i \frac{\partial \phi_i}{\partial n} \qquad \text{drop interface} \qquad (2.4\text{ d})$$

$$-\nabla \phi_e = E_0 \qquad \text{far from the drop} \qquad (2.4\text{ e})$$

ϕ_i is finite at drop center (2.4 f)

where σ_e is the electrical conductivity of the external continuous phase and σ_i is the electrical conductivity of the internal drop phase. There are similarities between the mathematical equations describing the case of a perfect dielectric drop in another perfect dielectric and the case of a leaky dielectric drop in a leaky dielectric medium.

Taylor (1966) assumed that free charges were only present at the *interface*, and no free charges existed in the bulk. The electric fields inside and outside the drop are described by the Laplace equation instead of the Poisson equation. However, the boundary condition (2.1 d) is no longer valid because of the free charges present at the fluid interface. Taylor applied another boundary condition (2.4 d) because, as he pointed out, the conduction current normal to the fluid interface must be continuous when the system is in steady state. From the solution of the electric field, Taylor obtained the electrical stresses at the interface.

The flow field is governed by the Navier-Stokes equation. It is assumed that forces due to inertia are negligible compared to viscous forces, i.e., the case of creeping flow. Taylor balanced the electrical stresses with hydrodynamic stresses obtained from Stokes flow. In the limiting case of *creeping flow* and *very small deformation*, Taylor (1966) introduced a discriminating function β, which could indicate whether the drop shape is prolate, spherical or oblate. When β is greater than zero, the drop is deformed into a prolate spheroid. Here, $\beta < 0$ implies an oblate spheroid and the drop remains a perfect sphere when $\beta = 0$. The discriminating function can be expressed in terms of the physical properties of the dispersed and continuous phases,

$$\beta = \left(R^2 - 2S + 1\right) + 3(R - S)\left(\frac{2 + 3M}{5 + 5M}\right) \tag{2.5}$$

Equation (2.5) is a modified form of Taylor's original expression [Melcher & Taylor, 1969]. In this expression,

$$R = \frac{\sigma_i}{\sigma_e} \tag{2.6}$$

$$S = \frac{\varepsilon_i}{\varepsilon_e} \tag{2.7}$$

$$M = \frac{\mu_i}{\mu_e} \tag{2.8}$$

where σ is the electrical conductivity, ε is the dielectric constant, μ is the fluid viscosity, and R, S and M are the ratios of the respective properties between inside and outside, with i denoting the dispersed phase and e representing the continuous phase.

By measuring a large number of deformations in different systems, Vizika & Saville (1992) showed that the discriminating function β is useful for predicting drop shapes. Prolate and oblate drops are shown in Figure 2.2, with β being greater than and less than zero, respectively.

In the limiting case of creeping flow, and for very small drop deformations in a constant electric field, [although Taylor (1966) did not explicitly give an expression for D], the degree of deformation can be expressed as [Vizika & Saville, 1992]

$$D = m r_0 E_0^2 \tag{2.9}$$

where

$$m = \frac{9}{16} \frac{\varepsilon_0 \varepsilon_e}{\gamma} \frac{\beta}{(2 + R)^2} \tag{2.10}$$

Here m is the so-called deformation factor.

In the case of a water drop dispersed in oil, the electrical conductivity of water is much larger than that of the surrounding oil, i.e., $R >> 1$. The degree of deformation D can, in such a case, be simplified to

$$D = \frac{9}{16} We \tag{2.11}$$

where We is the Weber number defined as

$$We = \frac{\varepsilon_0 \varepsilon_e}{\gamma} r_0 E_0^2 \tag{2.12}$$

Equation (2.2) can be simplified to the same form as (2.11) if the dielectric constant of the drop phase is much larger than that of the continuous phase (i.e, S >> 1). These limits point to the similarity between the perfect dielectric system (when S >> 1) and the leaky dielectric system (when R >> 1).

To balance the radial components of the electrical displacement on the two sides of the interface, there must exist a surface charge density given by [Taylor, 1966]

$$\rho_e = 3\varepsilon_0 \varepsilon_e E_0 \cos\theta \left(\frac{R - S}{2 + R} \right) \tag{2.13}$$

where θ is the angle between the electric field vector and the radial vector from the center of the drop to its surface, as shown in Figure 2.3(a).

In the system of a water drop in oil, with $R >> 1$, one can safely assume that R is greater than S. Thus, the charge density must have the same sign as $\cos\theta$. The free charge distribution and the tangential electric stress at the interface are shown in Figure

2.3 (a). To balance the tangential electric stresses, hydrodynamic stresses are required. The flow circulations inside and outside a water drop are shown in Figure 2.3 (b). Interfacial flow is directed from the equator ($\theta = \frac{\pi}{2}$) to the poles in this case.

After Taylor proposed the leaky dielectric theory in 1966, this model had been used extensively. Taylor's theory for drop deformation in steady electric fields was extended by Torza et al. (1971). The extended theory can be applied to both steady and alternating electric fields; it reduces to Taylor's theory in the case of DC fields. Torza et al. also conducted experiments to test Taylor's leaky dielectric theory. Twenty-two different systems were tested. In these systems, oils were selected as the continuous phase, while the dispersed droplet was either water or an immiscible oil. The experimental study only agreed with Taylor's theory qualitatively; the quantitative agreement was poor. It was found that in most cases, the measured deformations were greater than what was calculated based on the leaky dielectric theory (by a factor of two to four). The comparison of experimental and calculated deformations for fourteen systems is shown in Table 2.1.

Vizika and Saville (1992) chose the same experimental systems as Torza et al.'s (1971) and reported better agreement between Taylor's theory and their experimental results. However, discrepancies still remained for some systems. It was found that for drops that were deformed into prolate ellipsoids, Taylor's theory always underestimated the deformation; conversely, for drops that deformed into oblate shapes, Taylor's theory consistently overestimated the deformation by a small amount. Taylor's leaky dielectric model is capable of predicting the drop's electrohydrodynamics behavior only qualitatively.

As Taylor's leaky dielectric theory is valid only qualitatively, much work has been conducted to improve its accuracy. Ajayi (1978) extended Taylor's linear model to include higher order corrections in describing the drop profile as well as the resulting electric field and fluid motion. Taylor assumed that the drop deformed only slightly from

a sphere, while Ajayi considered second order perturbation terms for the drop shape. However, the discrepancies between theory and experiment cannot be reconciled even when higher order terms were included in the expansions of the electric field and fluid motion. Later, Baygents & Saville (1989) employed another approach (electrokinetic model of charge transport) to model the drop deformation, but obtained equivalent expressions for the drop deformation as the leaky dielectric theory.

With the development of modern computers, numerical techniques have been widely used in the past three decades. In the literature, there are publications that focus on the effect of an electric field on a drop's deformation behavior [Tsukada, et al., 1986; Tsukada, et al., 1994; Tsukada, et al., 1997]. It was claimed that these numerical results are in good agreement with Taylor's theory. However, there remain some shortcomings with regard to these results: certain assumptions such as creeping flow and small deformations were still employed.

Feng & Scott (1996) conducted a comprehensive numerical study of electrically deformed drops by extending Taylor's linear results to include finite inertial effects and nonlinearities arising from large deformations. They reported detailed analysis of the electrohydrodynamics of a leaky dielectric drop in an electric field. Flows of finite Reynolds number and drop shapes with large deformations were examined in their study. A comparison between Feng & Scott's computational results and Taylor's analytical prediction at the limit of creeping flow is shown in Figure 2.4. The numerical analysis is based on creeping flow and very large conductivity ratio (electrical conductivity of the drop phase to that of the continuous phase). Feng & Scott showed in Figure 2.4 that their results were essentially the same as Taylor's theory in the limit of small deformations. However, as the drop deformation becomes larger, the discrepancy between Feng & Scott's numerical results and Taylor's theory increases. For large deformations, Taylor's theory always underestimated the distortion of the drop. As shown in Figure 2.4, Vizika & Saville's experimental results shown on Figure 2.4 (1992) agreed better with Feng & Scott's numerical predictions in the range of large deformation.

2.1.2 Deformation of a Single Drop in Systems with Nonionic Surfactants

Although surfactants are commonly present in many applications, their influence on electrohydrodynamic behavior remains largely unexplored. There is a need to understand the effects of an applied electric field on dispersed drops when surfactants are present in the system. Surfactants tend to adsorb onto a liquid-liquid interface and can lead to several effects: (1) reduction of interfacial tension, (2) suppression of internal fluid circulation, and (3) creation of interfacial viscosity variation. In most studies, the changes in surface viscous effects are neglected.

When a water drop is suspended in oil in the presence of surfactants (either added deliberately or present as impurities), the surfactants will be adsorbed and distribute uniformly on the drop surface. That creates the first effect: the interfacial tension between water and oil is reduced. When an electric field is applied, the induced fluid flow is directed from the drop's equator to the two poles (as shown in Figure 2.3). Thus surfactants are also swept toward the poles from the equator. The surfactant distribution on the drop surface is changed and there are more surfactants at the poles than at the equator. There is thus a concentration gradient of surfactants along the drop surface. Consequently, an interfacial tension gradient is established with the lowest interfacial tension at the poles of the drop where surfactant concentration is the highest. As the concentration of the surfactants at the interface is not uniform, the so-called Marangoni flow (surface flow caused by interfacial tension gradients that results from nonuniform distribution of surfactants) is induced to satisfy the continuity of tangential stress. The direction of the Marangoni flow is opposite to the fluid flow induced by the electric field. Thus, Marangoni surface flow will retard the induced fluid circulation near an interface. This is the second effect brought about by surfactants.

Ha & Yang (1995, 1998) studied the effects of nonionic surfactants on the deformation and stability of a liquid drop in an electric field. The effect of surfactants is shown in Figure 2.5. When compared to Taylor's theory, appreciable discrepancies exist

in the range of large deformations, while the agreement is quite good when drop deformation is small. The degree of deformation becomes larger as the surfactant concentration increases. The presence of surfactants influences the drop deformation behavior in an electric field by reducing the interfacial tension and inducing Marangoni surface flow. As the regions near the poles of the drop have lower interfacial tensions (higher concentration of surfactants), larger local deformations are created. Ha & Yang also concluded that the nonuniform distribution of surfactants are important only during droplet breakup, and has negligible effects in the steady state drop deformation for a conducting drop. For a highly conducting drop in an electric field, the fluid is nearly motionless. In other words, the electric field-induced flow is too weak to cause any transport of the surfactants. Significant convection of the surfactants at the interface does not occur; therefore, the surfactants can be considered uniformly distributed.

Ha & Yang (1995, 1998) employed two parameters to express the drop deformation in the presence of surfactants: the surface Peclet number and the Gibbs elasticity. The surface Peclet number represents the relative importance of surfactant convection to surface diffusion on the interface; it is defined as

$$P_e = \frac{u_c r_0}{D_s} \tag{2.14}$$

where D_s is the surface diffusivity of surfactants, r_0 is the undistorted drop radius, and the characteristic velocity u_c is given by

$$u_c = \frac{\varepsilon_0 \varepsilon_e r_0 E_0^2}{\mu_e} \tag{2.15}$$

with ε_e being the dielectric constant of the continuous phase, E_0 is the applied electric field strength, and μ_e is the viscosity of the continuous phase. When $Pe \to 0$, there is no surfactant concentration gradient because of the large surface diffusivity. When $Pe \to \infty$, the transport of surfactants along the interface is effectively zero.

Gibbs elasticity measures changes in the interfacial tension in response to variation of the surfactant concentration. It can be expressed as

$$E_s = -\frac{1}{\gamma_0}\frac{\partial \gamma}{\partial \Gamma} \tag{2.16}$$

where γ_0 is the interfacial tension in the absence of surfactants and Γ denotes the surface concentration of the surfactants. When $E_s \to 0$, the surfactants have no effects on the interfacial tension. Conversely, as $E_s \to \infty$, the interface behaves effectively as a rigid film. These two parameters will be discussed later in the thesis. In terms of *Pe* and E_s, Ha & Yang made predictions of the steady state drop deformation in the presence of nonionic surfactants for small deformations. Their solution reduced to Taylor's theory when there was no surfactant present.

From the above discussion, it was noted that Taylor's leaky dielectric theory was a good approximation for small deformations in creeping flow situations. However, in the experimental studies, because of the need to avoid significant drop movement due to buoyancy or gravity, the continuous phase either had to have the same density as the drop phase, or must be very viscous. This is why mineral oils were commonly chosen as the continuous phase in the experiments conducted ([Allan & Mason, 1962], [Torza et al, 1971], [Vizika & Saville, 1992]). Only a small number of fluids satisfied the density or viscosity requirements. Experiments with a wider range of fluid properties, such as oils that do not meet the density or viscosity requirements, were not possible. The deformation of water drops in diluted bitumen has not been explored either. Experimental studies of water-oil and diluted bitumen systems will not only contribute to the understanding of the mechanism of electrical coalescence, but also add to the existing experimental data based in this area of research.

2.2 Deformation of a Drop Pair in an Electric Field

When two drops are placed close to each other in an electric field, each drop will influence the other's deformation behavior. For simplicity, the line that connects the centers of the two drops is assumed parallel to the direction of the electric filed. In contrast to a single drop, less investigation was devoted to the complex mechanism of drop pair deformation in an electric field. As observing the deformation of two freely moving drops is very difficult, only limited experimental studies on drop pair deformation have appeared in the literature. Consequently, much of the information on the deformation behavior of drop pairs is only qualitative.

When two drops are placed in an electric field, the electric field strength between the drops is enhanced due to mutual interactions of the polarization charges, provided the line of centers of the drops is not perpendicular to the electric field. The electric field strength at the inside surface of the drops, e.g., point A in Figure 2.6, has the maximum field strength, with x_0 is the initial edge-to-edge separation distance between the two drops. The enhancement factor of the electric field is defined as

$$\Omega = \frac{E_A}{E_0} \tag{2.17}$$

where E_A is the electric field at the inside surface of the drop and E_0 is the applied electric field strength. Davis (1964) presented numerical results for two conducting spheres in a uniform electric field. The prediction was based on rigid spheres. It is shown in Table 2.2 how rapidly the enhancement factor Ω increases as the separation distance decreases. For example, when the initial separation distance (edge-to-edge) between two equal-sized spheres is one thousandth of the radii of the spheres, the electric field at the near surfaces will be about seven hundred times that of the applied electric field.

Latham & Roxburgh (1966) used Davis's results to study the behavior of water drops in air. Water drop pairs were suspended from thin Teflon rods and were elongated

along the electric field direction. With the assumption of rigid spheres, it was concluded that a drop can be considered isolated if it were separated by several radii from its neighboring drops. Leaky dielectric model was not used in this study. Later, Brazier-Smith et al. (1971) attempted to remove the effects of distorting forces produced by the Teflon supports by studying the interactions between falling drop pairs. The deformation behavior of uncharged drop pairs was investigated using incompressible potential flow to simulate the deformations. Brzaier-Smith et al. concluded that if the initial separation distance (edge-to-edge) between the drops was less than 1.2 times the drop radius, the drops would deform until they contacted each other. The degree of deformation was only recorded at the moment of drop disintegration. No quantitative model was given for all these experimental studies. It should also be noted that only Columbic interactions were considered in these reported investigations. Thus, all of the aforementioned studies were not rigorous as none of them accounted for electrically driven fluid circulations.

Sozou (1975) used the leaky dielectric model to analyze two-drop systems with the assumption of very small deformation and zero relative motion between the drops. It was concluded that the local electric field and fluid motion of one drop were not affected by the other if the separation distance was several times the drop diameters. That was the same conclusion made by Latham & Roxburgh (1966). Only when the distance was on the order of one radius, was there a substantial modification in the tangential electric stress at the surface of the drops and in the induced flow field. Otherwise, two widely separated drops can be considered as isolated entities.

Recently, Baygents et al. (1998) modeled the electrohydrodynamic deformation and interaction of drop pairs using the leaky dielectric model. They obtained the same result as Sozou's (1975) for the tangential electrical stress along the drop surface, as shown in Figure 2.7. The drop deformation and translation as a function of the initial separation distance is shown in Figure 2.8. This figure shows that fluid circulation plays an important role in the collective behavior of a drop pair in an electric field. When the center-to-center distance is sufficiently large (in this study, greater than approximately 9.8 times the radius), the drops would deform and move apart due to repulsive

hydrodynamic interactions. The hydrodynamic interactions resulting from fluid circulation can be significant and may even be stronger than the direct electrical interactions between the drop pair, as in the case of Figure 2.8 (c). When the separation distance is small, electrical interactions will be dominant and the two drops would move toward each other. Nevertheless, the validity of the numerical data needs to be confirmed.

For water drop pairs in oil, flow is drawn from the equator to the pole, as shown in Figure 2.9. Thus, the hydrodynamic interactions are always repulsive. It is reasonable to suggest that water drops will attract each other when the separation distance is very small compared to the drop radius. This is because, at small distances, the electrical attractive force would be greater than the hydrodynamic repulsive force. When two water drops are far away from each other (e.g., the separation distance is ten times the radius), they will be pushed apart because of the dominant hydrodynamic repulsive forces.

In summary, there appears to be a lack of experimental data in the literature to verify most of the above-mentioned theoretical or numerical results. Thus, an experiment investigation of water drop pair deforming in various systems is needed to attain more understanding, at least qualitatively. As it is difficult in practice to study the deformation of two free drops, capillaries will be used in this study to hold the water drop pair, thus maintaining an equilibrium state.

2.3 Coalescence of a Drop Pair in an Electric Field

Although there is abundant literature on demulsification, not much has been reported on the electrically-induced coalescence of two liquid drops. This may be due to insufficient knowledge of the interaction between the flow fields and the electric fields, as well as of the surface properties of the liquid drops. It is also very difficult to conduct experimental investigations on the coalescence of two freely moving drops. For these

reasons, much of the work was conducted on the collision rate or collision efficiency of large population of drops. For example, Zhang et al. (1995) used trajectory analysis to follow the relative motions of pairs of drops, to calculate the collision and coalescence rate. However, the work was based on perfectly conducting drops in perfect dielectric liquids. All these investigations had concluded that an external electric field promoted coalescence between drops, but no fundamental or quantitative information on the electrically-induced coalescence between two drops is available.

Coalescence of two drops occurs when they collide and remain in contact with each other for a certain time. This happens in two stages. First, the drops approach each other and the intervening liquid between the drops drains from the region until the liquid is reduced to a very thin film. Second, the film ruptures and makes way for coalescence. The attractive forces between the drops must make the film sufficiently thin so that film rupture becomes possible. The rate of thinning of the film and its stability against rupture are two main factors determining the possibility of coalescence. As for the system without surfactants, the intervening film could become very thin. However, if stabilizing agents are present, they may accumulate at the liquid-liquid interface and increase the difficulty of film rupture, thus reducing the rate of coalescence.

Electric fields could facilitate drop coalescence by bringing two drops very close to each other. When an electric field is applied to water drops in an oil-continuous system, polarization charges are induced on the drops. For two liquid drops that are sufficiently far apart, the mutual attractive forces between two equal size water drops in a uniform electric field can be expressed approximately as,

$$F_a = 24\pi\varepsilon_0\varepsilon_e \frac{E_0^2 r_0^6}{x_c^4} \qquad (2.18)$$

where ε_0 is the permittivity of vacuum, ε_e is the dielectric constant of the continuous phase, r_0 is the radius of the undistorted drop, and x_c is the drop separation distance (center-to-center). Details of the derivation can be found in Appendix III. A similar

expression for the attraction force between two drops is given by Waterman (1965). As noted in equation (2.18), the force increases sharply ($\sim 1/x_c^4$) as the drop separation decreases. When the water drops are very close to each other, the electrical attractive force will be the dominant force. Enhanced electric field between two water drops will not only help in the drainage of the intervening oil film, but it also makes the water drops deformed more. The chance of coalescence increases as the drop separation distance is decreased due to water drop deformation.

In the literature, there have been very few experimental studies on the electrical coalescence between two drops. Taylor (1968) studied the coalescence of closely spaced soap bubbles, but no image of the coalescence process was reported. It is very helpful to conduct a visualization study on the coalescence process to enhance understanding of electrical coalescence; this will be one of the objectives of this present work.

Table 2.1 Comparison of experimental and calculated deformations for different systems (reproduced from [Torza et al. 1971])

System #	Calculated value m (cm/kV^2)	Experimental value m^* (cm/kV^2)	Discrepancy factor m^*/m
1	0.24	0.39	1.6
2	0.31	1.31	4.2
3	0.38	0.91	2.4
4	0.23	0.88	3.8
5	0.30	0.90	3.0
6	0.38	0.93	2.4
7	0.24	0.51	2.1
8	1.05	2.04	1.9
9	0.12	0.36	3.0
10	0.40	1.58	3.9
11	0.05	0.19	3.8
12	0.15	0.25	1.7
13	0.05	0.19	3.8
14	0.15	0.35	2.3

Note: Calculated value $m = \frac{9\varepsilon_0\varepsilon_e}{16\gamma}\frac{\beta}{(2+R)^2}$, experimental value $m^* = \frac{D}{r_0 E_0^2}$

[see equations (2.9) and (2.10)]

Table 2.2 Electric field enhancement factor Ω with regard to the initial separation distance of two rigid spheres (reproduced from [Davis, 1964])

x_0/r_2	Ω (r_1/r_2 =1)	Ω (r_1/r_2 =2)	Ω (r_1/r_2 =5)
10	3.004	3.027	3.215
1	3.718	4.741	6.556
0.1	14.17	18.16	22.03
0.01	92.48	117.2	137.5
0.001	696.7	883.4	1022.7

Note: x_0 is the initial separation distance (edge-to-edge) between two rigid spheres; r_1 and r_2 are the radii of the two spheres.

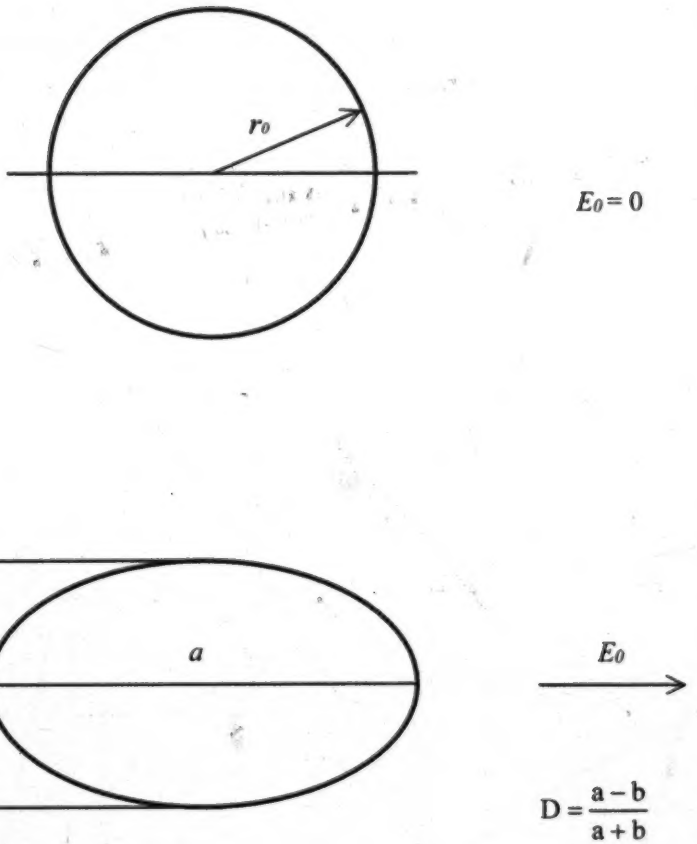

Figure 2.1. Definition of the degree of drop deformation

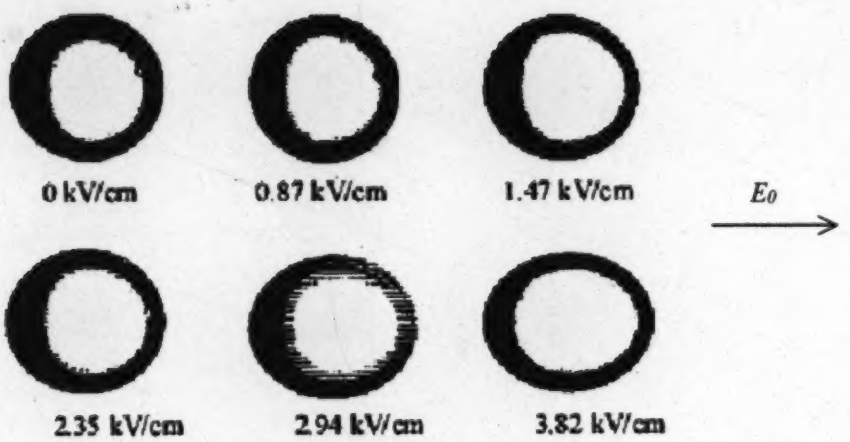

(a) a water drop suspended in castor oil ($\beta > 10^6$)

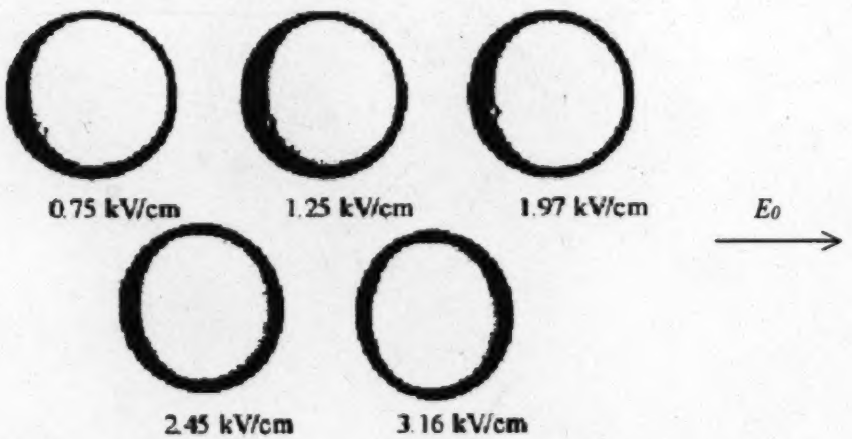

(b) a silicon oil drop suspended in castor oil + Triton ($\beta = -1.7$)

Figure 2.2 Sequence of photographs of prolate and oblate drops as the horizontally electric field increases (reproduced from [Vizika & Saville, 1992])
(a) A water drop suspended in castor oil ($\beta > 10^6$)
(b) A silicon oil drop suspended in castor oil + Triton ($\beta = -1.7$)

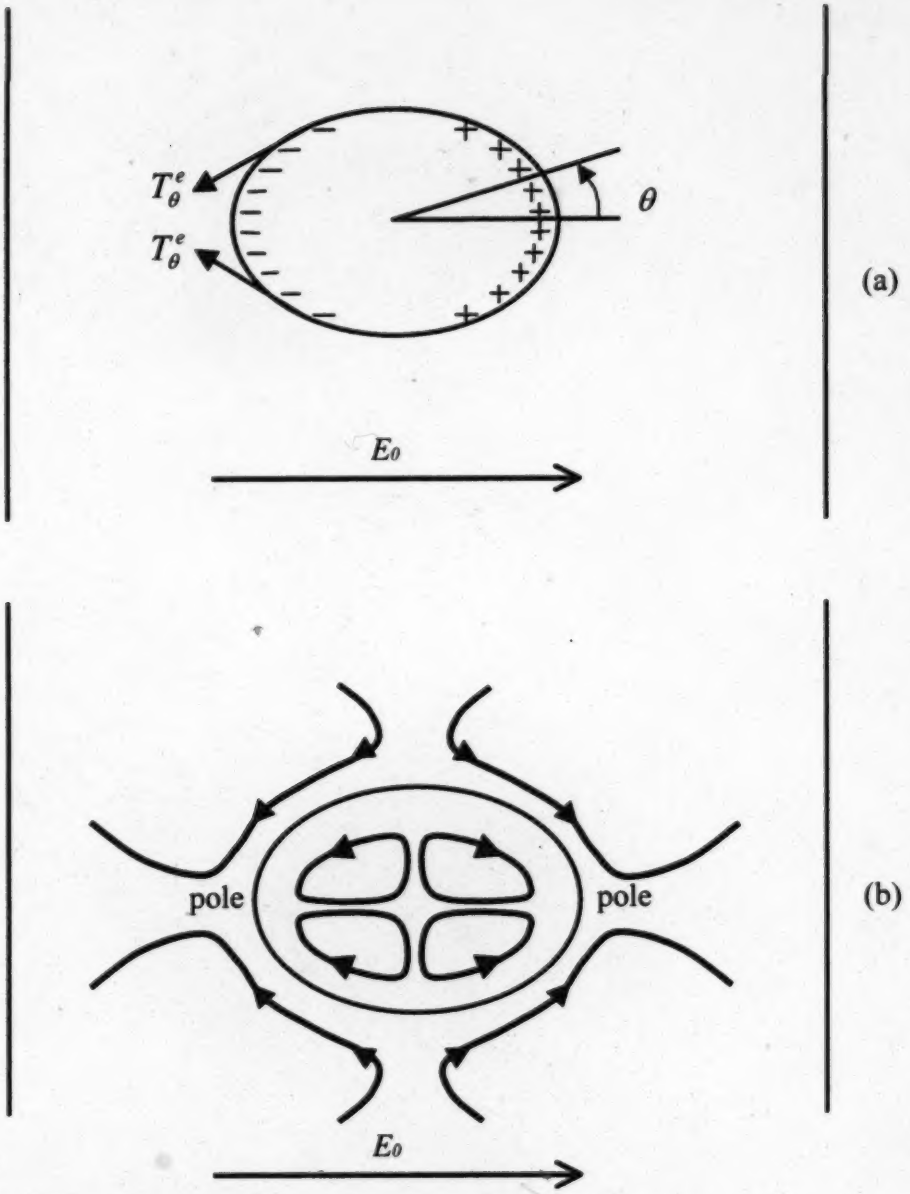

Figure 2.3 Schematic representation of a water drop suspended in oil under an applied electric field

(a) Free charge distribution and transverse electric stress at the interface of a drop

(b) Circulation inside and outside a water drop

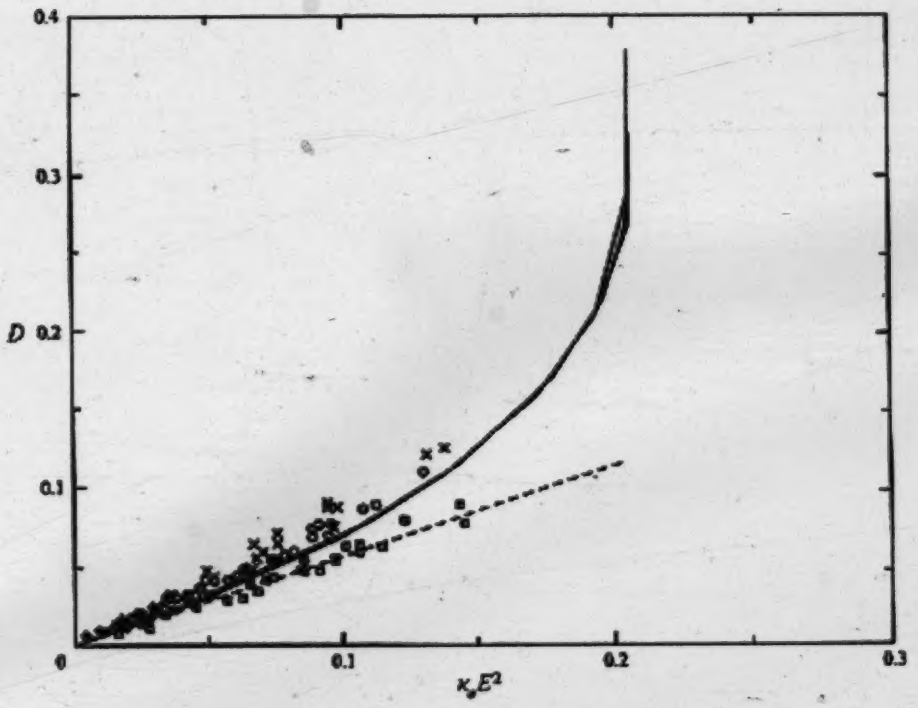

Figure 2.4 Computational results for degree of deformation in the case of very large R at the limit of creeping flow. Solid curve represents Feng & Scott's numerical result, dash line represents Taylor's theoretical result, symbols represents Vizika & Saville's experimental result (κ_o is the dielectric constant of continuous phase, E is dimensionless electric field strength) [Feng & Scott, 1996]

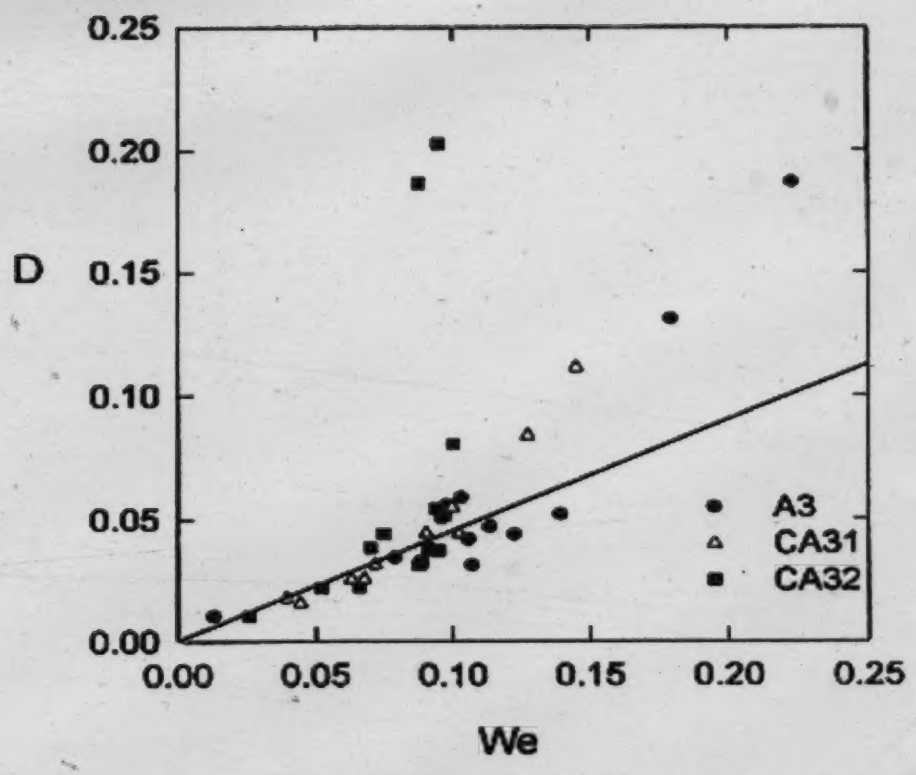

Figure 2.5 Comparison of experimental results with Taylor's theory in the presence of surfactant PS-b-PMMA, solid line represents Taylor's theoretical result. (reproduced from [Ha & Yang, 1995])

A3: Dispersed phase – 5 wt% PVDF, Continuous phase – 20 wt% PS;

CA31: Dispersed phase – 5 wt% PVDF + 0.05 wt% PS-b-PMMA, Continuous phase – 20 wt% PS;

CA32: Dispersed phase – 5 wt% PVDF + 0.15 wt% PS-b-PMMA, Continuous phase – 20 wt% PS

(PS: polystyrene, PVDF: polyvinylidene fluoride, PS-b-PMMA: polystyrene and polymethyl methacrylate)

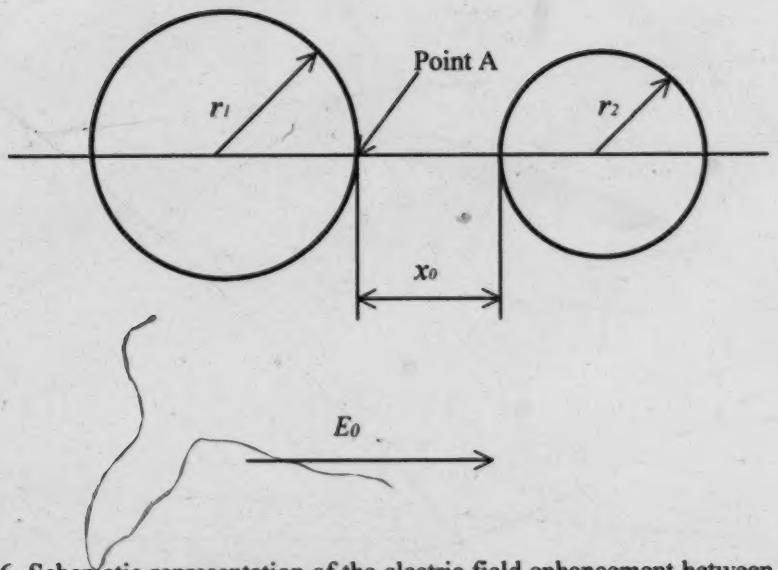

Figure 2.6 Schematic representation of the electric field enhancement between two rigid spheres in a uniform electric field

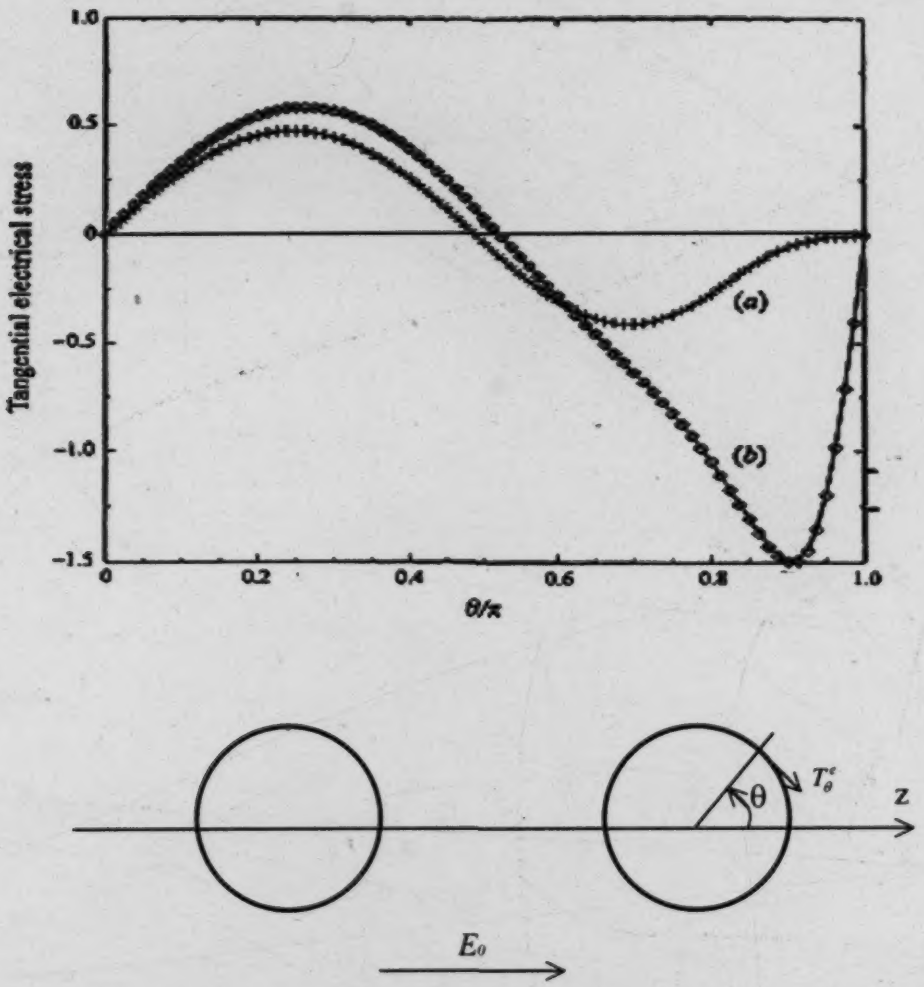

Figure 2.7 Tangential component of the electrical stress along the drop surface of one drop when two drops are placed in an electric field. Symbols represent Baygents et al.'s numerical results while solid curve represents Sozou's (1975) analytical result. Here, θ is the usual polar angle measured from the positive z-axis [Baygents et al., 1998] (a) $R = 0.05, S = 1$ (b) $R = 10, S = 1$

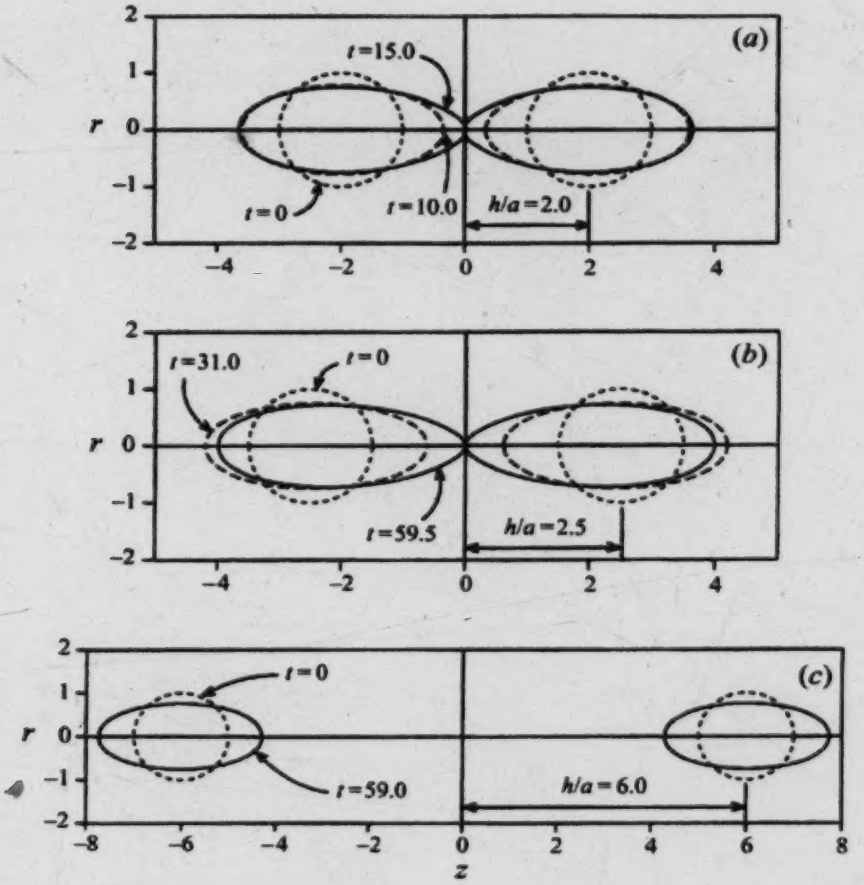

Figure 2.8 Drop deformation and translation as a function of the initial separation distance h/a and time t; $R = 5$, $S = 4$, $M = 1$, and $We = 1$ [Baygents et al., 1998]

(a) Initial center-to-center separation distance is 4 radii and the drops touch owing to deformation

(b) Initial center-to-center separation distance is 5 radii and the drops translate together owing to dielectrophoretic interactions

(c) Initial center-to-center separation distance is 12 radii and the drops deform and drift apart slowly owing to the induced circulatory flows which are repulsive in character

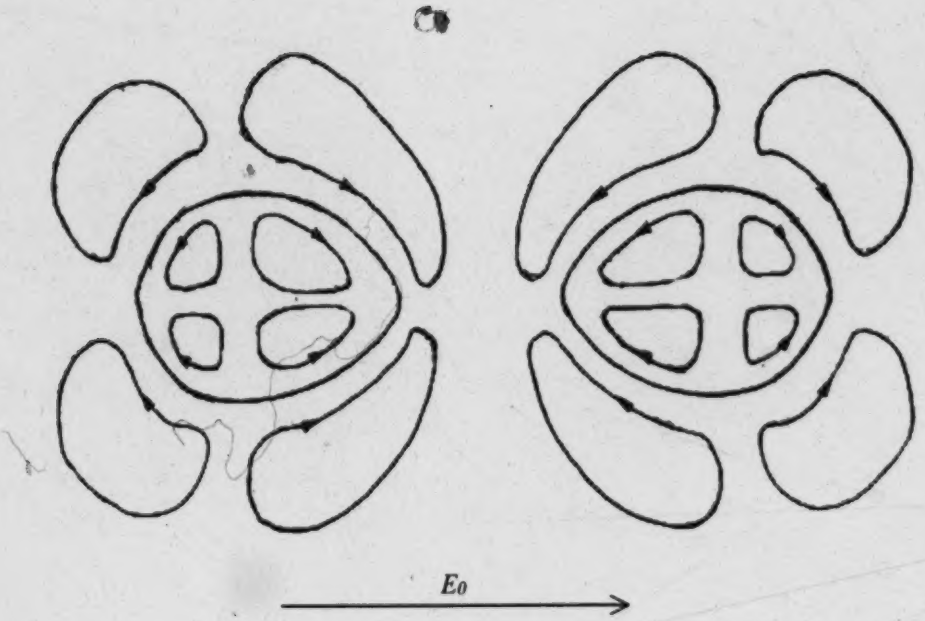

Figure 2.9 Circulation pattern according to the leaky dielectric model for water drop pairs in a uniform electric field

Chapter 3
Interfacial Tension Measurements

Interfacial tension measurement is the first step in understanding the behavior of a water drop as it is an important parameter in determining of drop shapes. For water drops in hydrocarbon oils, the degree of deformation decreases for high interfacial tensions liquids. However, interfacial tensions of chosen oils over water were not available. Therefore, to obtain a rigorous comparison between theory and experiment, interfacial tension between the water and oils must be measured accurately.

3.1 Materials

The liquids chosen as the continuous phase must satisfy the following requirements: insoluble or very slightly soluble in water, non-conductive, transparent, and non-toxic. According to Taylor's leaky dielectric theory, the degree of deformation of a water drop suspended in oil is directly proportional to the dielectric constant of the continuous phase, and inversely proportional to the interfacial tension between the oil and water. Thus, to obtain larger deformations for the same electric field strength, it is desired that the oils have high dielectric constants and low interfacial tensions with water. Seven different oils were chosen in this study, namely, decyl alcohol, diethyl phthalate, cycloheptanone, alpha-ionone, cyclohexyl acetate, ethyl benzoate and 2-ethyl-3,3-hexanediol. These systems of water and oil will be called model systems. The physical properties of these organic solvents are listed in Table 3.1. Details about the organic compounds can be found in Appendix IV.

One of the objectives of this study is to understand the behavior of water drops in bitumen, so a bitumen system was also chosen as the oil phase. As optical transparency is necessary for the observation of drop deformation as well as the coalescence process, bitumen was diluted with toluene. In this present study, the bitumen used was Syncrude

coker feed bitumen, while the solvent was Certified A.C.S. grade toluene (Fisher Scientific). Different amounts of bitumen were dissolved in toluene. The amounts of 0.5g, 1.0g, 1.5g, and 2.0g bitumen were used in 100 ml of solvent. The corresponding weight concentrations were 0.57%, 1.14%, 1.70% and 2.25%, respectively. According to Strausz (1989), the density of Alberta bitumen varied between 970 to 1020 kg/m^3. A density of 1000 kg/m^3 was assumed and the volume concentrations of bitumen were about 0.5%, 1.0%, 1.5%, 2.0%.

The drop phase was de-ionized ultra-filtered water (DIUF), which was produced with ultra-pure water system (Millipore, H20). The DIUF water has a density of ρ_w = 998kg/m^3 and a liquid-air surface tension of 72.7 mN/m at 22 ± 0.5 °C.

Two types of surfactants were used in this study: sodium dodecyl sulphate SDS (Aldrich, 95% pure), which is an anionic surfactant, and sodium naphthenate (Pfaltz & Bauer, aqueous). The surfactant solutions were prepared by adding different amounts of the two surfactants, either SDS or sodium naphthenate, to the DIUF water. The critical micelle concentration (CMC) for SDS in water was reported to be about 1.3x10^{-3} M [Zhou, 2000] at 25°C . Two amounts of 0.7mM and 2.0mM of SDS were added to DIUF water to measure the interfacial tension. Interfacial tensions of toluene over water, with different concentrations of sodium naphthenate dissolved in the water phase, were also measured. The corresponding volume concentrations were 0.13%, 0.2%, 0.4% and 1%.

3.2 Interfacial Tension Measurements

In the present study, both the ring and pendant drop methods were used to measure the interfacial tensions between the various oils and the DIUF water.

3.2.1 Ring Method

3.2.1.1 Apparatus

A Kruss process tensiometer (model K12) based on the ring method, was used to measure interfacial tensions. The basic setup consists of the measuring and the processor units. The parameters set for the experiment are listed in Table 3.2. The parameters of the platinum ring used are:

- Mean radius of the ring: R_m = 9.545 mm
- Radius of the cross-section: r = 0.185 mm

The measuring part of the apparatus is shown schematically in Figure 3.1 (a) and a photograph is shown in Figure 3.1 (b). The balance lock knob (1) is used to lock the force measuring system when not performing measurements. The ring suspension (2) serves to connect a ring to the balance system and the guidance of the suspension will keep the ring in vertical position. The thermostat vessel (4) holds the sample container (3) and can be filled with a liquid which is maintained at a constant temperature. The height of the thermostat vessel can be controlled by adjusting the height control knob (6). The weight display window (5) shows the measured pulling force in grams. It could also display error messages. For example, it will display "Lamella broke" if the interface at the ring is broken by strong vibrations.

3.2.1.2 Principle of Ring Method

Measurements of interfacial tensions follow the Du Nouy ring method [Shaw, 1980]. This is perhaps the most commonly used technique because of its simplicity in operation and low cost. When a ring is pulled through an interface from the heavy phase to the light phase, there are three forces that are involved. The upward pulling force is balanced by two downward forces: the ring's weight and the interfacial tension multiplied

by the circumference of the ring. At the moment the ring detaches from the interface, the pulling force F could be expressed as

$$F = W_{ring} + 2\pi(R_{in} + R_{out})\gamma \tag{3.1}$$

where W_{ring} is the weight of the ring, R_{in} is the inner radius of the ring, R_{out} is the outer radius of the ring, and γ is the interfacial tension between the heavy phase and light phase. As the mean radius of the ring R_m could be expressed as

$$R_m = \frac{R_{in} + R_{out}}{2} \tag{3.2}$$

equation (3.1) could be simplified to

$$F = W_{ring} + 4\pi R_m \gamma \tag{3.3}$$

In practice, the axial force F is measured. With the known parameters of the ring, i.e., its weight W_{ring} and mean radius R_m, the interfacial tension γ can be calculated from equation (3.3).

When the ring is pulled above the level of the liquid surface, the measured force also includes the weight of liquid lamella, as indicated in Figure 3.2. Taking account of weight, Harkins and Jordan (1930) introduced an empirical correction factor C that depends on two dimensionless ratios,

$$C = f(\frac{R^3_m}{V}, \frac{R_m}{r}) \tag{3.4}$$

where V is the volume of the lifted liquid, R_m is the mean radius of the ring, and r is the radius of the wire cross-section. Empirical correction factors are tabulated by Harkins

and Jordan. In 1941, Zuidema and Waters adopted a modification function, which was developed from extrapolation of the tables of Harkins and Jordan, to make the correction. It is a function of ring parameters, measured interfacial tension value and density difference. The correction process could be performed automatically by the process tensiometer K12.

One of the difficulties in using du Nouy method is the disturbance of the interface at the moment of detachment. It is also required to have a zero or near zero contact angle to get accurate interfacial tension. This is particularly important in measuring interfacial tensions in the presence of surfactants, as adsorption on the ring could change the wetting characteristics.

3.2.1.3 Experimental Procedure

The "pull" method was chosen to measure the interfacial tension. For the different systems, the heavy phase and light phase could be found in Table 3.3. The accuracy of the measurement was checked first by measuring the surface tension of water. The measured value was considered accurate if the surface tension of the DIUF water was in the range of ±0.5 mN/m of literature value (72.75 mN/m).

The procedure for conducting interfacial tension measurements was quite straight forward. First, the densities of the heavy phase and light phase were entered through the control panel of the process tensiometer. The light phase was then poured into the sample container and the ring was dipped into it. Next, the force to hold the ring in the light phase was measured using the tensiometer. After that, the light phase was removed and the ring was cleaned. The heavy phase was then poured into sample container and the ring was dipped into it. The light phase was then poured into sample container. An automatic measurement was started by pressing the "start" key in the control panel. At the end of the measurement, the interfacial tension value was displayed in the weight display window.

The ring and sample containers were cleaned thoroughly after each measurement. It is extremely important that they are clean, as chemical residues are most often the reason for erroneous measuring results. Details of the cleaning procedure were as follows: first, for the bitumen solution, the ring and sample containers were rinsed in toluene; for oils, acetone was used for rinsing. Next, the container and the ring were rinsed with warm tap water and then with distilled water. After this, the ring was heated to red-hot in a Bunsen burner flame and allowed to cool to room temperature before the next measurement.

For diluted bitumen systems, the interfacial tension can vary with time, as there may have diffusion between the two phases. Time dependence of the interfacial tensions was also measured. All measurements were taken at 22 $\pm$ 0.5 °C. Each interfacial tension value was an average of three repeated measurements.

3.2.2 Axisymmetric drop shape analysis method

As a comparison, the axisymmetric drop shape analysis (ADSA) method [Kwok, et al., 1994; Li & Neumann, 1992] was also used to measure the interfacial tensions. ADSA is one type of pendant drop method, which uses drop profiles to determine interfacial tensions.

3.2.2.1 Apparatus

The apparatus is shown schematically in Figure 3.3. A Cohu 4910 monochrome camera is mounted on a Lecia Wild M3B microscope. The test cell is placed between the light source and the microscope. The drop profile was monitored on the computer monitor. When the video signal was transmitted to the Videopix digital video processor, it was grabbed and digitized into a field of 640x480 pixels with 256 gray levels (0 for black, 255 for white). A Sun Sparc20 station was used to acquire the image from the

Videopix and perform the image analysis and computations. A standard grid image was taken first as a calibration. The apparatus, except for the Sun station, was placed on a vibration isolation table.

3.2.2.2 Principle of ADSA Method

The ADSA method is based on the concept that the shape of a drop is determined by a balance between the interfacial tension and gravity forces. Small drops in an immiscible liquid tend to be spherical. However, when gravitational and interfacial tension effects are comparable, a drop hanging from a tube tip will elongate in the direction of gravity force. Thus, the interfacial tension can be determined by analyzing the shape of the drop.

The Young-Laplace equation [Shaw, 1980] is a statement of mechanical equilibrium between two homogeneous fluids separated by a curved interface. It relates the pressure difference across an interface to the interfacial tension and the local curvatures,

$$\Delta P = \gamma(\frac{1}{R_1} + \frac{1}{R_2}) \tag{3.5}$$

where ΔP is the pressure difference across the interface, γ is the interfacial tension between the two liquids, and R_1 and R_2 are the two principal radii of curvature. In the case where gravity is the only body force, ΔP can be expressed as a linear function of the elevation z:

$$\Delta P = \Delta P_0 + \Delta\rho g z \tag{3.6}$$

where ΔP_0 is the pressure difference at a reference elevation, $\Delta\rho$ is the density difference between the two liquids, g is the gravitational acceleration, and z is the height of the drop measured from the reference elevation.

From equations (3.5) and (3.6), the shape of a drop may be obtained through the principal radii of curvature if interfacial tension is given. Conversely, the interfacial tension can be determined from the shape of the drop. In ADSA method, an objective function that expresses the discrepancy between the calculated Laplacian profile and the experimental result is constructed. The function is numerically minimized, with the interfacial tension being one of the adjustable parameters. Experimental drop profiles are matched with theoretical shapes using different interfacial tension values. The best match provides the interfacial tension.

The ADSA method has several advantages over other interfacial tension measuring techniques. In comparison with the ring method, only small amounts of the liquid are required in ADSA. In addition, since the drop profile could be rapidly recorded by imaging techniques, it is possible to study time dependent interfacial effects. Furthermore, in other shape analysis methods [Hartland and Harley, 1976], the accuracy of the measurement depends critically on the precision of several preselected points, such as the location of the apex. In the ADSA method, all measured points on the surface are given the same statistical weight. Thus, it is not necessary to identify the apex of the drop profile as in other drop shape analyses.

3.2.2.3 Experimental Procedures

In this study, pendant drops were used to measure interfacial tensions. The experimental procedure followed was to fill the test cell with oil, then a water drop was created at the end of a capillary using a microsyringe. The drop was made as large as possible. The image of the drop profile was taken when the drop was in steady state. A typical image is shown in Figure 3.4.

The procedure was slightly modified for measuring the interfacial tensions of diethyl phthalate and ethyl benzoate over water as these compounds were heavier than water. In these two cases, the continuous phase in the test cell was water and pendent drops of diethyl phthalate and ethyl benzoate were generated, respectively. The other remaining steps of the procedure were the same.

All digital images of the pendant drops were automatically stored in the computer's hard drive, so they could be retrieved and analyzed after the experiment was finished. A special image-processing software was used to digitize the drop profiles. By implementing spline curve fitting, the accuracy of the digitized profiles is about 1.0 μm at 40x magnification. After image processing, several coordinate points could be obtained from the drop profile. Then, a computational program was run to match the theoretical drop profile with the experimental one. The input parameters for this calculation were the local gravity, the densities of the drop phase and the continuous phase, as well as the location of several points at the drop shape. The output of the program were the values of interfacial tension, drop volume and surface area.

Cameras and lenses can produce slightly distorted optical images, as shown in Figure 3.5. As the distortion could cause significant errors in interfacial tension measurements, a specific calibration method was used. For each image taken during the experiment, a standard grid image was taken at the same position. After mapping the distorted grid image and compared with an undistorted one, appropriate corrections could be made.

3.3 Results of Interfacial Tension Measurements

Table 3.3 shows measurements of interfacial tensions between water and several oils using the ring method. The system with SDS (a surfactant) is also listed in this

Table. The measured results using ADSA are shown in Table 3.4. The interfacial tension values measured are fairly close to the literature values (less than 3% error).

For the system that contained surface-active species, the interfacial tension varied with time after the two liquid phases were placed in contact with each other. The time-dependent interfacial tension between diluted bitumen and water is shown in Figure 3.6. It can be seen that, after half an hour, the interfacial tension decreased by about 1~1.5 mN/m. The value was 2% to 3% higher than what it was observed after equilibrating for one hour. The system can thus be considered in steady state after about half an hour. Thus, in drop deformation experiments, the dilute bitumen solution was equilibrated with the water drop for half an hour before the electric field was applied.

The results for water-toluene systems in the presence of sodium naphthenate are shown in Figure 3.7. There was a significant change in the interfacial tension within the range of surfactant concentrations tested. The interfacial tension decreased more than 50% when the surfactant volume concentration increased from 0.2% to 1%.

After comparing the results from the ring method and the ADSA method, the interfacial tension values measured using the ADSA method were selected for use, as the overall measurement result of ADSA method is closer when comparing with the literature values.

Table 3.1 Physical properties of various oils used

Oil name	Dielectric constant [a]	Density [b] (kg/m^3)	Viscosity (mPa•s)
Decyl alcohol	8.1	827	8.7 (22°C) [c]
Diethyl phthalate (99%)	7.86	1116	10.86 (21°C) [d]
Cycloheptanone (99%)	13.16	949	2.59 (25°C) [e]
Alpha-ionone (90%)	10.78	928	N/A
Cyclohexyl acetate	5.08	964	2.57 (20°C) [f]
Ethyl benzoate (99%)	5.99	1049	2.22 (20°C) [g]
2-ethyl-1,3-hexanediol	18.73	931	67.8 (20°C) [h]

(a) – [CRC handbook of Chemistry and Physics, 72nd ed.]

(b) – [Corresponding material safety data sheet]

(c) – [Measured]

(d) – [Journal of Chemical and Engineering Data; 1959(4); 336]

(e) – [Journal of Chemical Society; 1914 (105); 2011]

(f) – [Journal fur praktische chemie; 1935(142); 225]

(g) – [Journal of Chemical Society; 1950; 75]

(h) – [Journal of American Chemical Society; 1949 (71); 508]

Table 3.2 Parameters set in the setup menu of process tensiometer K12

General Parameters	
Parameter	Value
Vessel diameter (cm)	6.4
Vessel height (cm)	3.6
Vessel speed [10…100% max speed]	20% (4.8 mm/min)
Gravity factor (m/s^2)	9.80665
No.of values for standard deviation [2~10]	10
Maximum number of values [10~999]	10
Minimum standard of deviation [0~9]	2
Parameters of Ring Method	
Return distance [1…100%]	10%
Margin searching (mg)	1.0
Margin measuring (mg)	1.0
Ring correction [0 = No 1 = Z&W]	1 (Zuidema & Waters equation)
Lamella height [0 = NO 1 =YES]	0
Density of water (kg/m^3)	998.6
Density of air (kg/m^3)	1.3

Table 3.3 Surface and interfacial tension of various systems measured with ring method

Heavy phase	Light phase	Measured value (mN/m)	Literature value (mN/m)
Water	Air	72.4	72.75[a]
Water	Toluene	34.4	34.47[b]
Water	Decyl Alcohol	8.7	8.97 [c]
Water (0.7mM SDS added)	Decyl Alcohol	8.5	
Water (2.0 mM SDS added)	Decyl Alcohol	6.1	
Diethyl phthalate	Water	14.1	
Water	Cycolheptanone	6.9	
Water	Alpha-ionone	18.0	
Water	Cyclohexyl acetate	14.0	
Ethyl benzoate	Water	17.2	
Water	2-ethyl-1,3-hexanediol	3.3	

(a) – [Adamson, 1990]

(b) – [Yan, 1999]

(c) – [Aveyard, R. et al., Journal of Chemical Society, Faraday Transactions I; 1972 (68); 12]

Table 3.4 Surface and interfacial tension of various systems measured with ADSA method

Drop phase	Continuous phase	Number of drops	Measured value (mN/m)	Literature value (mN/m)
Water	Air	8	72.0	72.75 [a]
Water	Toluene	9	34.2	34.47 [b]
Water	Decyl Alcohol	9	8.9	8.97 [c]
Diethyl phthalate	Water	8	14.5	
Water	Cycloheptanone	5	6.9	
Water	Alpha-ionone	9	17.4	
Water	Cyclohexyl acetate	8	14.3	
Ethyl benzoate	Water	11	17.2	
Water	2-ethyl-1,3-hexanediol	6	3.3	

(a) – [Adamson, 1990]

(b) – [Yan, 1999]

(c) – [Aveyard, R. et al., Journal of Chemical Society, Faraday Transactions I; 1972 (68); 12]

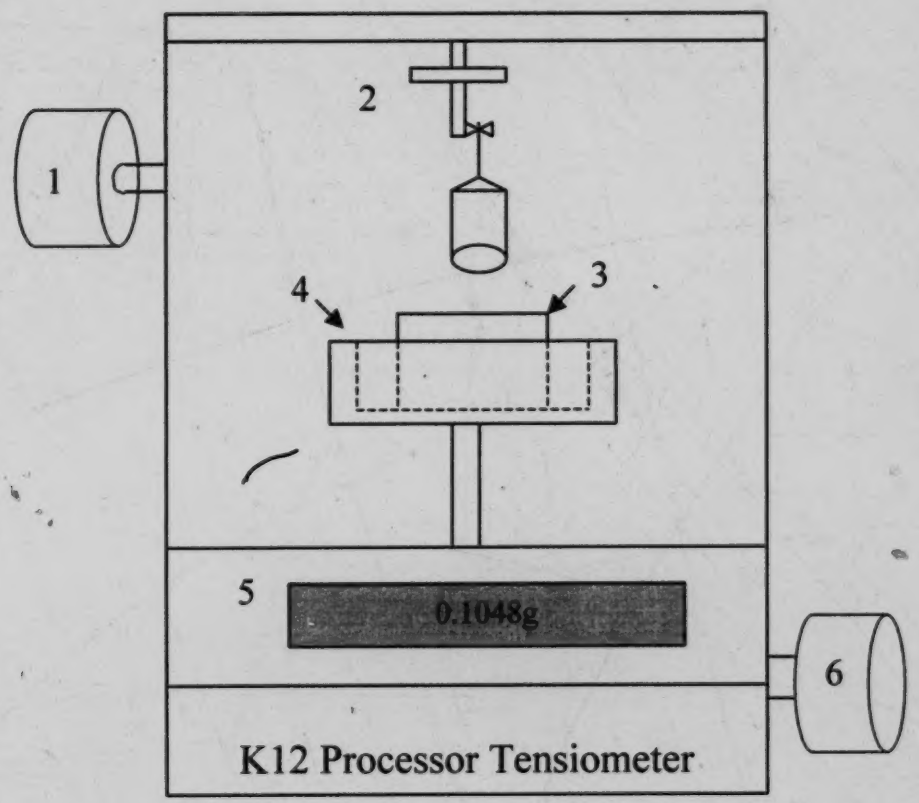

Figure 3.1 (a) Scheme of K12 measuring unit

(1) Balance lock knob (2) Ring suspension (3) Sample container
(4) Thermostat vessel (5) Weight display window (6) Height control knob

Figure 3.1 (b) Photograph of K12 Processor Tensiometer

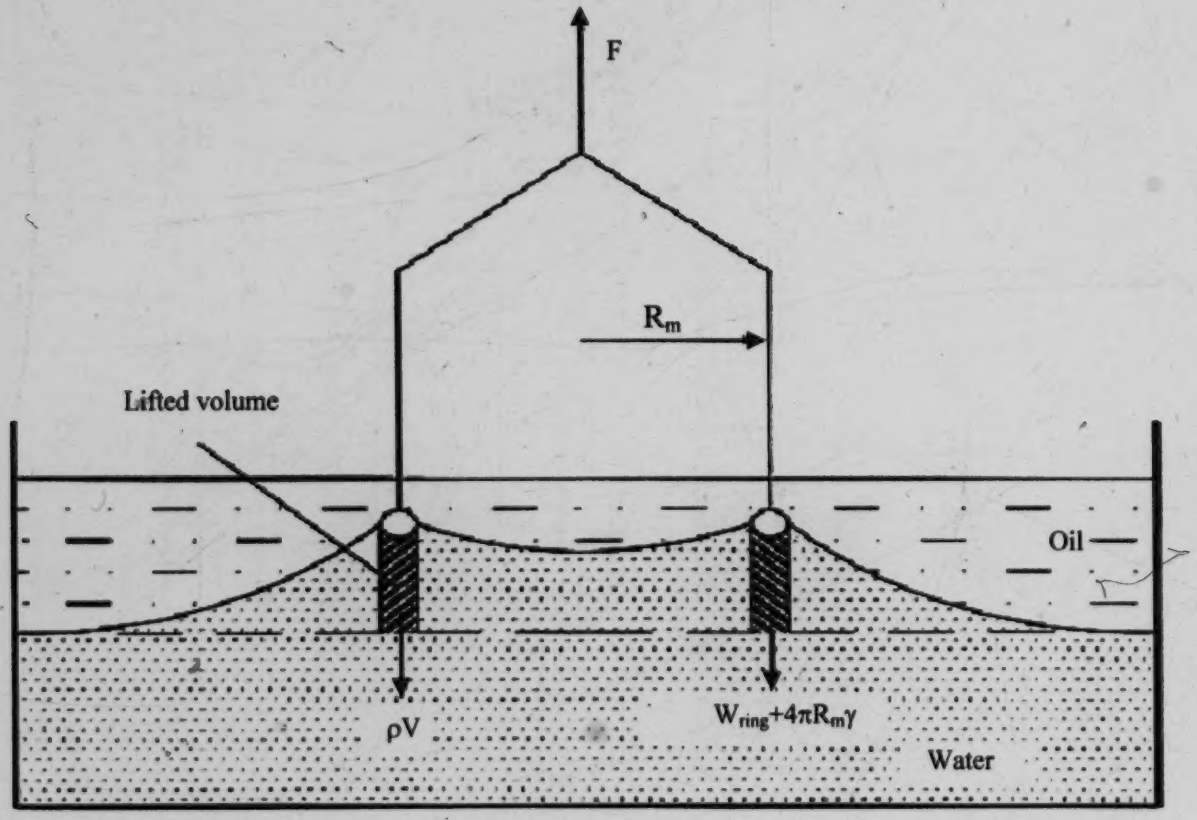

Figure 3.2 Measured force including lifted volume in the ring method

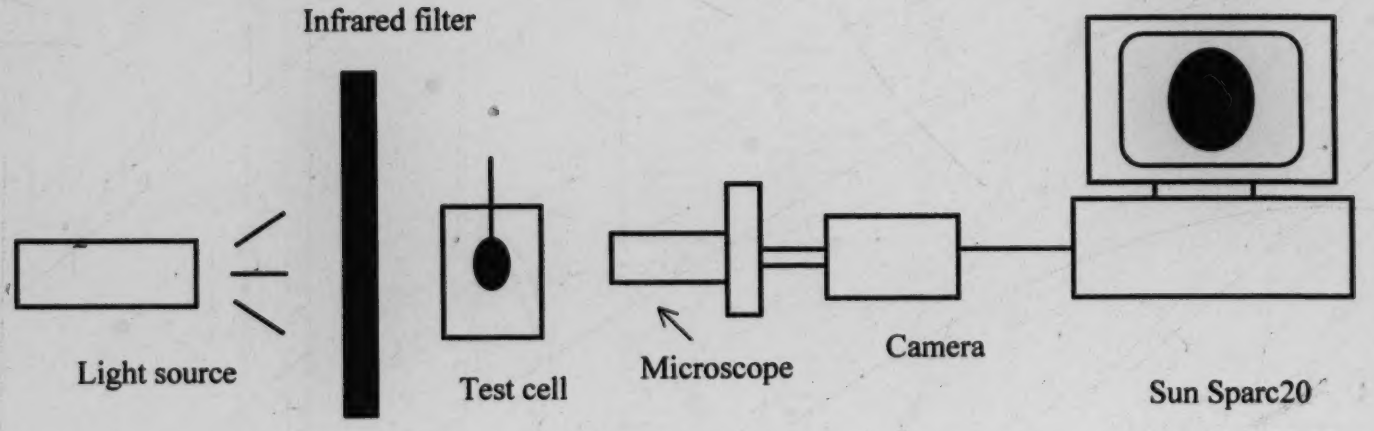

Figure 3.3 Schematic diagram of interfcial tension measurements using ADSA method

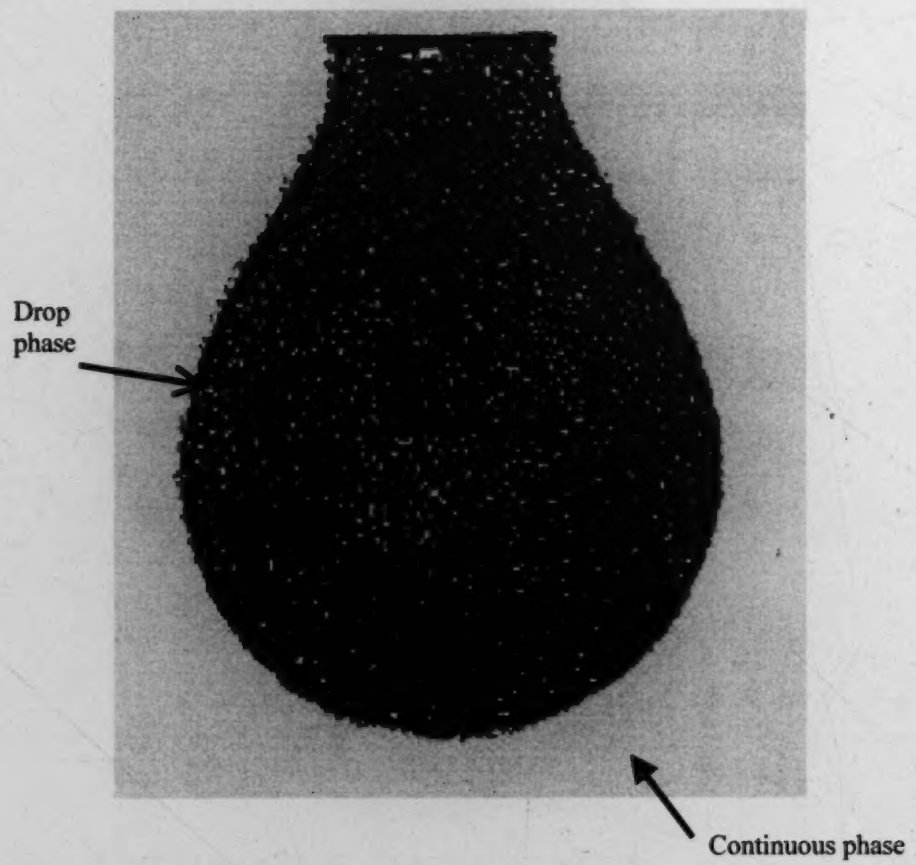

Figure 3.4 A digital image of water drop in decyl alcohol for interfacial tension measurement using ADSA method

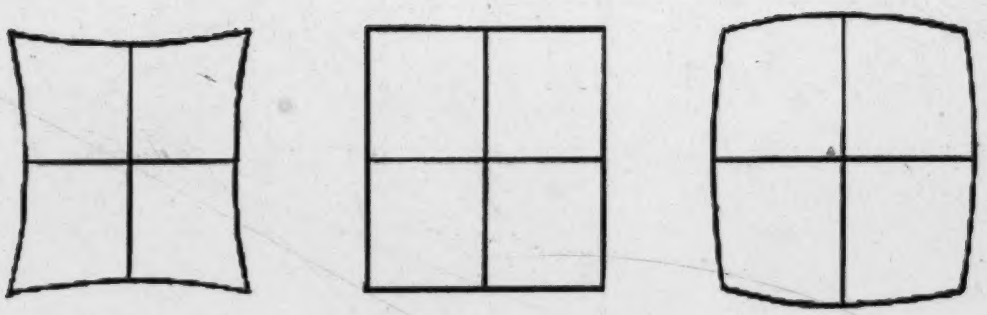

(I) Pin cushion distortion (II) Original (III) Barrel distortion

Figure 3.5 Examples of optical distortions in digital images

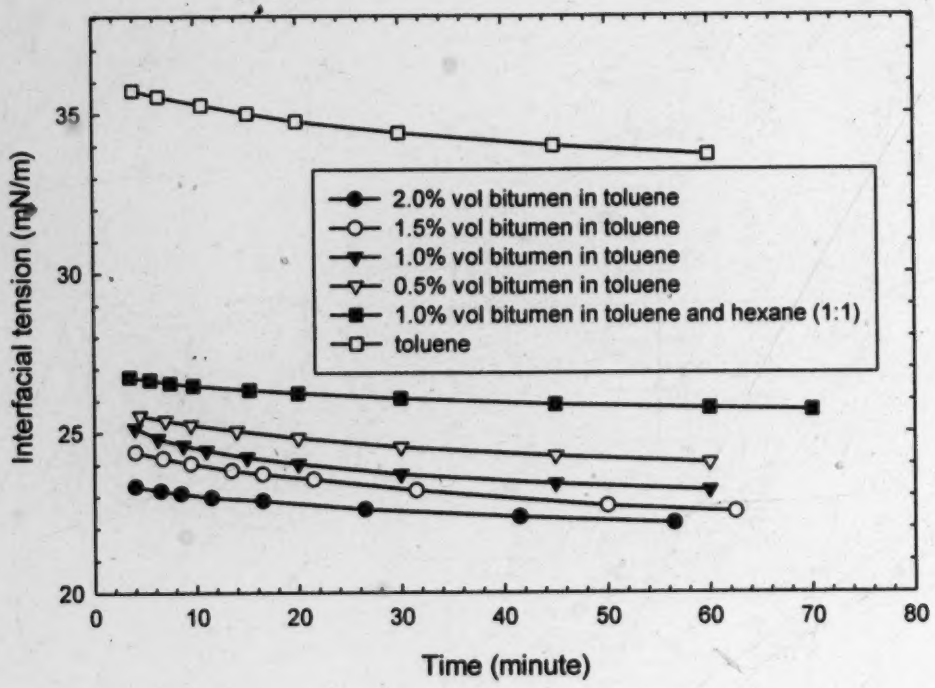

Figure 3.6. Time dependence of the interfacial tension of diluted bitumen solution over water

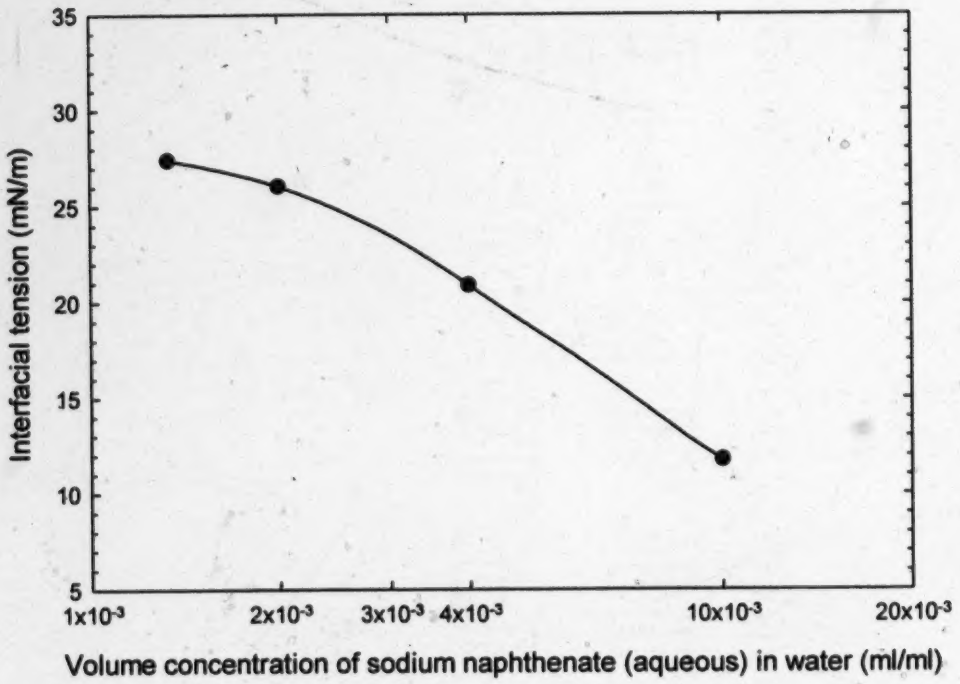

Figure 3.7. Equilibrium interfacial tension of toluene over water with different concentration of sodium naphthenate (aqueous) added to water

Chapter 4

Experimental Protocol for the Measurement of Drop Deformation and Coalescence in an Electric Field

4.1 Introduction

As previous investigations of electrical coalescence were focused primarily on collision rates and coalescence efficiency, there is a need for more fundamental studies on the effect of electric field on water drop coalescence. Naturally the first step is to study electric field effects on water drop(s) deformation, followed by the effects of electric field on the coalescence of two water drops. Carefully designed and executed experiments under a different conditions should lead to a better understanding of electrohydrodynamics, especially in relation to the phenomena of electrical coalescence.

As mentioned earlier, with regard to the deformation of a water drop, only a small number of fluids had been studied owing to the need of avoiding drop movement due to gravity. For the purpose of studying water drop deformation in a wider variety of oils, glass capillaries were used to hold the water drops, thus preventing drop movements caused by buoyancy or gravity.

De-ionized and ultra-filtered (DIUF) water was used for the drop phase. For the dispersed phase, seven types of oils were chosen in this study, namely, decyl alcohol, diethyl phthalate, cycloheptanone, alpha-ionone, cyclohexyl acetate, ethyl benzoate and 2-ethyl-3, 3-hexanediol. Toluene solutions with 0.5%, 1.0%, 1.5%, 2.0% (by volume) bitumen were also chosen as the continuous phases; they will be called "diluted bitumen systems". The previous water in oil sysfems are referred to as "model systems".

Two types of surfactants, sodium dodecyl sulphate (SDS) and sodium naphthenate (aqueous), were used in this study to investigate the role of surfactants in the deformation of a water drop. The surfactants were dissolved first in the aqueous phase. Interfacial tensions of the surfactant systems were measured according to the methods described in Chapter 3. As the addition of surfactants did not appreciably change the bulk physical properties of the systems (except for interfacial tension), physical properties corresponding to surfactant-free systems will be assumed.

Details about the materials used were described previously in Section 3.1.

4.2 Experimental Set-up and Procedures

4.2.1 Single Drop System

4.2.1.1 Experimental Set-up

A schematic diagram of the experimental apparatus for single drop system is shown in Figure 4.1 (a). A photograph of the setup is shown in Figure 4.1 (b). In this set-up, a square glass cell was mounted on the moveable stage of the microscope (Zeiss, Axiovert 25C), i.e., between the light source and objective lens. The illumination was from the top.

A photograph of the test cell is shown in Figure 4.2 (a), and its dimensions are labeled in Figure 4.2 (b). The cell was made by first gluing a square glass tube to the glass slide, then cementing two thin brass plates (electrodes) to the inner walls of the square tube. The dimensions of the electrodes are 20x20 mm, and its thickness is 0.2 mm. Three different cells were used and the distance between the two parallel electrodes were 0.95, 1.94 and 1.95 cm, respectively.

An electric field was applied across the electrodes through a high voltage D.C. power supply (Spellman, SL20x10). The power supply is equipped with a prohibitor that

could prevent over current by setting a maximum current level. If the current is over the preset value, the prohibitor will disconnect the circuit. In this study, the maximum safety current was set at 10 mA. The two outputs of the power supply were connected to the brass electrodes, creating a potential difference of 0 to 20 kV. The voltage was read directly from the digital display on the power supply. Voltage drops in other parts of the circuit was considered negligible. The small water drop (diameter of about 1.5 mm) was positioned in the center region of the test cell. As the water drop is small compared to cell size, it may be assumed to be subjected to a uniform electric field. The electric field strength was obtained by dividing the voltage by the distance between the two electrodes. The applied electric field strength ranges from 0 to 4 kV/cm.

The deformation of a single water drop was observed through a microscope where the line of view is perpendicular to the electric field direction. A photograph of the microscope is shown in Figure 4.3. The microscope is equipped with an X-Y manipulator that can control the position of the test cell relative to the objective lens. The light bulb is in the cylindrical housing located at the top of the microscope. As the original light source (25W light bulb) could not provide enough illumination for water drop(s) in diluted bitumen systems, it was changed to a 50W bulb. The drop deformation process could be recorded continuously by a CCD camera (Hitachi, KP-M1U back and white) and VCR (Sony, EV-S5000 videocassette recorder). A black and white video monitor (Sony, PVM-137) was used for online monitoring.

As mentioned earlier, glass capillaries were used to hold the water drop. As the drop deformation was viewed from below, the capillaries needed to be bent to avoid obstructing the view. Straight glass capillaries were heated with a Bunsen burner and bent to the shape of a right angle. A support stand that could be placed on the microscope's movable stage was constructed to support the capillary. The capillary was fixed to the groove of the stand by a screw, as seen in Figure 4.1 (b). A microsyringe was connected to the capillary through a Teflon tube.

As the glass capillary is naturally hydrophilic, the water drop tends to spread onto the outer surface of the capillary, as shown in Figure 4.4. To make the capillary tube hydrophobic, it was treated with trimethylchlorosilane (Aldrich, 99%) solution for 20 seconds. Trimethylchlorosilane (TMCS) solution was prepared by adding TMCS to cyclohexane (Fisher Scientific) to make a 5% volume solution. A syringe was connected to the capillary through a Teflon tube. When the capillary was placed into the TMCS solution, air was continuously pushed out from the capillary. Thus, the inner surface of the capillary remains untreated (hydrophilic) while the outer surface was modified to become hydrophobic. All manipulations were performed under a fume hood.

4.2.1.2 Experimental Procedures

In this study, the continuous phase (i.e., suspending liquid) was either an organic solvent or diluted bitumen. The deformation of a single water drop was test in the following suspending liquids: decyl alcohol, diethyl phthalate, cycloheptanone, alpha-ionone, cyclohexyl acetate, ethyl benzoate and 2-ethyl-1, 3-hexanediol. The deformation of a single water drop in diluted bitumen (0.5, 1.0, 1.5 and 2.0 vol% bitumen in toluene) was also tested.

To study the effect of surfactants, certain amounts of surfactants were added to the systems of a water drop in decyl alcohol and a water drop in diluted bitumen. In the former system, 0.7mM sodium dodecyl sulphate (SDS) was added to the aqueous phase. In the latter system, 0.4% vol. sodium naphthenate (aqueous) was added to the aqueous phase. The drop deformation behaviors in these systems were then compared to the systems without surfactants.

With the experimental set up illustrated in Figure 4.1, the experiment was conducted according to the following procedure:

First, the test cell was filled with the continuous phase. The end of a water-filled capillary was carefully placed at the center region of the test cell. Then a water drop was generated from the end of the capillary using the microsyringe, which was held by a clamp mounted on a rod. The water drop diameter was about 1.5 mm. In the model systems, the experiment was conducted immediately after the water drop was generated. In the diluted bitumen systems, the experiment was first conducted without aging time. For comparison, the test system of water drop in diluted bitumen was then aged for half an hour before an electric field was applied.

The drop shape was first recorded before the electric field was applied. This provides a recorded image of the undeformed water drop. Then, an electric field was applied across the electrodes; it normally took several seconds for the drop to reach a steady state shape. The transient process could be observed on the monitor and recorded from the capture of the CCD camera with the VCR. It took longer for the water drop to reach steady state in 2-ethyl-1, 3-hexanediol, as the organic solvent is very viscous.

The applied electric field strength was increased gradually from low to high. For each value of the applied electric field strength, drop deformation was recorded when steady state was reached. For each system tested, the water drop size was kept the same. All experiments were conducted at 22 ± 0.5 °C.

After the deformation process was recorded, the water drop was discarded and the continuous phase removed from the test cell. If the continuous phase was an organic solvent, the test cell was cleaned with acetone, hot tap water, distilled water and then left to dry. If the continuous phase was diluted bitumen, the test cell was cleaned with toluene, hot tap water, distilled water in succession and then left to dry.

4.2.2 Drop Pair System

4.2.2.1 Experimental Set-up

For the drop pair system, two capillaries and two micromanipulators were used. Other parts of the experimental set-up were identical to the single drop system. Figure 4.5 only shows the difference between the single drop and drop pair experimental systems. Capillaries were treated by TMCS solution in the same way as described in Section 4.2.1.1.

A new X-Z micromanipulator was built for this study by attaching a two-dimensional micromanipulator to an aluminum base. A photograph of the micromanipulator is shown in Figure 4.6. The microscope's X-Y manipulator allows rough alignment and could move one capillary within the horizontal plane. The X-Z micromanipulator allows fine adjustment and could move the other capillary along the vertical direction. Thus, the ends of the two capillaries could be positioned at the same height and their axes be aligned along the direction of the electric field.

4.2.2.2 Experimental Procedures

For the model systems, the deformation behaviors of the water drop pairs in decyl alcohol were studied in an applied electric field. For the diluted bitumen system, the deformation behaviors of water drop pairs in toluene solutions with 0.5% and 1.5% vol. bitumen, were selected for study when an electric field was applied.

The experiment was conducted according to the following procedure:

First, glass capillaries were positioned at the center of the test cell. Two micromanipulators were adjusted until the ends of the two water-filled capillaries were at

the same height and the lines of center were in alignment with the direction of the electric field. Then, the test cell was filled with the continuous phase. Two water drops were injected into the continuous phase through the microsyringes. It was important to keep the drop sizes the same as those in the previous experiments involving single drops. In this way, the experimental results of single water drops could be compared to those of water drop pairs. Next, the initial centre-to-centre separation of the two water drops was adjusted to about four times the radius of the undeformed drops.

The recording process began when the electric field was applied. After the water drops had reached steady state, the separation distance of the water drops was reduced to the next preset value. The separation distance was reduced until the water drops were very close and steady state could not be maintained. To check for repeatability, the procedure was carried out several times with the same drop size and the same initial separation distance for the same electric field strength. Then the electric field was increased to a higher value and the same procedure repeated. For each system tested, the experiment was conducted for four different electric field strengths.

In some tests, the two water drops coalescenced and the resulting drop fell to the bottom of the cell. After the tests, the water drops were discarded. The cleaning process was the same as described in the previous section for single drops.

All experiments were conducted at 22 ± 0.5 °C.

4.2.3 Drop Coalescence

4.2.3.1 Experimental Set-up

The experimental setup for recording the drop coalescence process is shown in Figure 4.7. For simplicity, the two microsyringes and manipulators are not shown in this figure. The coalescence process was recorded with a high speed digital imaging system

(MotionScope, PCI8000S). The imaging system could record sequences of digital images at a maximum rate of 8000 frames per second. These images could be stored in the memory of the controller unit. The system is capable of storing up to two seconds of digital images at different rates, as shown in Table 4.1. The resolution of the images is also indicated in the Table for different frame rates. These sequences could be saved as video clips or individual images for further analysis. The video could be replayed (forward or reverse) at frame rates between 1 to 8000 frames per second to allow detailed analysis.

The camera head is a 6.25 x 6.25 x 10 cm enclosure that contains a CCD sensor and imaging circuits. It is connected to the microscope through a C-mount. There is a locking ring under the lens to provide coarse focus adjustment. Because the computer monitor shows no images during the recording process, it was necessary to view the video on a remote monitor. For this purpose, the "composite out" cable connector of the imaging system is connected to the video input of a Sony monitor, as shown in Figure 4.7.

The experiment setup, i.e., the drops, has to receive sufficient light for the recorded images to be clear, otherwise, the motion of the water drops could not be observed in detail. To enhance illumination, the infrared filter of the CCD camera was removed. The light source for the microscope was also changed from a 25W bulb to a 50W bulb. It should be mentioned here that since the exposure time of each frame is reduced at higher frame rates, more illumination was required as a result. To eliminate image blurring due to the rapid motion of the water drops, the shutter speed of the camera was also adjusted for every event. For example, as there was ample illumination in the case of water drops in decyl alcohol, the shutter speed was increased to 20 times the frame rate.

The recording process was initiated by clicking the REC button in the menu of the high speed imaging system. The REC button flashed to indicate that the system was recording live images from the camera. The display in the computer went blank but the image from the camera could be seen on the remote monitor.

As the maximum recording time of an event is two seconds, the oldest images are replaced by the latest images after a two-second duration. The total number of images is the number of frames in the image memory at different frame rates, as indicated in Table 4.1. As the coalescence process took place very fast, it was necessary to find a way to stop the recording immediately after the process. There are two ways to stop a recording process in this high speed imaging system: using the STOP command in the menu or using a trigger. The STOP command terminates the sequence and may record a few more frames after the stop command is received. That is due to the delay through the system. The MotionScope imaging system also has a trigger system that could detect a signal from an external source and stops the recording once the triggering signal is received. There is no delay when operating the trigger. The trigger point could be set from 0% to 100% at increments of 10%. For example, if the trigger point is set at 50%, the imaging system will record the sequence for one more second after the trigger is received. Half of the stored images would precede the trigger and half of it would follow the trigger. This makes it possible to record an event that either occurs very quickly, or happens without warning. As the image memory could store image sequences for up to two seconds and the coalescence process happened in less than one tenth of a second, the delay of STOP command could be ignored. For simplicity, this study utilized the STOP command to terminate the recording process.

Images stored in the memory will be overwritten if another recording is made. Therefore, the images in the memory were transferred to a hard drive file before recording another sequence. The old images could be saved as video clips, such as AVI files, or as sequences of BMP, JPEG, PCX or TIFF images. Three compression methods can be chosen when the sequence is saved as an AVI file. In this study, the sequences were saved as AVI files with the default of no compression.

4.2.3.2 Experimental Procedures

The drop phase was water while the continuous phase could be one of the following: decyl alcohol, toluene solution with 0.3% vol. or 0.5% vol. bitumen, heptane and toluene mixture (1:1) with 0.5% vol. or 1.5% vol. bitumen. The coalescence process of two water drops in 2-ethyl-1, 3-hexanediol was also studied because of the high viscosity of the organic phase. Coalescence in a high viscosity medium occurs at a slow rate and requires more time. Details of the coalescence process could be observed. For several systems, the water drops were aged for 30 and 60 minutes in the continuous phase before the experiment began. Detailed information about the aging time for different systems can be found in Table 4.2. The frame speed was varied from 500 to 4000 frames per second. For each system, the frame rate, the shutter speed and the applied electric field strength are summarized in Table 4.2.

The experiment was conducted according to the following procedure:

First, the ends of the two water-filled capillaries were set at the same elevation and the axes of the capillaries were aligned parallel to the electric field using the two micromanipulators. After the test cell was filled with the continuous phase, two water drops of the same size were generated by expelling small amounts of water from the capillaries. The drops were then brought close to each other.

The REC button on the menu of the high speed imaging system was clicked on and the system began recording. The power supply was then turned on to apply the electric field. When coalescence was observed on the monitor, the STOP button was clicked to terminate the recording.

The coalescence process was then saved as an AVI file with no compression. It was then stored as successive images. The photographs were subsequently analyzed. All experiments were conducted at 22 ± 0.5 °C.

4.3 Drop Deformation Measurements

4.3.1 Single Drops

The entire drop deformation process was recorded on video and could be processed by a personal computer. During playback of the video recording, the data was digitized to a 1500 by 1280 pixel digital image using an image capture software (Play Inc., Snappy 2.1). A typical image of an undeformed drop occupies about 370x370 pixels, while a deformed drop usually occupies an area of 250 to 450 pixels. Figure 4.8 shows a typical image of a deformed water drop in 0.5% vol. diluted bitumen. The electric field was applied horizontally. In this image, the central ellipsoid represents the deformed water drop and the remaining gray space was the continuous phase. The water drop deformed into a prolate spheroid with increasing electric field.

Measurements of the degree of deformation were carried out according to the following procedure. First, a standard grid image was used for length scale calibration. Next, drop lengths along perpendicular axes were directly determined by measuring the number of pixels. The undeformed drop radius was also obtained by counting the number of pixels in the image taken without the electric field. For each measurement, the number of pixels was counted three times and an average value obtained. The degree of deformation was then calculated for each drop at different electric field strengths in the different systems.

4.3.2 Drop Pair

When an electric field is applied to two water drops in a continuous phase, in addition to drop deformation, there will also be displacement of the entire water drops, as shown in Figure 4.9. That is because of the net charges on the water drops. As such, the initial separation distance before the electric field is applied becomes meaningless, as there will be different amounts of whole-body displacements for different field strengths.

In this study, the separation distance x (after the electric field was applied) was used instead of the initial separation distance x_0 (before the electric field was applied).

Figures 4.10 (a) and 4.10 (b) show two images of the drop pair deformation under an electric field. The continuous phase in Figure 4.10 (a) was 1.5% vol. diluted bitumen, while that in Figure 4.10 (b) was decyl alcohol. The electric field was applied horizontally. Note that, the drops in Figure 4.10 (b) possessed sharp tips at locations of close approach.

Measurements of the degree of deformation were carried out according to the following procedure:

The drop lengths along parallel and perpendicular axes were determined directly by measuring the number of pixels for each drop. For drop pair systems, the digitized images also provided the separation distance between the drops. The separation distance was obtained by counting the number of pixel between the tips of two water drops. The number of pixels was measured three times and an average value obtained. The degree of deformation with the corresponding separation distance was thus obtained for different electric field strengths and different separation distances.

4.4 Drop Coalescence Process

It was observed that under the condition of zero electric field, the two water drops in diluted bitumen (1.5% vol bitumen in toluene) would not coalescence even when one water drop was pushed very hard against the other. However, under an electric field, the two water drops coalesced in less than 0.1 second upon contact.

Table 4.1 MotionScope PCI8000S frame storage and recording time

Frame Rate (Frame per second)	Resolution (Pixels)	Number of Frames	Recording Time (Second)
500	320x280	1024	2
1000	240x210	2048	2
2000	160x140	4096	2
4000S	160x68	8192	2
4000	100x98	8192	2

Table 4.2 Aging time, frame rate and shuttle speed of the systems tested for drop coalescence

Continuous phase	Aging time (minute)	Frame rate (frames per second)	Shutter speed (seconds)	Applied electric field strength (kV/cm)
Decyl alcohol	0	1000	1/10000	1.031
Decyl alcohol	0	4000	1/4000	1.031
Decyl alcohol	10	1000	1/20000	1.031
Decyl alcohol	30	1000	1/10000	1.031
2-ethyl-1, 3-hexanediol	0	500	1/1000	0.515
2-ethyl-1, 3-hexanediol	0	1000	1/20000	0.515
2-ethyl-1,3-hexanediol	0	4000	1/20000	3.093
0.3 vol% bitumen added to toluene	0	2000	1/2000	3.093
0.3 vol% bitumen added to toluene	0	4000	1/4000	3.093
0.5 vol% bitumen added to toluene	30	1000	1/1000	1.795
0.5 vol% bitumen added to toluene	60	1000	1/1000	3.350
0.5% vol% bitumen added to heptane + toluene(1:1)	30	500	1/500	3.350
0.5% vol% bitumen added to heptane + toluene(1:1)	30	1000	1/1000	3.350
1.5% vol% bitumen added to heptane + toluene(1:1)	30	500	1/500	3.350

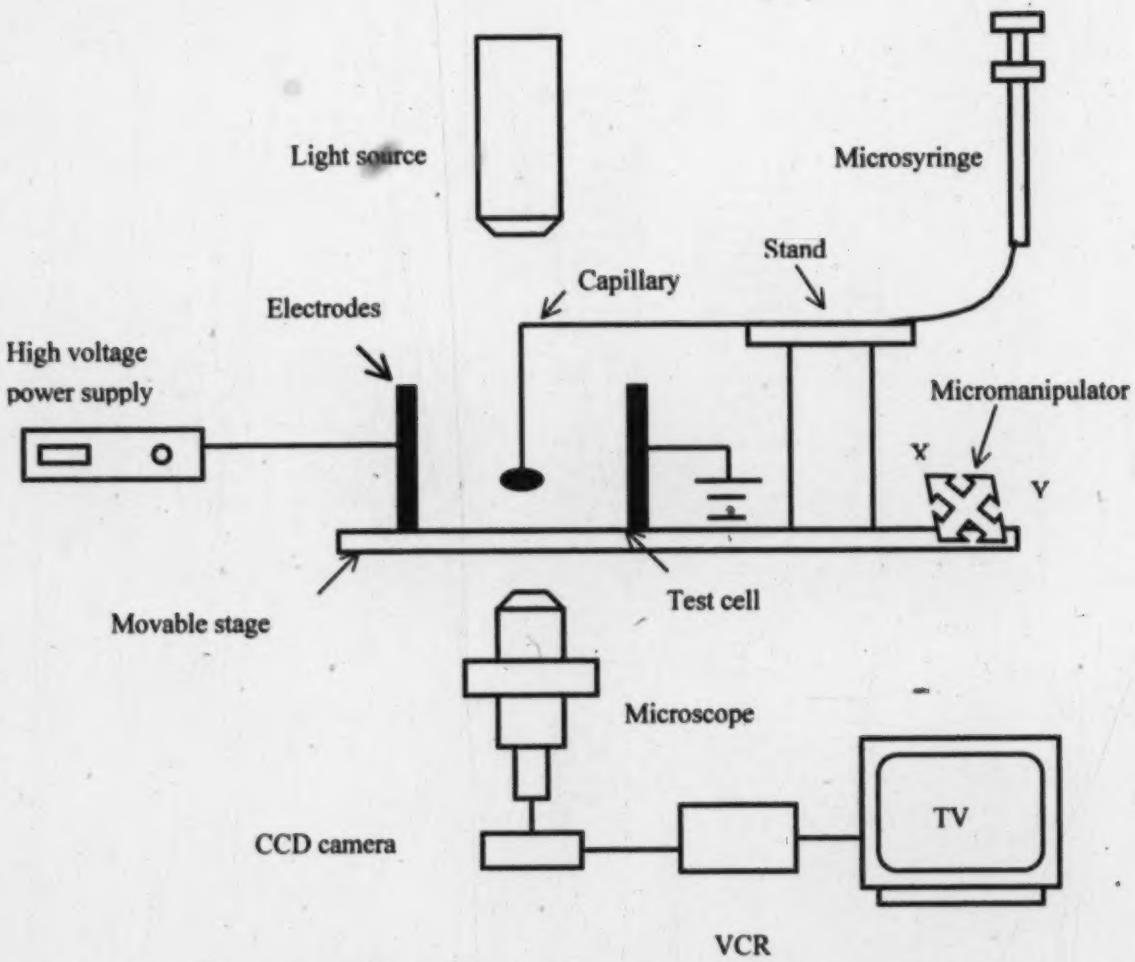

Figure 4.1 (a) Block diagram of experimental set-up for single drop system

Figure 4.1 (b) Photograph of experimental set-up for single drop system

Figure 4.2 (a) Photograph of glass test cell

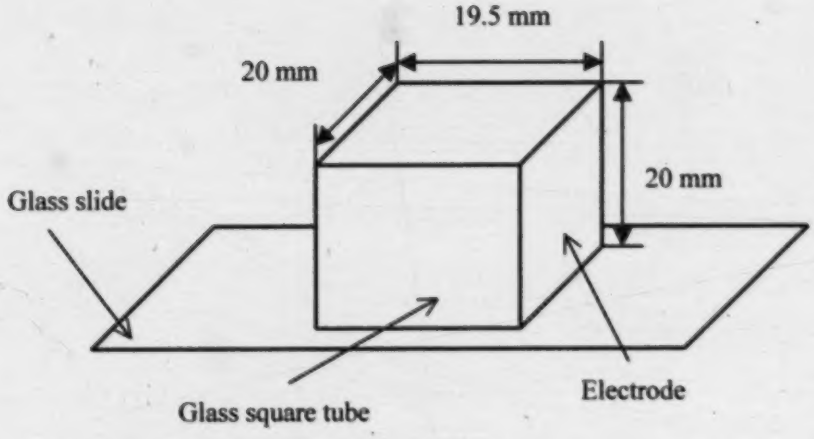

Figure 4.2 (b) Dimensions of glass test cell

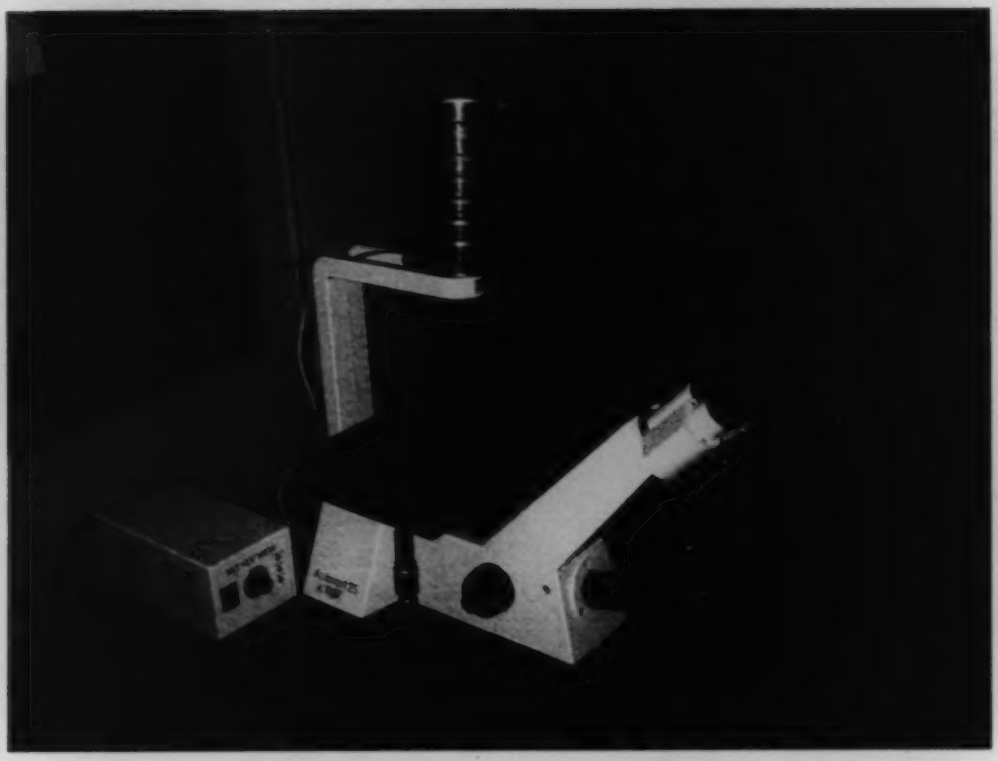

Figure 4.3 Photograph of microscope

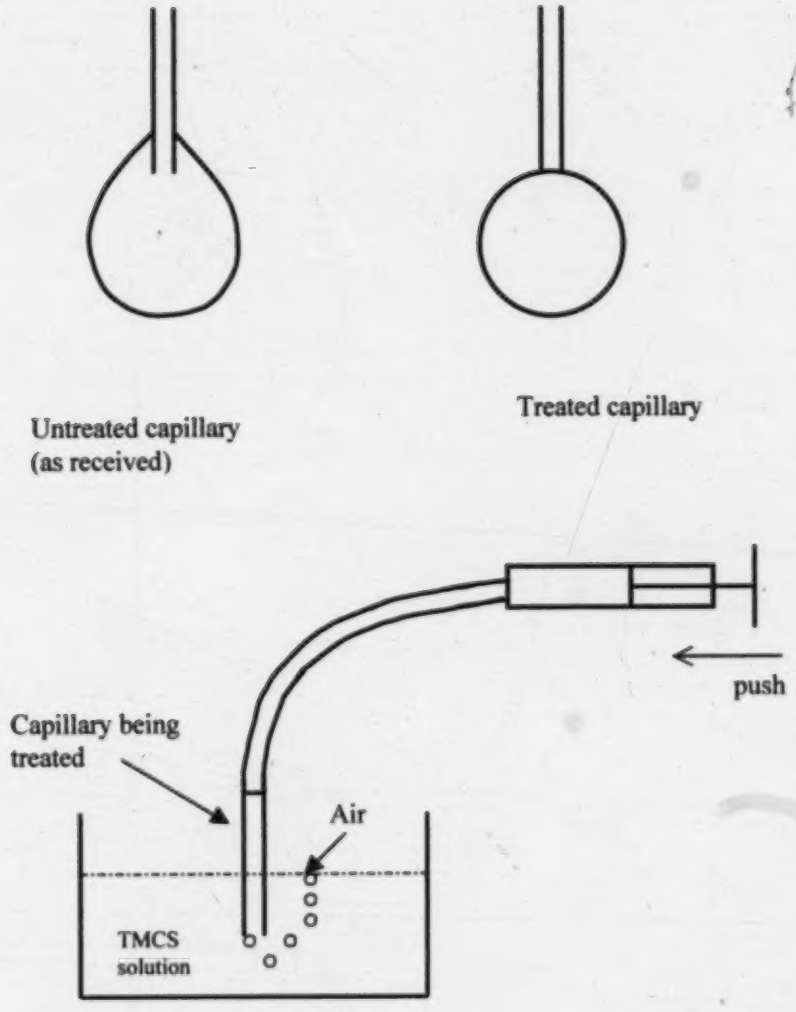

Figure 4.4 The process of making the outer surface of the capillary hydrophobic

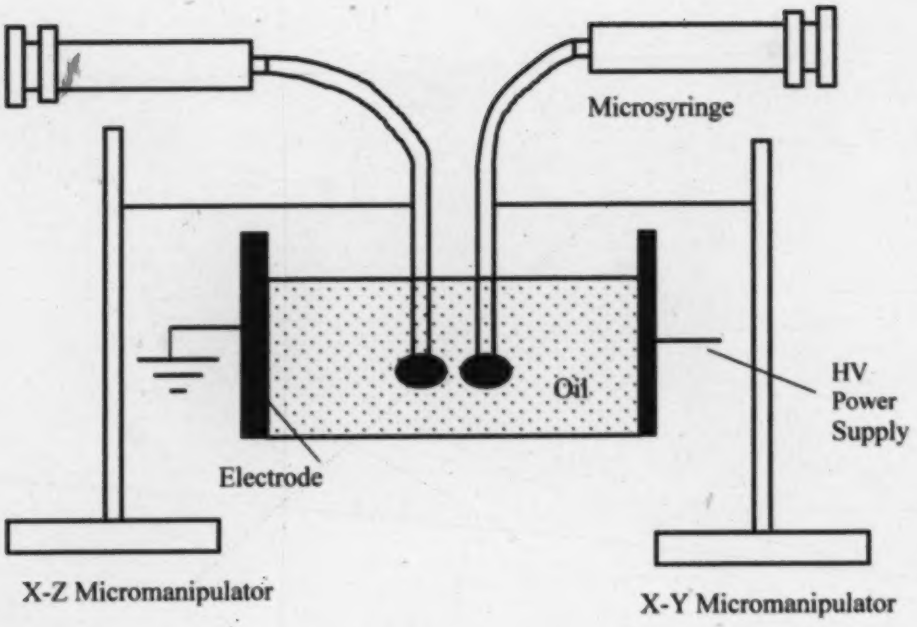

Figure 4.5 Schematic diagram of the difference between a drop pair system and a single drop system experimental set-up

Figure 4.6 Photograph of micromanipulator

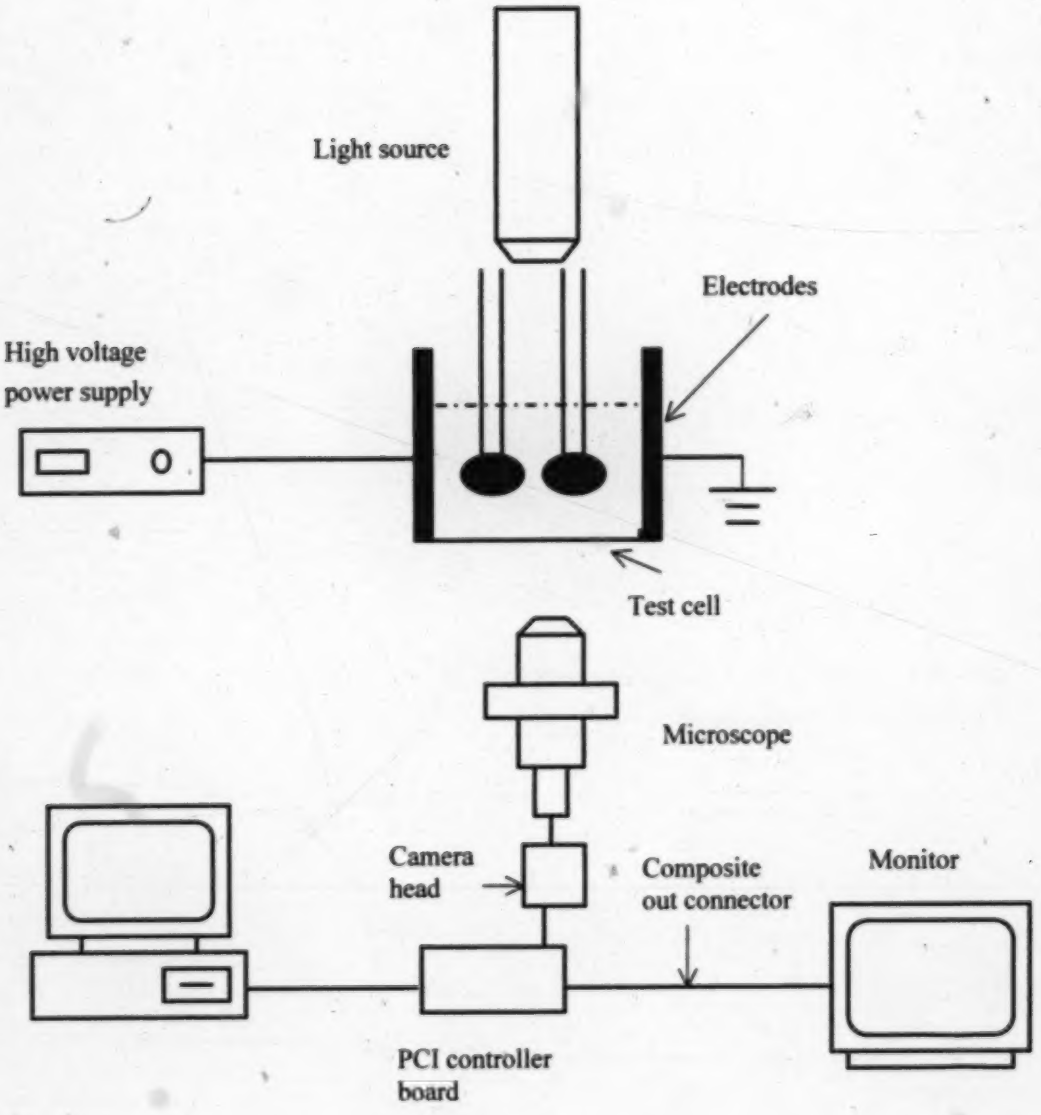

Figure 4.7 Block diagram of experimental set-up for drop coalescence record

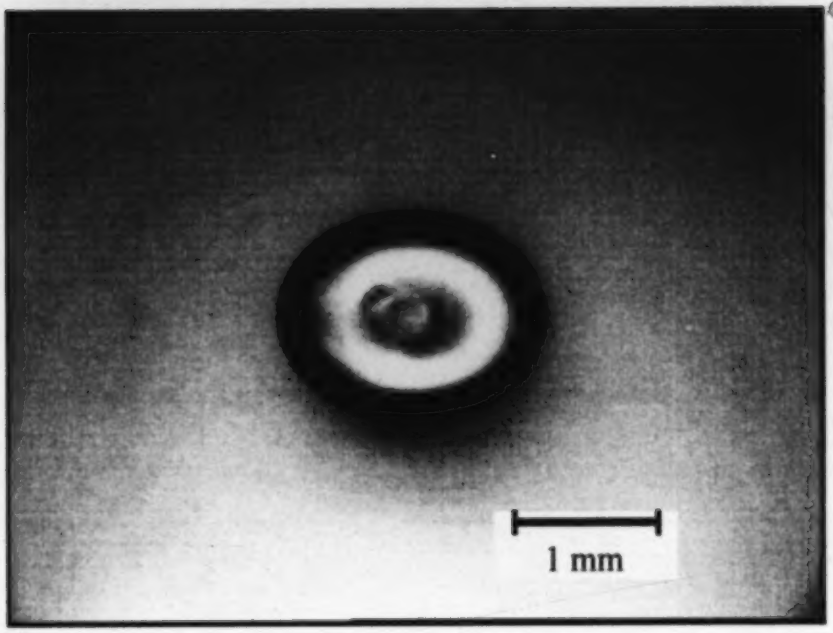

Figure 4.8 Water drop in 0.5% vol. diluted bitumen solution in 1.5 kV/cm electric field being applied horizontally

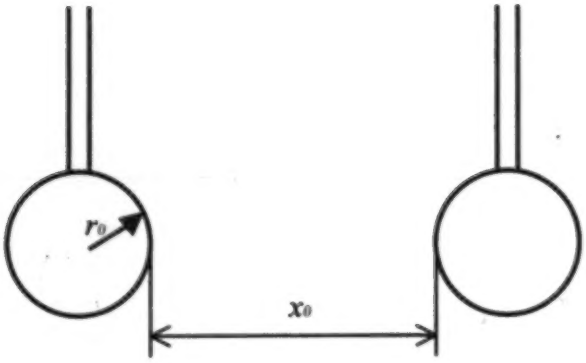

(a) Before the electric field is applied

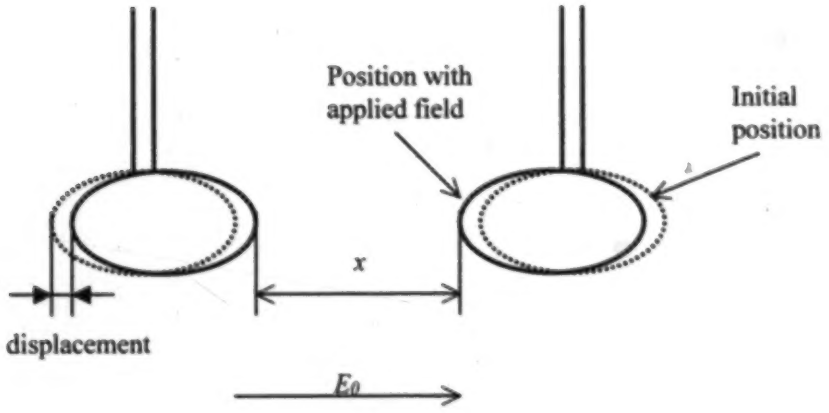

(b) When the electric field is applied

Figure 4.9 Displacement of the entire water drops in addition to the deformation when an electric field is applied

(a) Before the electric field is applied

(b) After the electric field is applied

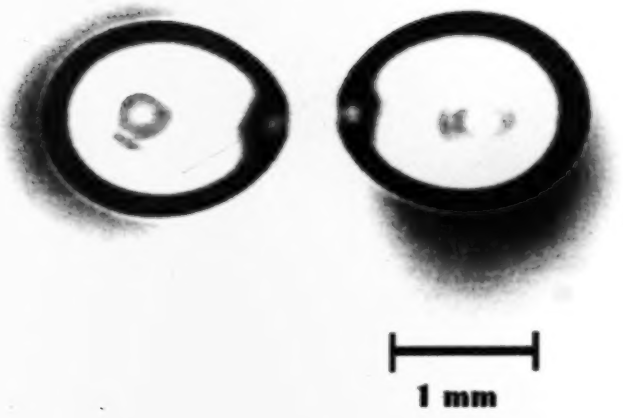

Figure 4.10 (a) Water drops in 1.5% vol. diluted bitumen solution when applying 2.4 kV/cm electric field horizontally

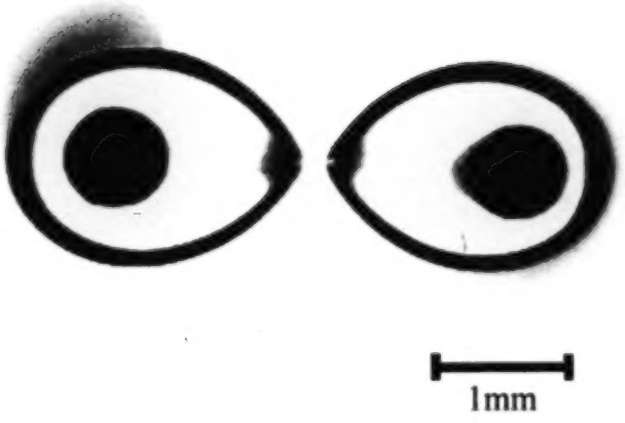

Figure 4.10 (b) Water drops in decyl alcohol when applying 1.0 kV/cm electric field horizontally

Chapter 5

Results and Discussion

5.1 Single Drop Deformation

From the equations describing the electric field and flow field of a leaky dielectric drop freely suspended in a leaky dielectric medium under an electric field, six dimensionless groups could be derived:

$$We = \frac{\varepsilon_0 \varepsilon_e}{\gamma} r_0 E_0^2 \qquad (5.1\ a)$$

$$\mathrm{Re} = \frac{\rho r_0 U}{\mu_i} \qquad (5.1\ b)$$

$$Ca = \frac{\mu_i U}{\gamma} \qquad (5.1\ c)$$

$$R = \frac{\sigma_i}{\sigma_e} \qquad (5.1\ d)$$

$$S = \frac{\varepsilon_i}{\varepsilon_e} \qquad (5.1\ e)$$

$$M = \frac{\mu_i}{\mu_e} \qquad (5.1\ f)$$

with i denoting the inner dispersed phase and e representing the outer continuous phase. Here, ε_0 is the permittivity of free space, ε_i is the dielectric constant of the internal (drop) phase, ε_e is the dielectric constant of the external (continuous) phase, γ is the interfacial

tension between the drop phase and the continuous phase, r_0 is the radius of the undeformed drop, E_0 is the uniform electric field strength, ρ is the density of the drop phase, σ_i and σ_e are, respectively, the electrical conductivities of the internal and external phases, μ_i and μ_e are the viscosities of the same respective phases, and U is the maximum surface velocity given by Taylor (1966)

$$U = \frac{9\left|\frac{R}{S} - 1\right|}{10(2+R)^2(1+M)} \frac{\varepsilon_0 \varepsilon_i}{\mu_e} r_0 E_0^2 \qquad (5.2)$$

Orders of magnitude of the dimensionless groups can be derived from the following parameters (representative value in the experiments):

$r_0 = 10^{-3} m$, $E_0 = 10^5 V/m$, $\varepsilon_0 = 8.854 \times 10^{-12}\ C^2/(N \cdot m^2)$, $\varepsilon_e = 8$, $\varepsilon_i = 80$,

$\rho = 1000 kg/m^3$, $\gamma = 30 \times 10^{-3} N/m$, $\sigma_i = 10^{-4} S/m$, $\sigma_e = 10^{-6} S/m$,

$\mu_e = 10^{-2} kg/(m \cdot s)$, $\mu_i = 10^{-3} kg/(m \cdot s)$

Thus, R = 100, M = 0.1, S = 10, U is of order 10^{-3} m/s, We is of order 10^{-2}, Re is of order unity and Ca is of order 10^{-4}.

In the case of a perfectly conducting drop in a perfect dielectric, the electric conductivity ratio R is infinite. The electric field is zero inside the conducting drop and the electrical stresses are oriented normal to the interface. No flow inside or outside of the drop is induced. The case of a water drop in a hydrocarbon is similar to the perfect drop case, as R is of order 100. The electric field inside the water drop is weak and the electrical stresses are effectively normal to the interface. The stresses resulting from the electric field play a dominant role, while the hydrodynamic stresses due to fluid flow are negligible by comparison. As the electric field-induced flow is very weak, the viscosity ratio M (which compares the viscosity of the internal phase to that of the external phase) and capillary number Ca (which measures the ratio of viscous forces to interfacial

restoring forces) do not play significant roles. On the other hand, the Weber number *We*, as indicated in equation (5.1 a), is a dimensionless parameter that is a measure of the relative importance of electrical distorting forces to interfacial restoring forces. This dimensionless group, whose definition is based on the electric field, will be used extensively in the analysis that follows.

5.1.1 Model Systems

5.1.1.1 Model Systems without Surfactant

Following Taylor's leaky dielectric theory (1966), a discriminating function β is defined in terms of the physical properties (electrical conductivity, dielectric constant and dynamic viscosity) of the fluid systems,

$$\beta = \left(R^2 - 2S + 1\right) + 3(R - S)\left(\frac{2 + 3M}{5 + 5M}\right) \tag{5.3}$$

As R, the conductivity ratio of the internal (drop) phase to the external (continuous) phase, is very large, the discriminating function β is always greater than zero. This means a single water drop will always be deformed into a prolate spheroid in the hydrocarbon systems in the presence of an electric field. Taylor's prediction is verified by experiments conducted on a single water drop suspended in model oils and diluted bitumen. In all the systems tested, the degree of drop deformation D was always greater than zero, which means that a single water drop was always elongated along the direction of the electric field. The degree of drop deformation D is defined as

$$D = \frac{a - b}{a + b} \tag{5.4}$$

where a and b are the drop axes parallel and perpendicular to the direction of the electric field, respectively. The reader is referred to Figure 2.1 for the definition. The experiments show that the discriminating function could successfully predict drop shapes for the system of a water drop suspended in a hydrocarbon.

For water drops in oil, the degree of deformation can be expressed as [Vizika & Saville, 1992]

$$D = \frac{9}{16}\frac{\varepsilon_0 \varepsilon_e}{\gamma} r_0 E_0^2 \qquad (5.5)$$

Alternatively, it can be expressed in terms of the Weber number We (cf. equation 5.1a)

$$D = \frac{9}{16} We \qquad (5.6)$$

For the case of decyl alcohol, the degree of deformation was measured and is shown in Figure 5.1 for a single water drop. Theoretical calculations based on Taylor's theory are also presented in the Figure as a dashed line. The solid line is a least squares fit of the experimental data. As can be noted from these results, the degree of deformation D exhibits a linear variation with We with increasing electric field strength, as predicted by Taylor's leaky dielectric theory.

Figures 5.2 to 5.7 show the experimental results for other model systems. Table 5.1 gives the comparison of calculated values and experimental values. Calculated values of m (the reader is referred to Table 2.1 for details) are derived from each system's physical properties, as was given by equation (2.10). Experimental values m^* are obtained from the data using least squares fits. The ratio of m^*/m falls between 1.0 and 2.0. The agreement with Taylor's theory is better than the result of Torza et al.(1971) (

where m^*/m falls between 2 and 4). Among the seven systems tested, the experimental result of a water drop in diethyl phthalate shows the best agreement with Taylor's theory, but the reason for that remains unclear. It is interesting that in all the cases, the experimental values are higher than the theoretical predictions, indicating a consistent deviation from equation (5.6). There is a larger deviation in the range of higher electric field strengths, consistent with the findings of Allan & Mason (1962), Torza et. al. (1971), and Vizika & Saville (1992).

All the experimental results are summarized in Figure 5.8 and compared with Feng & Scott's (1996) numerical calculations. It can be observed that almost all the experimental data are higher than Taylor's theoretical line. For large values of *We*, the degree of deformation no longer shows a linear relationship with Weber number. Compared with Taylor's first order prediction, Feng & Scott's numerical results are in better agreement with our experimental data. Within the small deformation limit, in the case of a water drop in a hydrocarbon, the viscosity ratio M and dielectric constant ratio S are not as important as the conductivity ratio R; this is because the electric induced flow is very weak. However, M and S may play important roles at higher electric field strengths.

Although the agreement of our experimental data and Taylor's theoretical prediction is better than with the data obtained by Torza et al. (1971), there still remains discrepancies. Allan & Mason (1962) suggested that the deviation from theoretical prediction may be due to an "electrocapillarity" effect by which the interfacial tension was lowered by the accumulation of electric charges at the interface. Discrepancies may also be caused by the non-homogeneity of the electric field and the effect of non-free drop (drop is held by the glass capillary). On the other hand, it should also be noted that Taylor's theory is limited only to small deformations and creeping flows. Feng & Scott's numerical approach might be a better alternative, as it is a more general model that

accounts for inertial effects and geometric nonlinearlities arising from large deformations.

5.1.1.2 Model Systems with Surfactants

The effect of surfactants on drop deformation was studied by adding sodium naphthenate (50% aqueous solution) and sodium dodecyl sulphate (SDS) to the drop phase. The degree of deformation of a single water drop in toluene is shown in Figure 5.9 as the Weber number was varied (for systems with and without sodium naphthenate).

The first system studied was a water drop in toluene, while 0.4% vol. of sodium naphthenate was added to the aqueous phase. The experimental result is compared with that of a water drop in pure toluene. The water drops were pulled away from the glass capillary by the electric field even when the electric field was fairly weak (2.3 kV/cm). The degree of deformation could not be measured when the Weber number was above 0.03, as the water drop could no longer remain attached to the capillary. When sodium naphthenate was added, the water drop was able to achieve a steady state even when the Weber number was 0.08. From Figure 5.9, it is seen that there is a significant difference between the deformations of a single water drop with and without surfactants. The water drop with adsorbed surfactants tended to deform less at the same Weber number.

Surfactants can lead to several effects: reduction of interfacial tension, suppression of internal fluid circulation by Marangoni flow, and creation of interfacial viscosities (as surfactants adsorbed at the interface cause a resistance to flow) As the effect of interfacial tension was already accounted for by the Weber number, any discrepancy must be due to the other two effects. Otherwise, the degree of deformation would be a function of the Weber number only and would be independent of other parameters. As mentioned above, surfactants not only play a role in lowering the

interfacial tension, but also induce Marangoni flows. The difference in drop deformation for the case with surfactants from that without surfactants may reflect the existence of Marangoni flow and its effects on the otherwise uniform distribution of sodium naphthenate at the interface. Another possible reason for the different behavior of the water drop in the two cases (with and without surfactants, as shown in Figure 5.9) could be due to interfacial viscosity created by the adsorbed surfactants.

The second system being studied was a water drop in decyl alcohol, with the aqueous phase containing 0.7 mM SDS. The degree of deformation is shown in Figure 5.10 as a function of the Weber number. The deformation of a water drop in the absence of surfactants is also shown in the same Figure. As is shown, the deformation is only a function of the Weber number and is independent of the presence of surfactants. As there is no noticeable difference between these two cases, it can be concluded that the surfactant SDS only played the role of reducing interfacial tension; no significant surface flow was induced to affect the uniform distribution of surfactants on the water drop surface. The system of a water drop in decyl alcohol could be considered as a perfectly conducting drop in a perfect dielectric, since there is no flow inside or outside of the conducting drop.

5.1.2 Diluted Bitumen Systems

One of the objectives of this study is to understand the behavior of water drops in bitumen, thus different amounts of bitumen are added to toluene solution for tests at different aging times (either zero or 30 minutes). As there are natural surfactants (i.e., asphaltenes and resins) in bitumen, the role of surfactants on drop deformation should be investigated.

5.1.2.1 Effect of Aging

The effect of surface aging on drop deformation was studied by comparing the behavior of fresh water drops with those that had been aged for half an hour. Figure 5.11 shows the deformation of a single water drop in 0.5% vol. bitumen for different aging times. There is no data for the fresh water drop when the deformation parameter D is above 0.02. This is because the fresh water drop could not remain attached to the capillary even when the electric field strength is very low (2.0 kV/cm). However, after the water drop was aged for 30 minutes, it could maintain a steady shape even when D was above 0.11. No clear trend was obtained for this experiment, as the degree of deformation was very small (of the same magnitude as the experimental error). Figure 5.12 shows the deformation behavior of a single water drop in toluene containing 1.0% vol. bitumen for different aging times. There is no difference between the water drop with zero aging time and that with 30 minutes aging time. However, it was noted that for water drops with longer aging times, it was possible to maintain stable equilibrium in larger electric fields.

Figures 5.13 and 5.14 show the deformation of a single water drop for different aging times at 1.5% and 2.0% vol. diluted bitumen. It can be observed from these Figures that there are appreciable differences between water drops without aging and those that had been aged for 30 minutes. This may be explained as following: compared with the fresh system, there was more surfactant adsorbed onto the water drop surfaces for the aged system. As the film around the water drop will presumably resist deformation, aged water drops deform less as compared with fresh water drops at the same Weber number.

5.1.2.2 Effect of Bitumen Concentration

Figure 5.15 shows the deformation of a fresh water drop (i.e., no aging) in toluene-diluted bitumen on all bitumen concentration. As there are natural surfactants in bitumen, it is reasonable to assume that more surfactants are present in the system as the bitumen concentration increases. From Figure 5.15, it is seen that the water drop deformed less with increasing bitumen concentration. Presumably, as more surfactants are adsorbed onto the water drop, the protective layer around the water drop becomes thicker. The protective layer may behave as a viscoelastic film which reduces the drop deformation.

But the experimental data are still above Taylor's theoretical line and Feng & Scott's numerical prediction. The reasons for this behavior remain unclear. Figure 5.16 illustrates the deformation behavior of a single water drop aged for half an hour in toluene solution with different amounts of dissolved bitumen. The experimental data showed a similar trend as in Figure 5.15. With more bitumen added to the continuous phase, the water drop deformed less at the same Weber number. The water drop could maintain a steady state at higher electric field strengths. As in Figure 5.15, the experimental data are above Taylor's theoretical line and Feng & Scott's numerical predictions. It is quite possible that the nature of the protective layer around the water drop has different characteristics at the different bitumen concentrations in toluene.

The surface Peclet number and Gibbs elasticity are two parameters that describe the drop deformation behavior in the presence of surfactants, as indicated by equations (2.14) and (2.16). Unfortunately, they are both difficult to quantify experimentally. The effects of surfactants on these two parameters are only qualitatively explained here. The surface Peclet number represents the relative importance of surfactant convection to diffusion on the interface. As the electrically induced flow is weak in the system of a

water drop in oil, which means there is effectively no surfactant concentration gradient at the oil-water interface, the surface Peclet number must be very small. The surfactants are almost evenly adsorbed onto the water drop. Gibbs elasticity measures changes in the interfacial tension in response to variation of surfactant concentration. When the Gibbs elasticity is small, the surfactant concentrations have little effect on the interfacial tension. Conversely, when the Gibbs elasticity is large, the interface behaves effectively as a rigid film. As more surfactants are added to the system, it is assumed that the protective layer around the water drop becomes thicker and will behave more like a rigid film.

5.2 Drop Pair Deformation

5.2.1 Model System

The deformation of a water drop pair in decyl alcohol as a function of the separation distance x is shown in Figure 5.17. The reader is referred to Figure 4.9 for the definition of x. When x is decreased at constant electric field strength, the drops tended to deform more. When the two drops were kept at the same distance, the drops deformed more when a higher electric field strength was applied. For example, when the separation distance x was equal to the undistorted drop radius r_0, the degree of deformation was 0.017 when the applied electric filed strength was 0.515 kV/cm. At the same initial separation, when the applied electric field strength was increased to 1.031 kV/cm (doubled), the degree of deformation extended to 0.08. It is also interesting to note that when the separation distance x is less than half the radius of the undeformed drop r_0, the degree of deformation increased rapidly with decreasing separation at constant electric field strength.

For the purpose of comparing with the experimental results of a single drop, the data in Figure 5.17 is replotted in Figure 5.18. In Figure 5.17, four points are obtained from the four different regression lines (different We's) at the separation distance of 0.6. These four points represent the different degrees of deformation at the same separation distance. The four points are presented as a regression line (x/r_0=0.6) in Figure 5.18, where the Weber number is plotted on the horizontal axis (instead of the separation distance x/r_0). This regression line expresses the corresponding degree of deformation with different Weber numbers at a separation distance of 0.6. In the same way, another regression line was obtained using three sets of points at separation distance 2.0 in Figure 5.18. For simplicity, only the results for x/r_0 = 0.6 and x/r_0 = 2.0 are presented. Figure 5.18 is a plot of the deformation D vs. the Weber number We at different separation distances x/r_0. It could be noted that each drop in the drop pair behaved very similarly to a single drop when the separation distance is large. More specifically, when the separation distance x is two times the radius of the undeformed drop, the degree of deformation (for drop pairs) is almost identical to that for single drops. This means if one water drop is separated from another by about a drop diameter, it can be considered an isolated drop and will not affect the other's deformation behavior. This result is consistent with Latham & Roxburgh's (1966) finding: for drop separation on the order of one radius or smaller, there is a substantial modification in the tangential electric stress at the surfaces of the drops and in the induced flow fields.

5.2.2 Diluted Bitumen Systems

The deformation of a water drop pair in diluted bitumen was also studied. The experimental results for a water drop pair in 0.5% vol. diluted bitumen is shown in Figure 5.19. The behavior is essentially the same as that for drop pairs in decyl alcohol. The drop deformed more with the increase of electric field and/or the decrease of separation

distance. For example, at a separation distance x/r_0 of 0.6, the degree of deformation more than doubled when the electric field strength was increased by 30%. The relationship between the deformation parameter D and the Weber number We for the same system is shown in Figure 5.20. It is replotted using the data of Figure 5.19. In Figure 5.19, four points are obtained from the four different regression lines (different We's) at the separation distance of 0.7. The four points represent the different degrees of deformation at the same separation distance. These four points are presented as a regression line (x/r_0=0.7) in Figure 5.20, where the Weber number is plotted on the horizontal axis (instead of separation distance x/r_0). This regression line expresses the corresponding degree of deformation with different Weber numbers at a separate distance of 0.7. In the same way, three other regression lines are obtained in Figure 5.20 using three sets of points at separation distances of 1.0, 1.3 and 1.6. Figure 5.20 is a plot of the deformation D vs. the Weber number We at different separation distances x/r_0. The results for x/r_0 = 0.6, 1.0, 1.3 and 1.6 are presented. When the separation distance x/r_0 increased from 0.7 to 1.6, each drop behaved similarly to a single water drop.

A plot of the deformation D vs. the separation x/r_0 at different Weber numbers is shown in Figure 5.21. Here, the oil phase is 1.5% vol. diluted bitumen. The water drops behave the same way as in the previous two systems (water drops in decyl alcohol and 0.5% vol. diluted bitumen), as they deformed more with increase in electric field and /or decrease in separation distance. The experimental data is replotted as Figure 5.22, using the method mentioned in the last paragraph. Figure 5.22 is a plot of the deformation D vs. the Weber number We at different separation distances x/r_0 = 0.5, 1.0, 1.5 and 2.0. When the separation distance between the water drops is decreased, the drops have less influence on each other and behaved in ways similar to single water drop.

However, the difference between this system (water drops in 1.5% vol. diluted bitumen) and the previous two systems (water drops in decyl alcohol and 0.5% vol.

diluted bitumen) is that, the present deformation deviates from that of a single drop even when the separation distance is two times the undeformed drop radius. This means when more surfactants are present in the system, each of the water drops could have effects on the other drop at a farther distance. It is speculated that when surfactants are present, they are swept to the poles of the water drop due to the electric field. The result is that there are more surfactants present at the poles than at other parts of the drop. The accumulated surfactants at the poles reduce the local interfacial tension and thus the drop has larger local deformations. If there are more surfactants present, the drop will deform more, resulting in larger modifications of the tangential electric stress at the surfaces of the drops and in the induced flow fields. Thus, the drops could influence each other at a farther distance when more surfactants are present in the system.

5.3 Coalescence between Two Drops

The coalescence of two water drops in 2-ethyl-1, 3-hexanediol is shown in Figure 5.23. The value of r_0 was about 0.7 mm. The viscosity of the continuous phase is about 60 times that of water. A more detailed sequence of images is shown in Figure 5.24, which reveals the coalescence of a water drop pair in decyl alcohol. The frame rate was 4000 frames per second. From Figures 5.23 and 5.24, it is noted that the two water drops are attracted to each other. This is due to the electrical attractive forces caused by the positive and negative polarization charges on the water drops. When the two water drops are very close to each other, it is noted that sharp tips are formed at the surfaces of the water drops. The two water drops then coalesced.

In the system of a water drop pair in diluted bitumen, there are natural surfactants present. Surfactants adsorbed at the drop surface may form a protective layer that acts as a barrier to coalescence. In Figure 5.25, the coalescence process of a water drop pair in heptane-toluene (1:1) solution (1.5% vol. bitumen added) is presented. The frame rate was 500 per second. One photograph ($f = -1$ and $t = 48$ ms) shows the drops just before

distance. The next photograph (f=0 and t=50ms) shows the start of the coalescence process.

The coalescence of a water drop pair in diluted bitumen is also shown in Figure 5.26 for a 0.3% vol. bitumen. The frame rate was 2000 frames per second. When the two water drops are sufficiently close, the sharp points at the closest separation appeared. Then, a water bridge was formed between the water drops. With the expansion of the width of water bridge, the two small water drops coalesced into one large drop.

From the above Figures, it is noted that the electric field will enhance the coalescence of two water drops in diluted bitumen. It brings two water drops very close to each other, either by electrical attractive force, or by drop deformation. Such a process is depicted in Figure 5.27.

Table 5.1 Comparison of calculated and experimental values for water drops in different continuous phases

Continuous phase	Calculated value m (cm/kV^2)	Experimental value m^* (cm/kV^2)	Discrepancy factor m^*/m
Decyl Alcohol	0.4637	0.6107	1.32
Diethyl phthalate	0.2776	0.2812	1.01
Cycloheptanone	0.9498	1.7197	1.81
Alpha-ionone	0.2982	0.4322	1.45
Cyclohexyl acetate	0.1803	0.2518	1.40
Ethyl benzoate	0.1735	0.2654	1.53
2-ethyl-1,3-hexanediol	2.8180	3.3371	1.18

Note: Calculated value $m = \frac{9\varepsilon_0\varepsilon_i}{16\gamma}\frac{\beta}{(2+R)^2}$, experimental value $m^* = \frac{D}{r_0 E_0^2}$ [as shown in equation (2.9) and (2.10)]

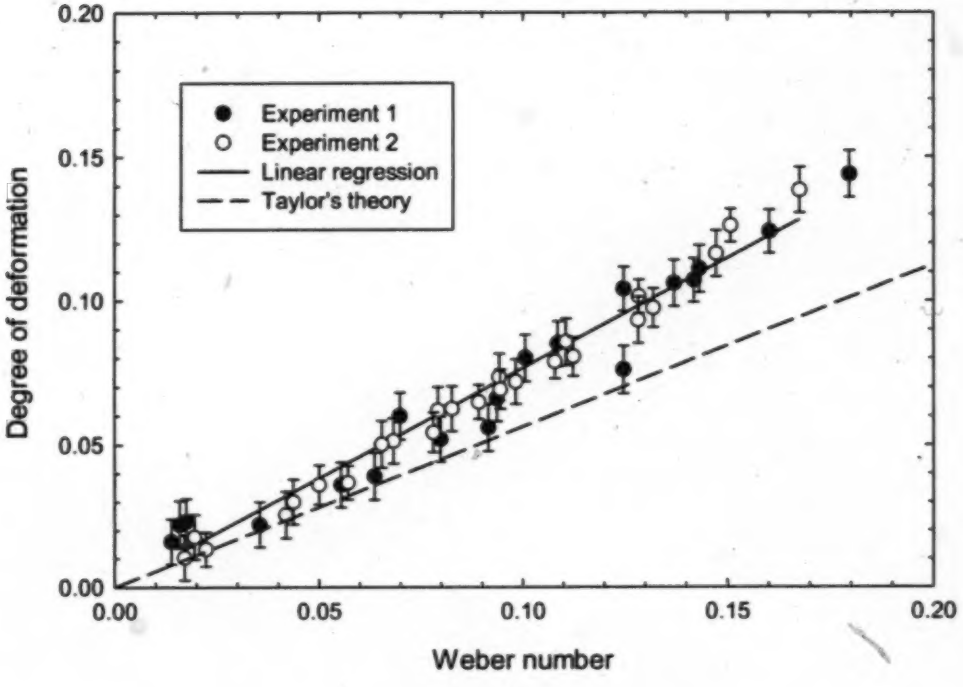

Figure 5.1. Degree of deformation as a function of Weber number for a single water drop in decyl alcohol

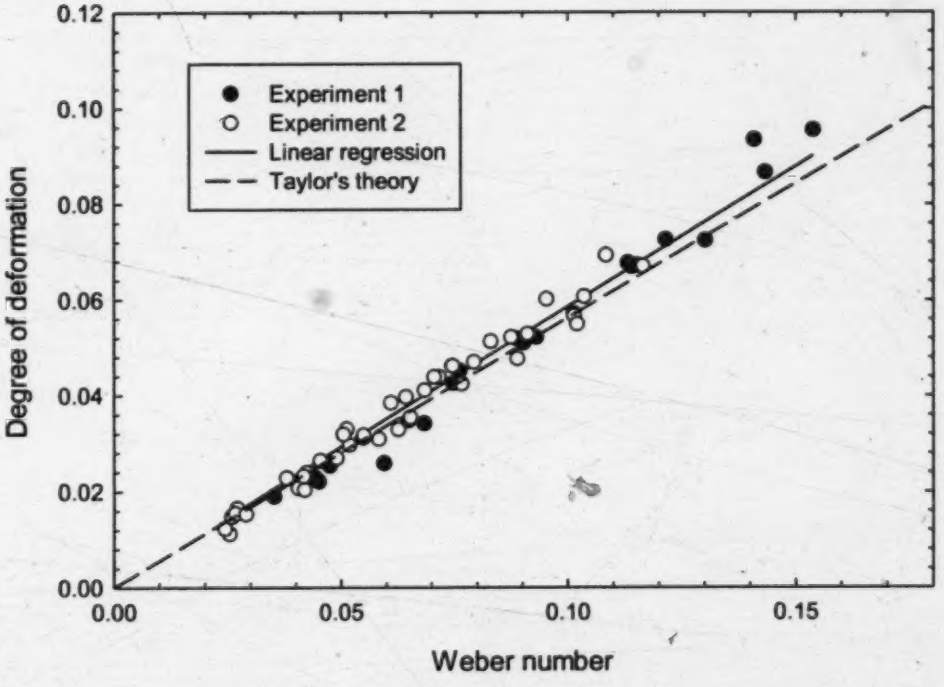

Figure 5.2. Degree of deformation as a function of Weber number for a single water drop in diethyl phthalate

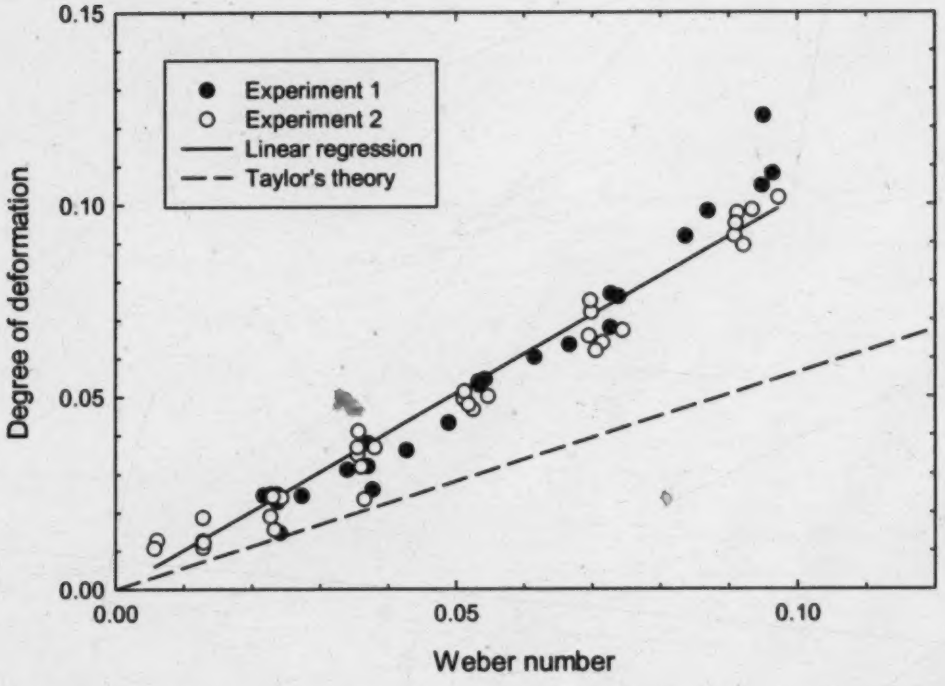

Figure 5.3. Degree of deformation as a function of Weber number for a single water drop in cycloheptanone

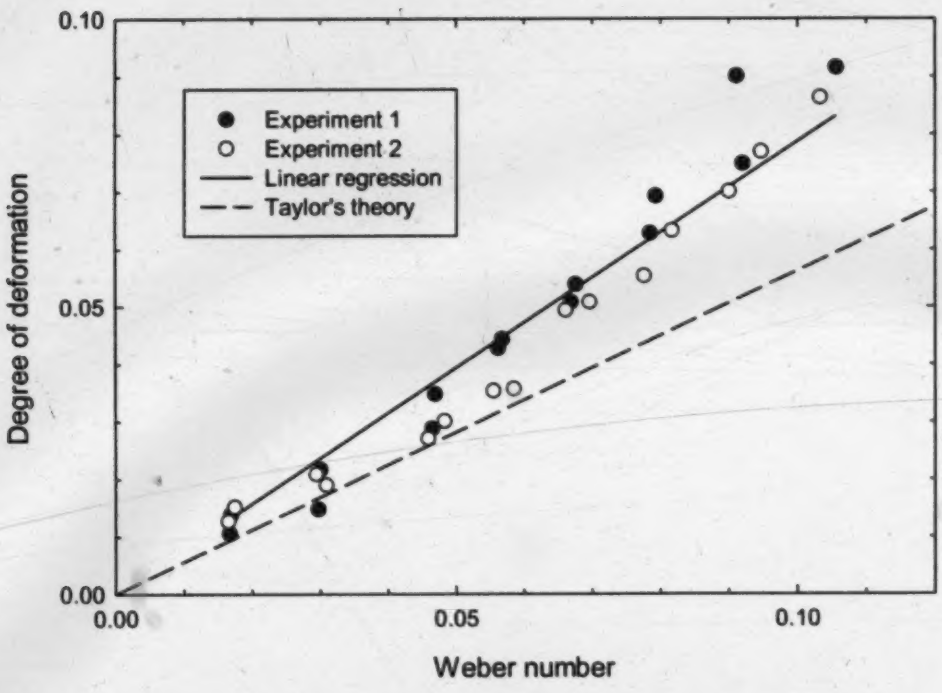

Figure 5.4. Degree of deformation as a function of Weber number for a single water drop in alpha-ionone

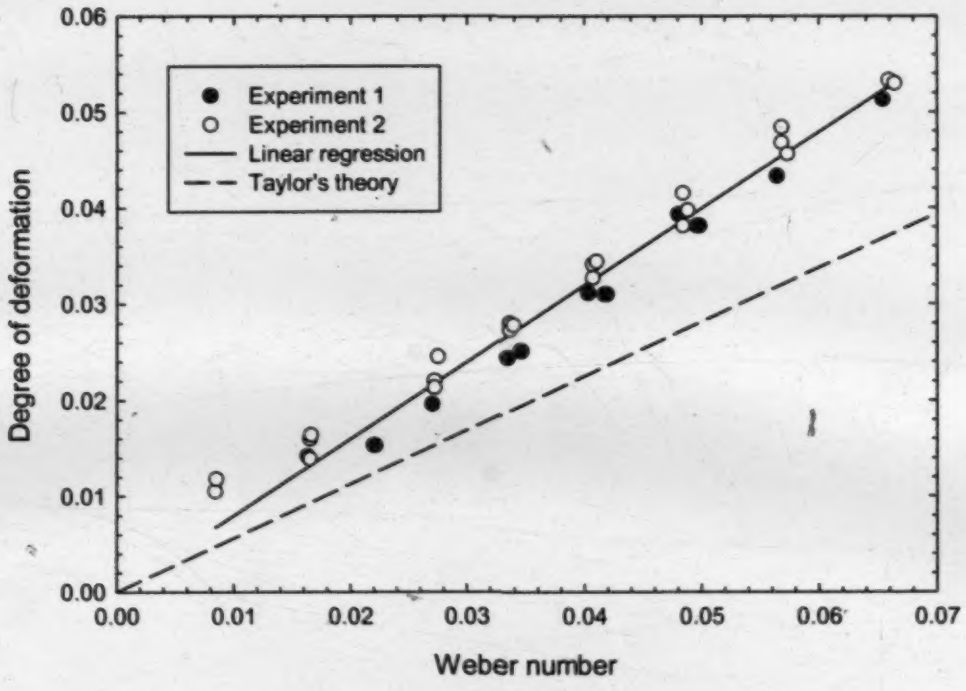

Figure 5.5. Degree of deformation as a function of Weber number for a single water drop in cyclohexyl acetate

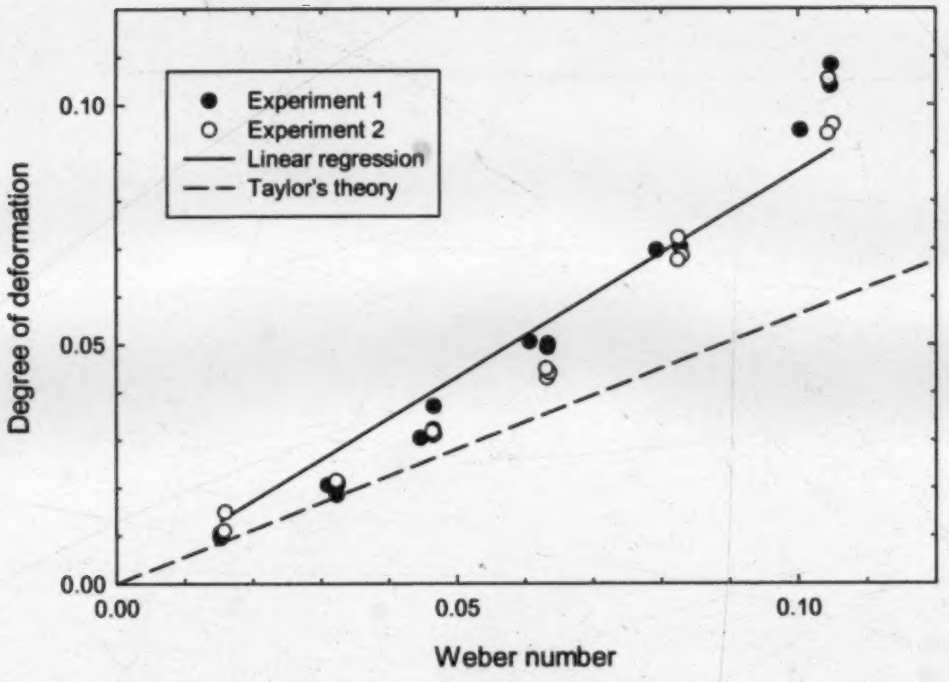

Figure 5.6. Degree of deformation as a function of Weber number for a single water drop in ethyl benzoate

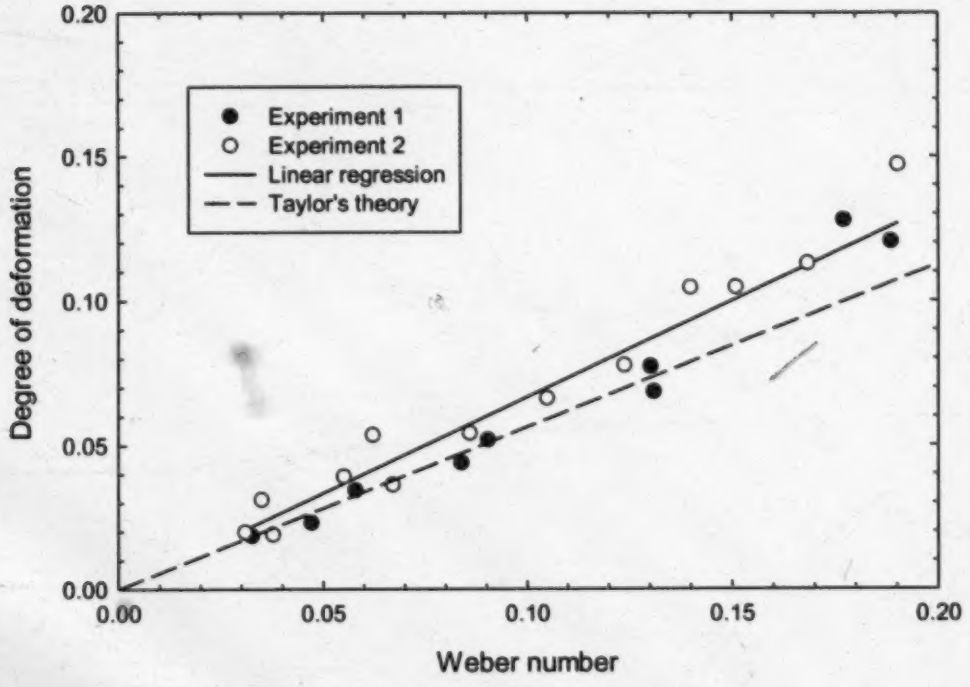

Figure 5.7. Degree of deformation as a function of Weber number for a single water drop in 2-ethyl-1, 3-hexanediol

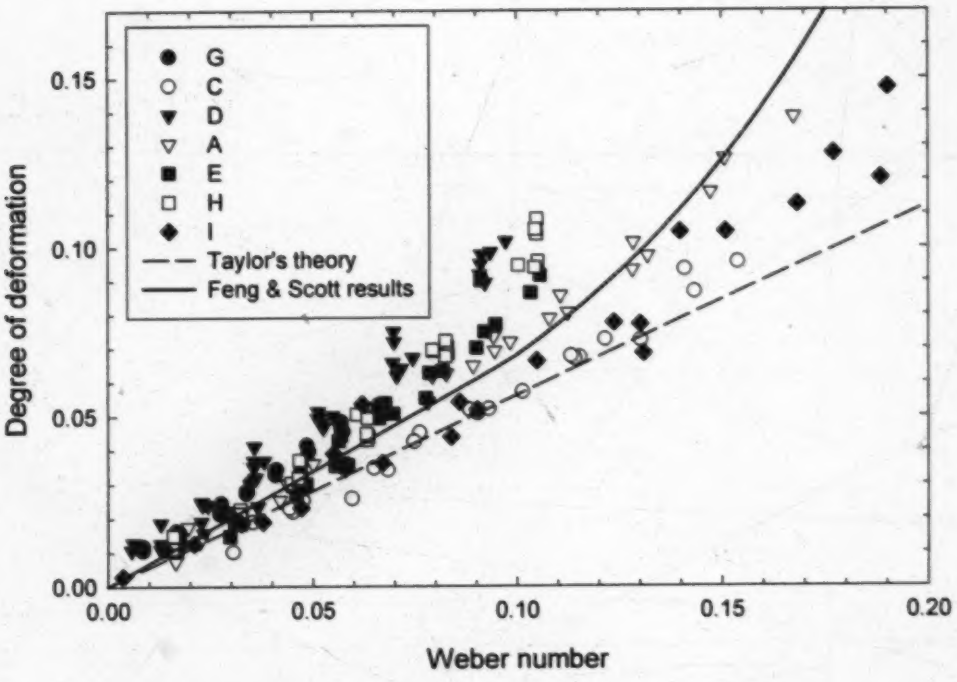

G: Cyclohexyl acetate C: Diethyl phthalate D: Cycloheptanone
A: Decyl alcohol E: Alpha-ionone H: Ethyl benzoate
I: 2-Ethyl-1,3-hexanediol

Figure 5.8. Degree of deformation as a function of Weber number for a single water drop in various organic compounds

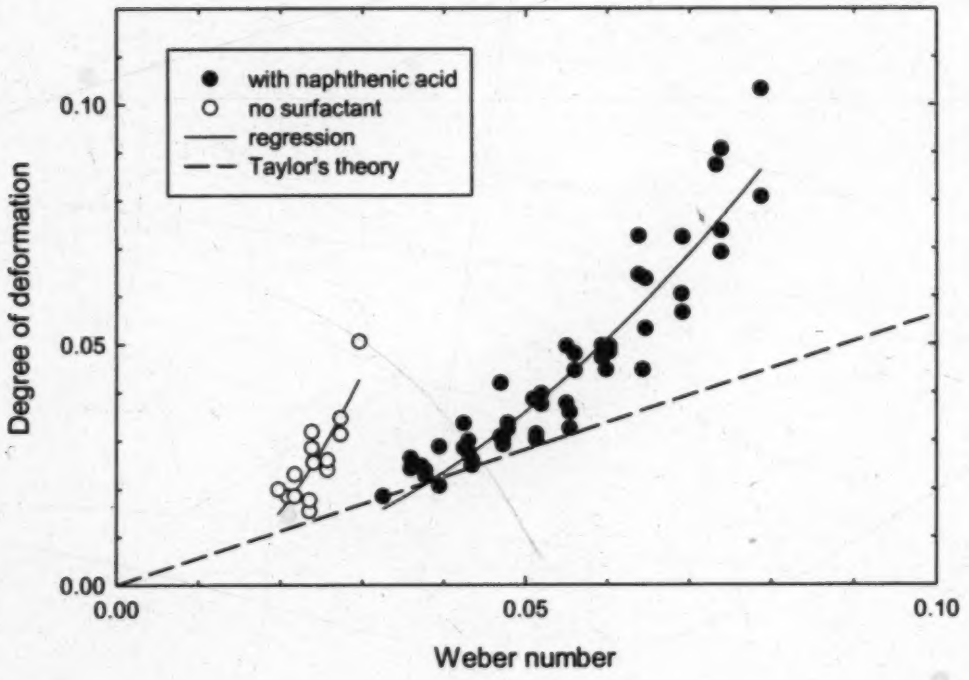

Figure 5.9. Degree of deformation as a function of Weber number for a single water drop in toluene (with and without surfactants added)

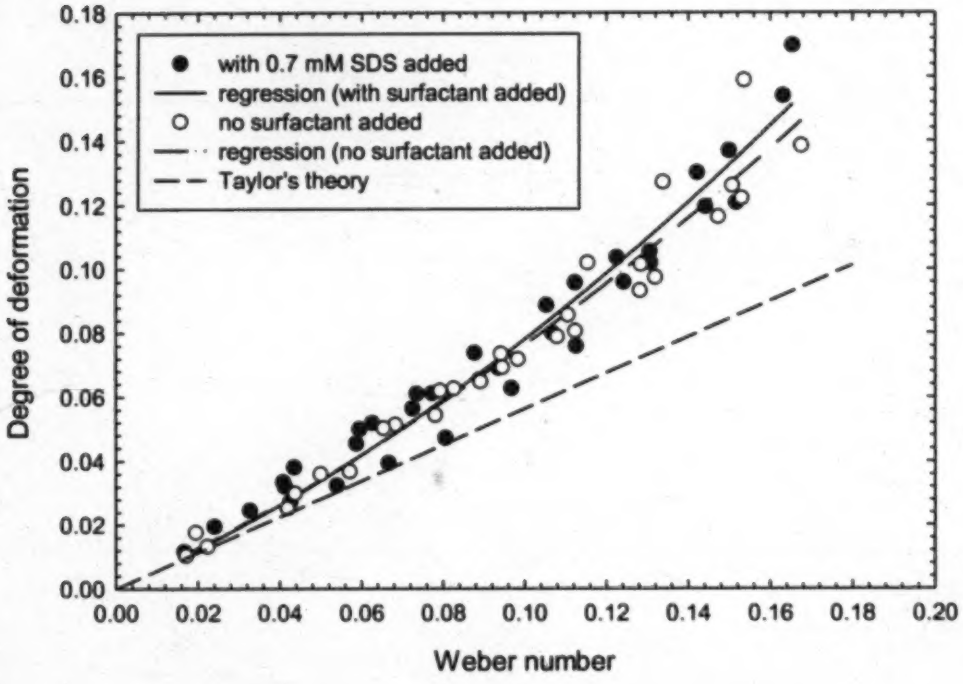

Figure 5.10. Degree of deformation as a function of Weber number for a single water drop in decyl alcohol with surfactant added

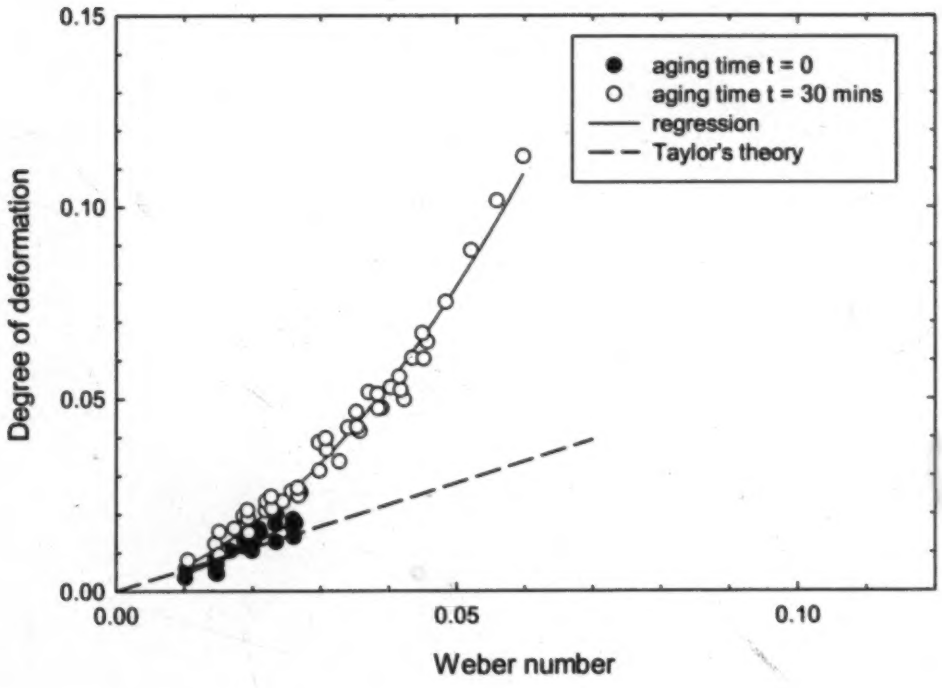

Figure 5.11. Deformation of a single water drop in toluene solution (0.5% vol. bitumen added) at two different aging times

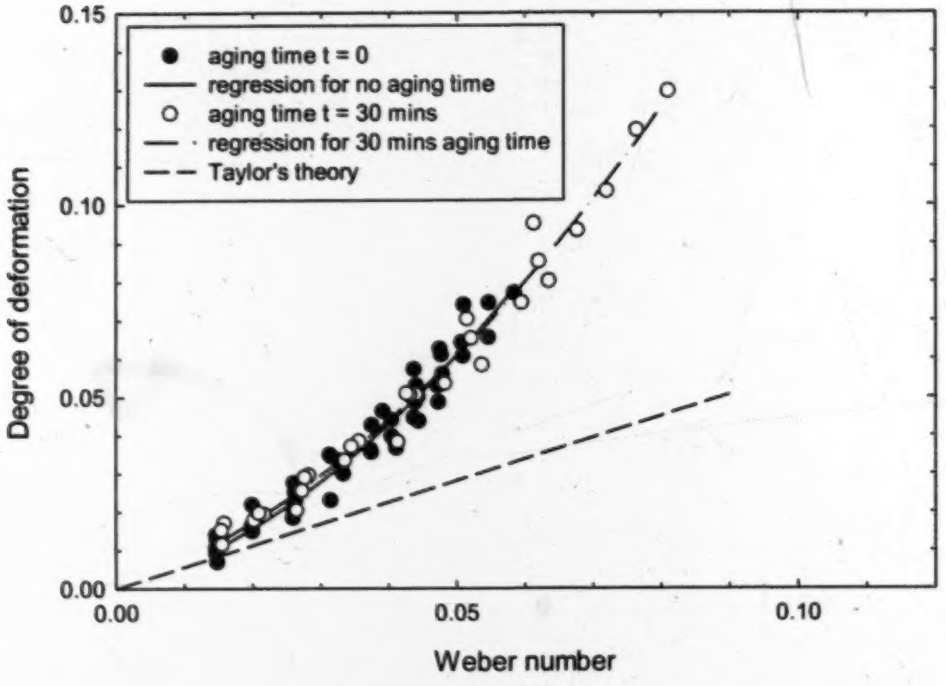

Figure 5.12. Deformation of a single water drop in toluene solution (1.0% vol. bitumen added) at two different aging times

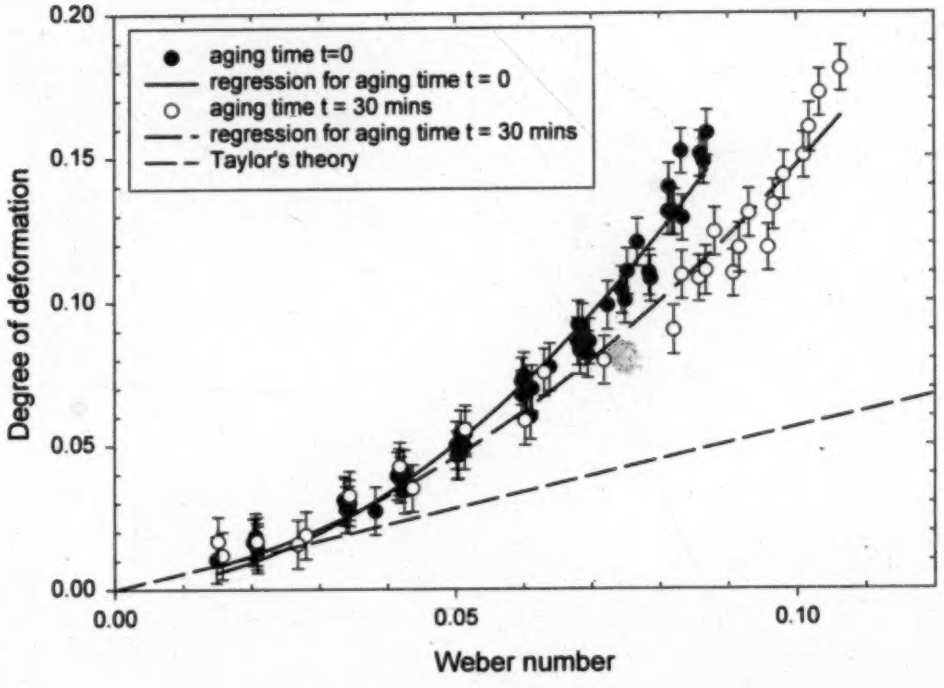

Figure 5.13. Deformation of a single water drop in toluene solution (1.5% vol. bitumen added) at two different aging times

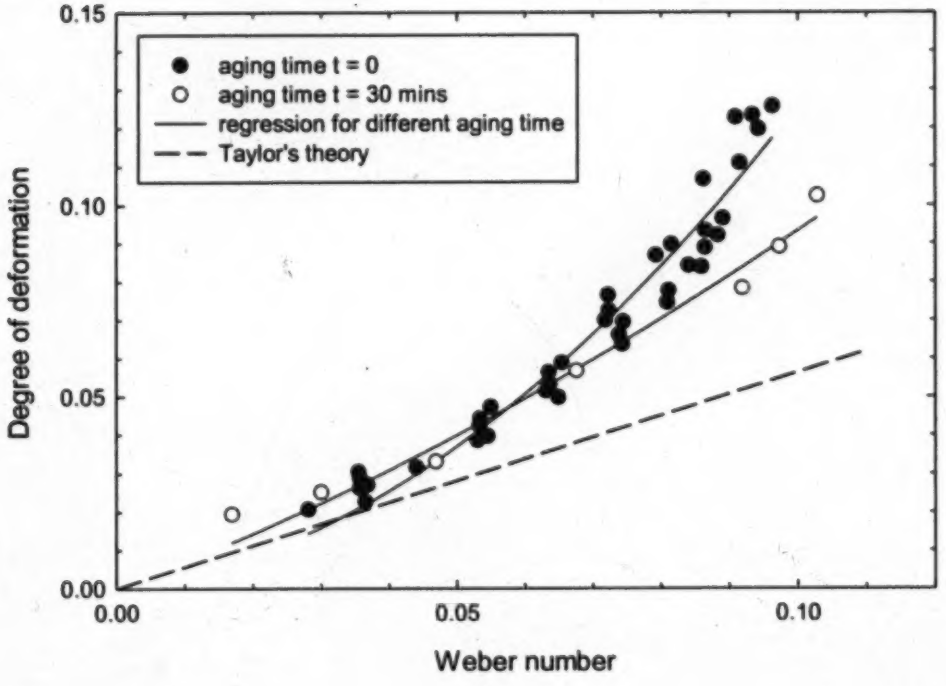

Figure 5.14. Deformation of a single water drop in toluene solution (2.0% vol. bitumen added) at two different aging times

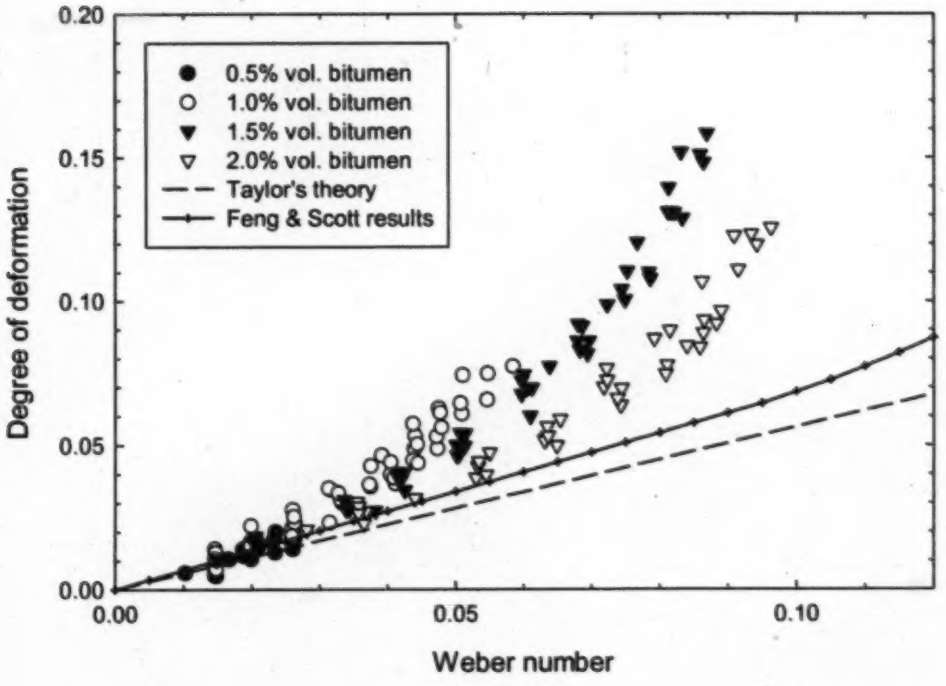

Figure 5.15. Deformation of a single water drop in toluene solution for different volume percent of bitumen added (no aging time)

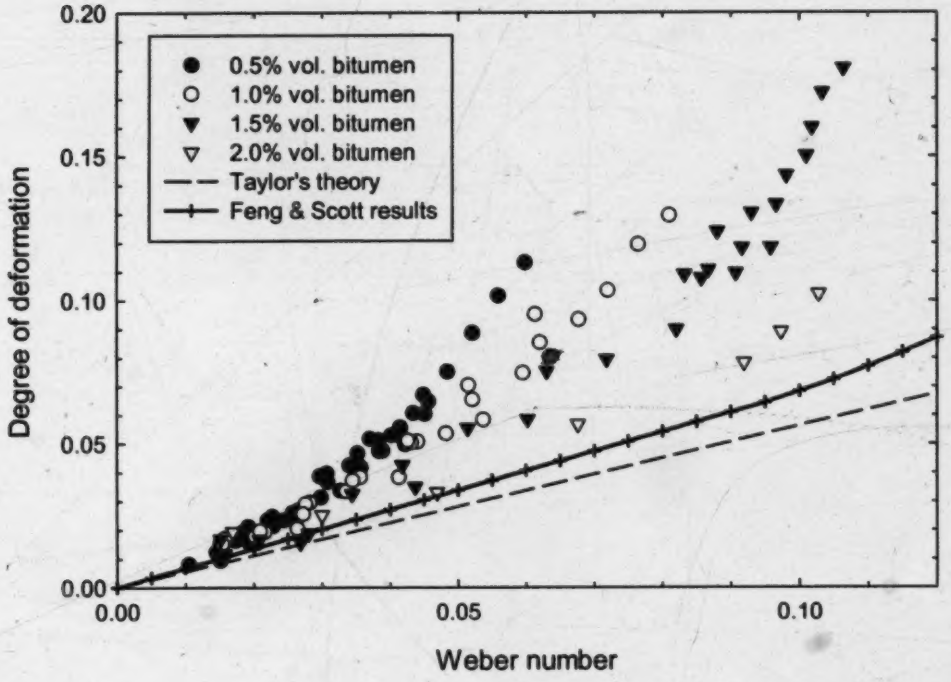

Figure 5.16. Deformation of a single water drop in toluene solution for different volume percent of bitumen added (30 minutes aging time)

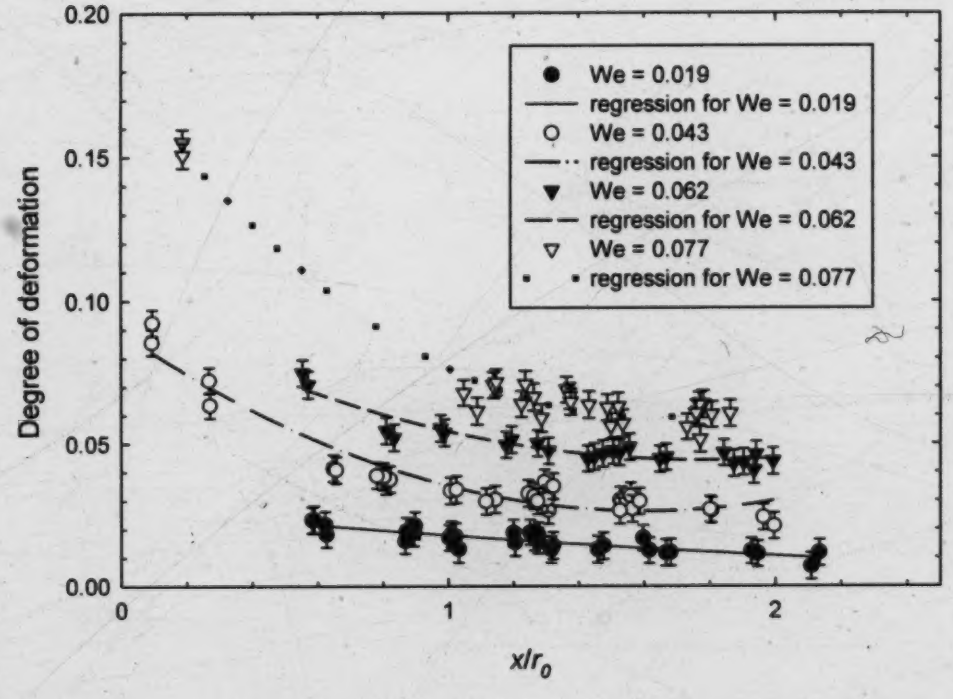

Figure 5.17. Degree of deformation as a function of distance for a water drop pair in decyl alcohol with no aging time

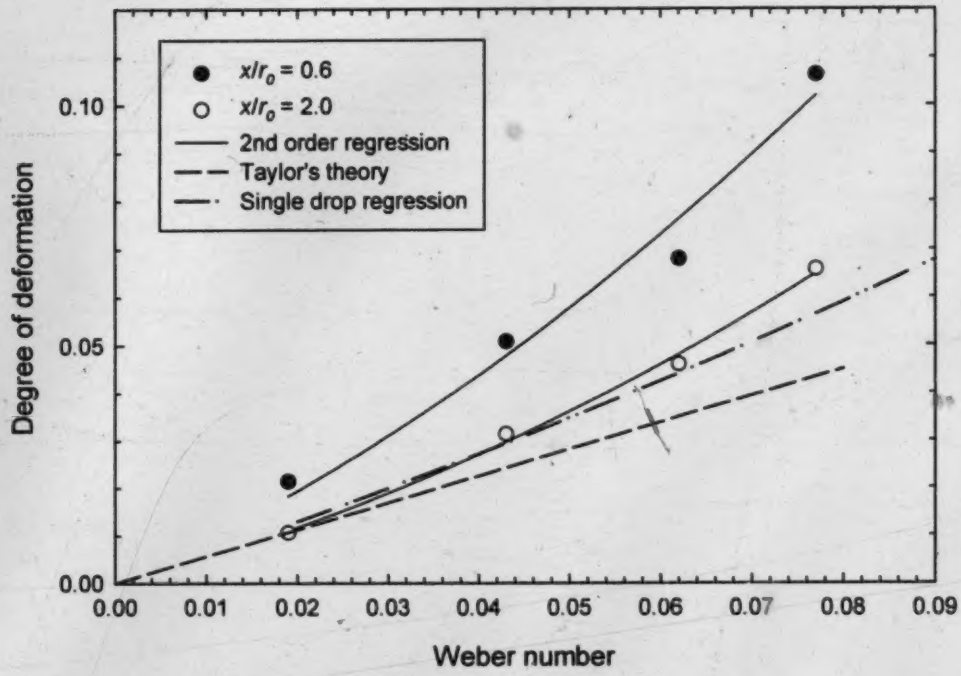

Figure 5.18. Degree of deformation as a function of Weber number for a water drop pair in decyl alcohol with no aging time

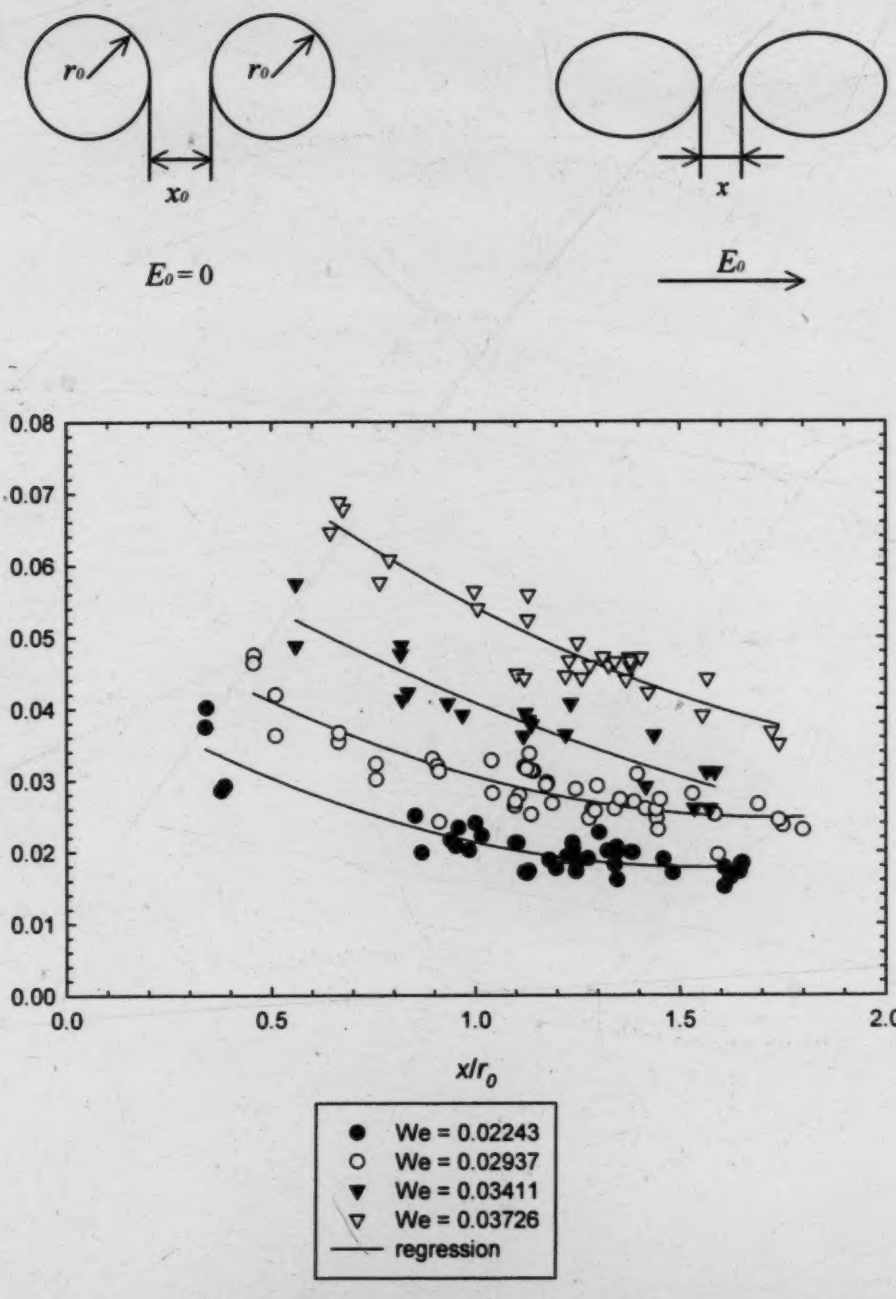

Figure 5.19. Degree of deformation as a function of distance with different Weber numbers for a water drop pair aged 30 minutes in toluene solution (0.5% vol. bitumen added)

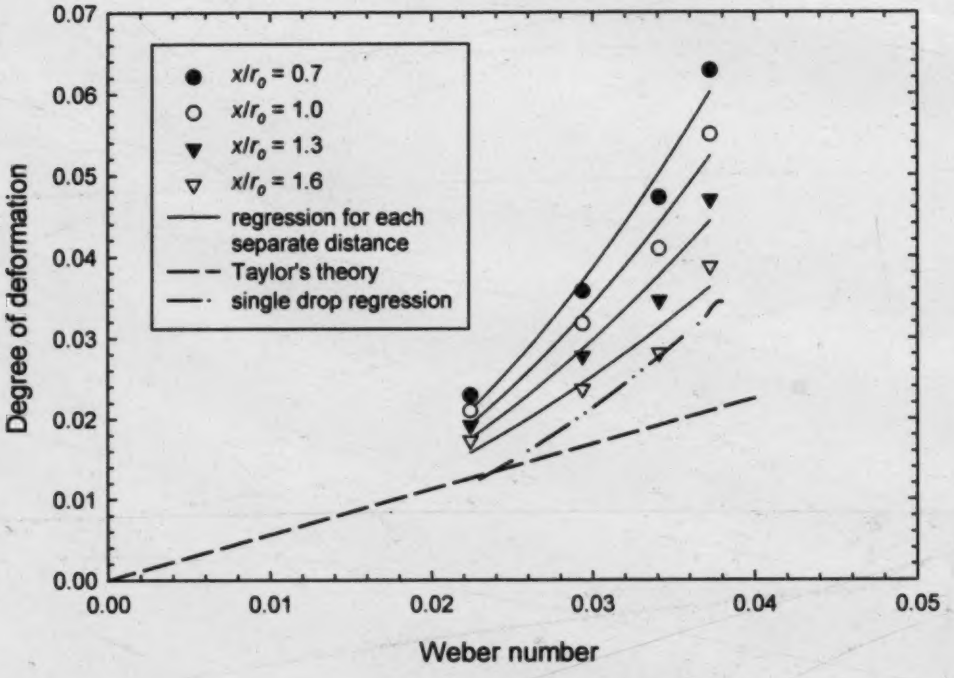

Figure 5.20. Degree of deformation as a funciton of weber number for a water drop pair aged 30 minutes in toluene solution (0.5% vol. bitumen added)

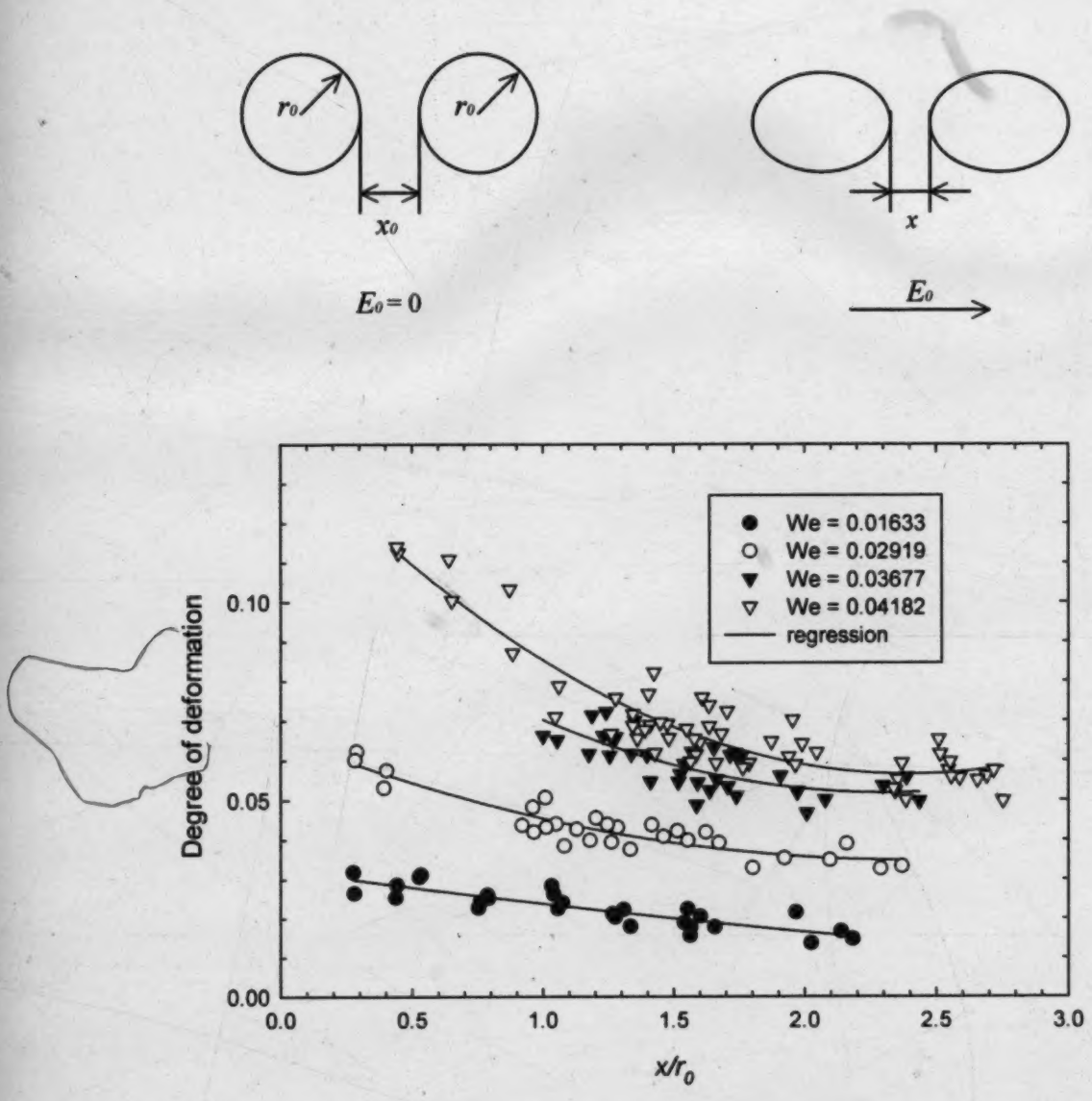

Figure 5.21. Degree of deformation as a function of distance with different Weber numbers for a water drop pair aged 30 minutes in toluene solution (1.5% vol. bitumen added)

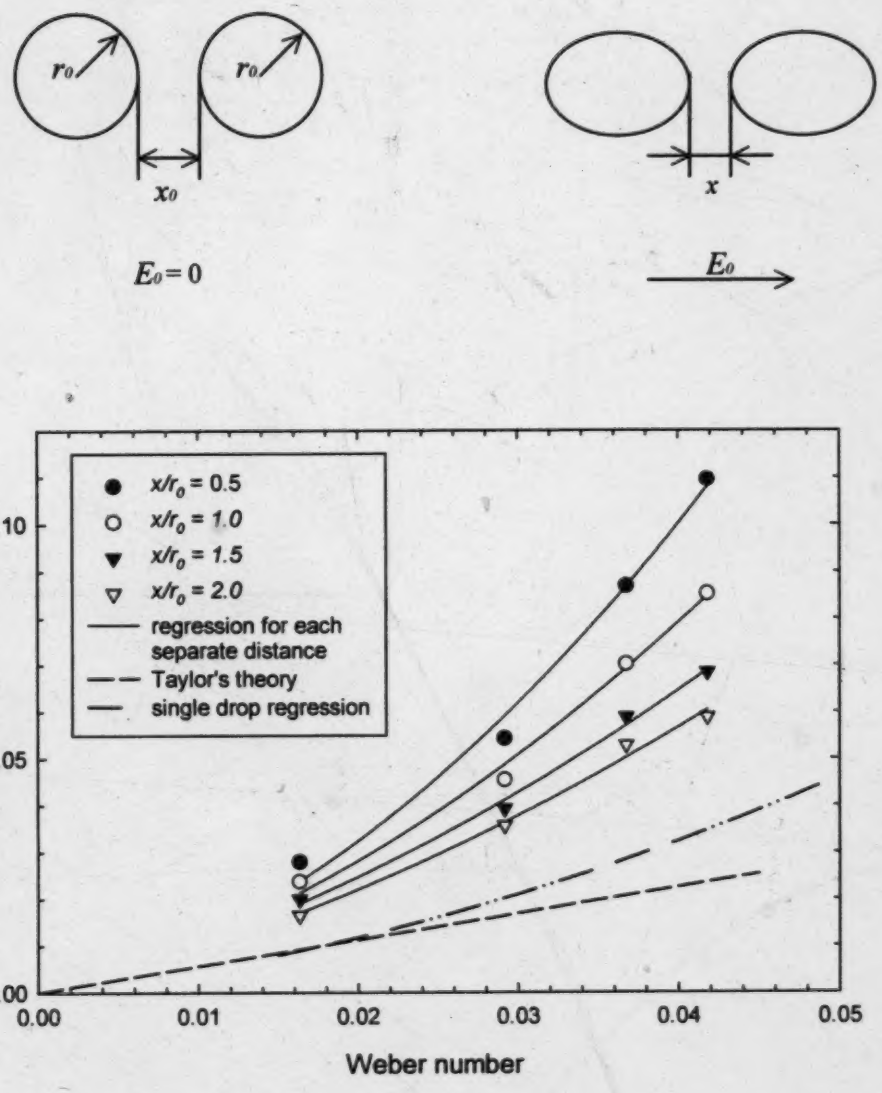

Figure 5.22. Degree of deformation as a function of Weber number for a water drop pair aged 30 minutes in toluene solution (1.5% vol. bitumen added)

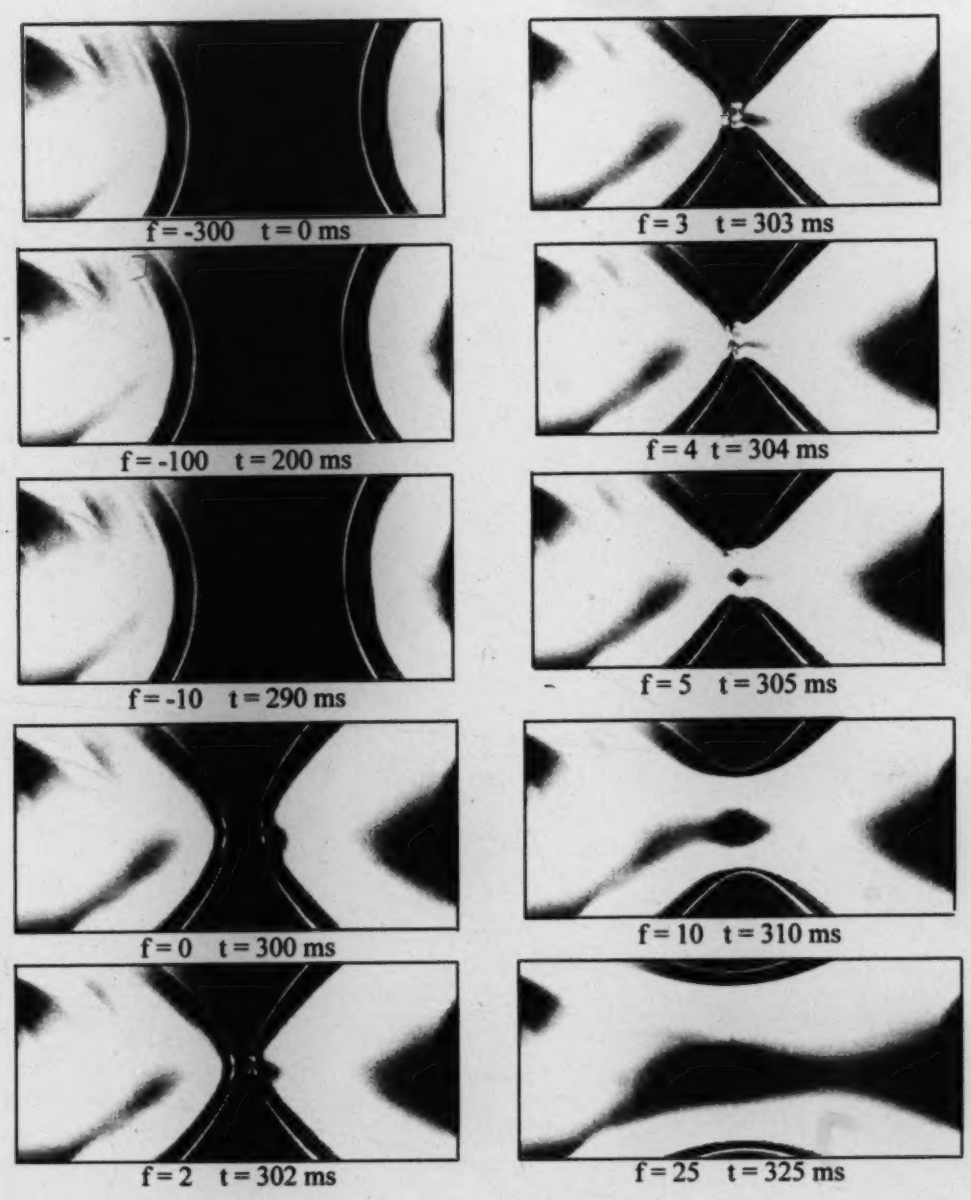

Figure 5.23 Coalescence process of a water drop pair in 2-ethyl-1, 3-hexanediol under an electric field (E = 0.515 kV/cm)
(f is the frame number, t is the time)

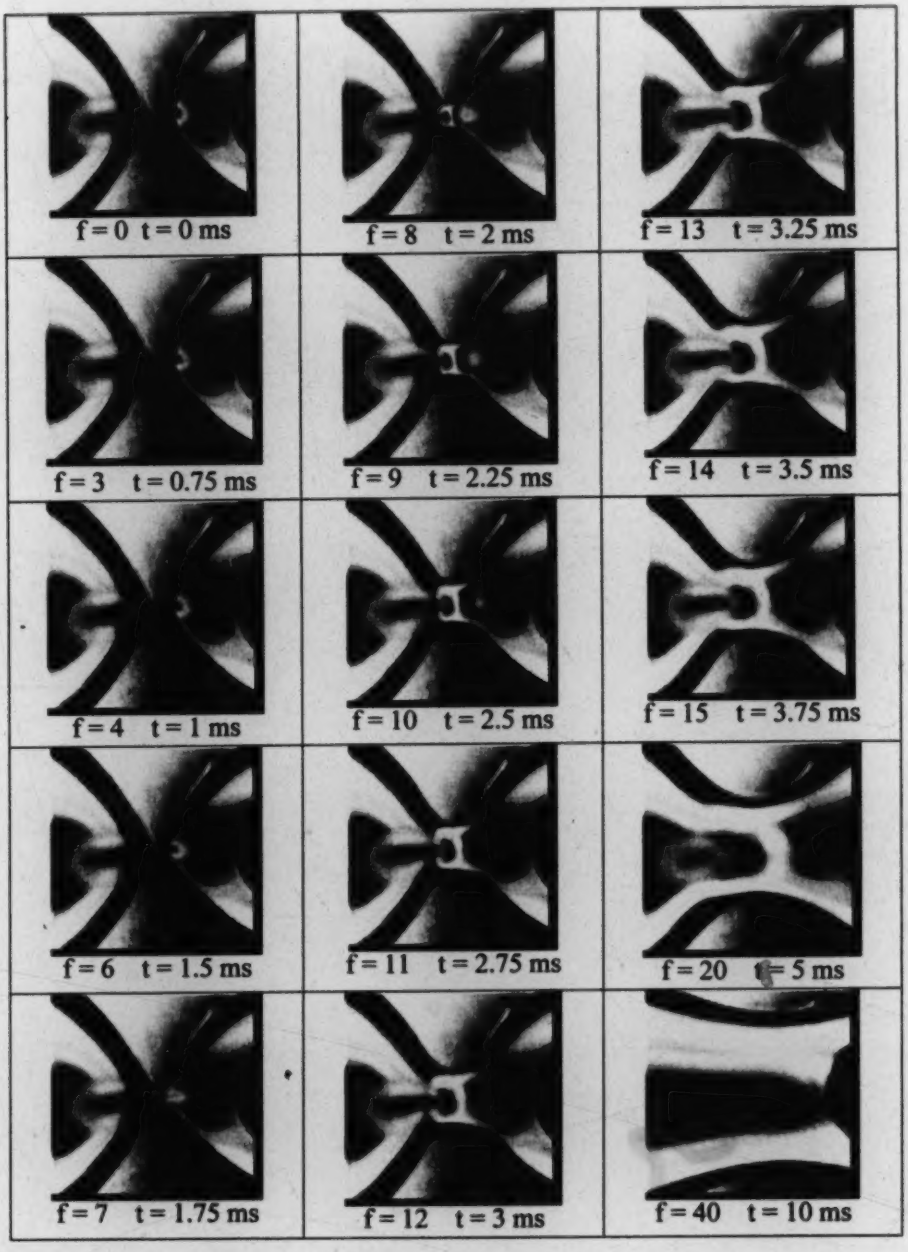
f = 0 t = 0 ms
f = 8 t = 2 ms
f = 13 t = 3.25 ms
f = 3 t = 0.75 ms
f = 9 t = 2.25 ms
f = 14 t = 3.5 ms
f = 4 t = 1 ms
f = 10 t = 2.5 ms
f = 15 t = 3.75 ms
f = 6 t = 1.5 ms
f = 11 t = 2.75 ms
f = 20 t = 5 ms
f = 7 t = 1.75 ms
f = 12 t = 3 ms
f = 40 t = 10 ms

Figure 5.24 Coalescence process of a water drop pair in decyl alcohol under an electric field (E = 1.031 kV/cm)
(f is the frame number, t is the time)

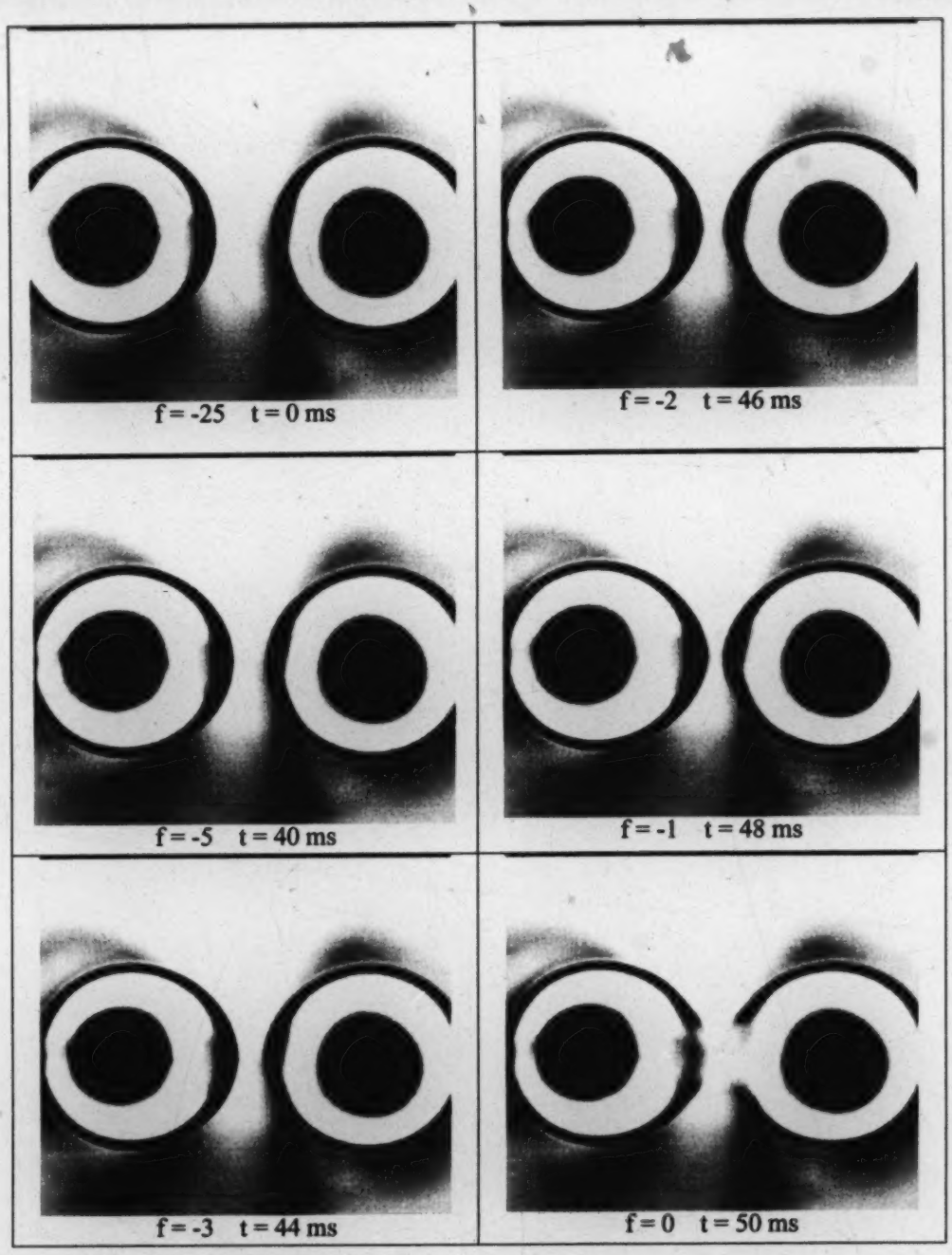

Figure 5.25 Coalescence process of a water drop pair in heptane-toluene (1:1) solution (1.5% vol. bitumen added) under an electric field (E = 3.350 kV/cm) (f is the frame number, t is the time)

Figure 5.25. (continued)

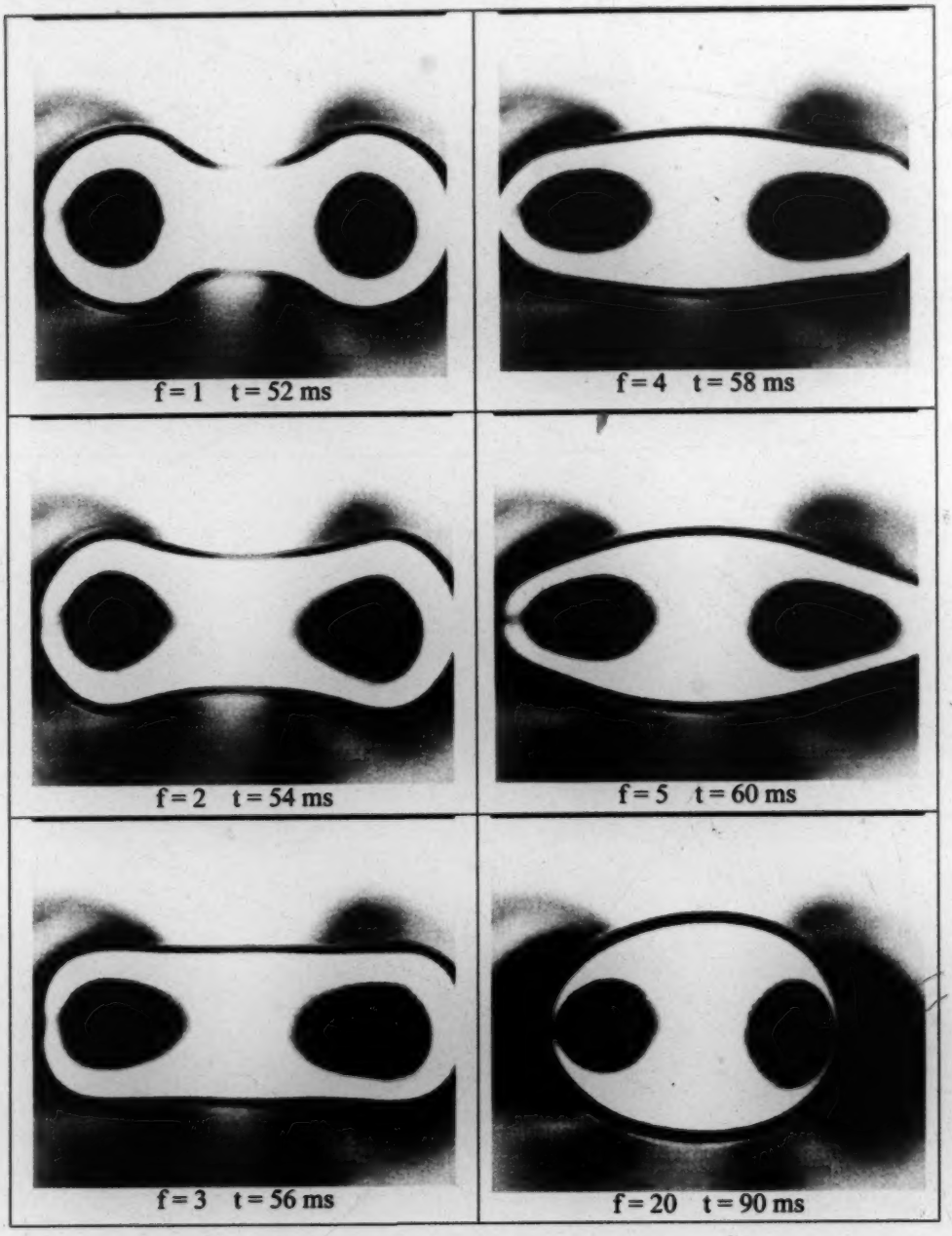

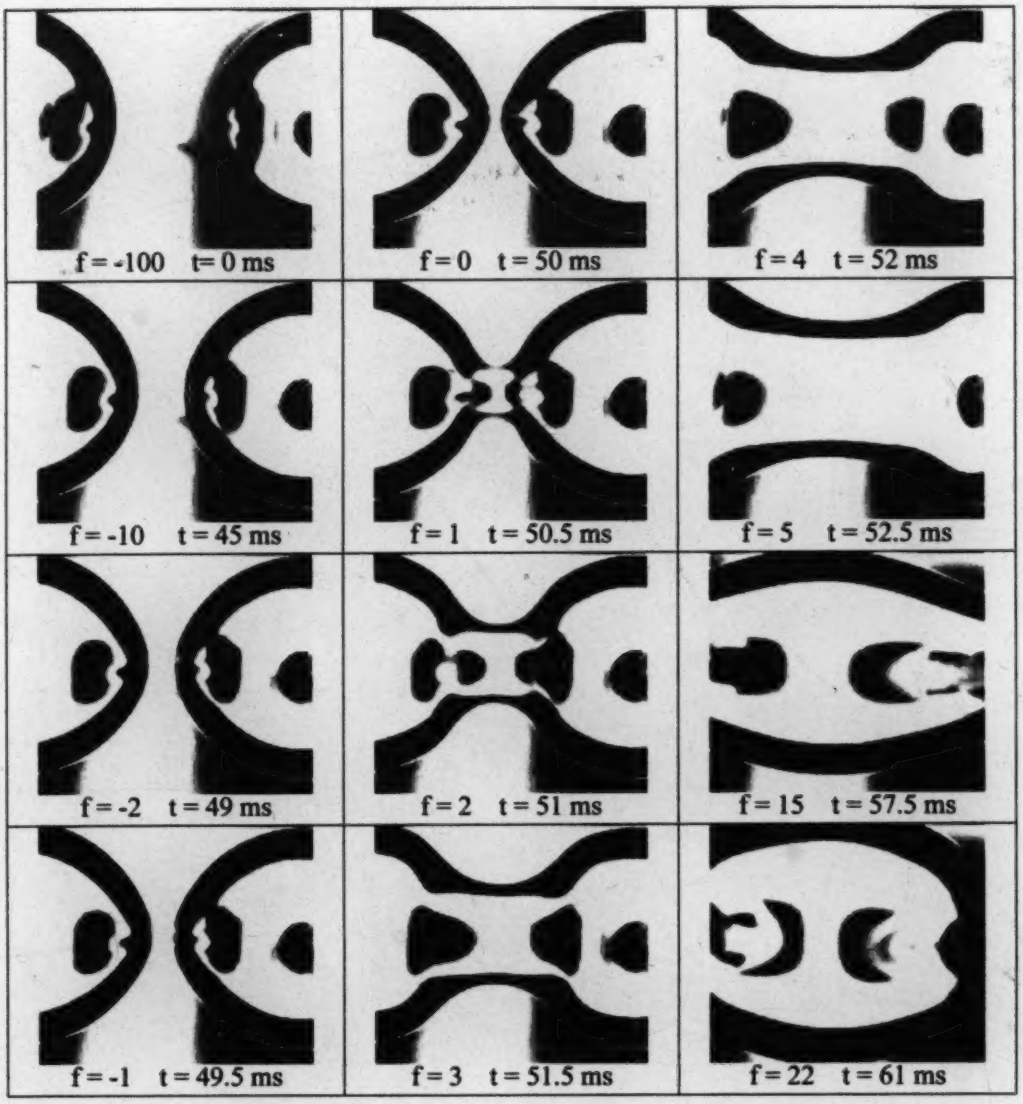

Figure 5.26 Coalescence process of a water drop pair in toluene solution (0.3% vol. bitumen added) under an electric field (E = 3.093 kV/cm) (f is the frame number, t is the time)

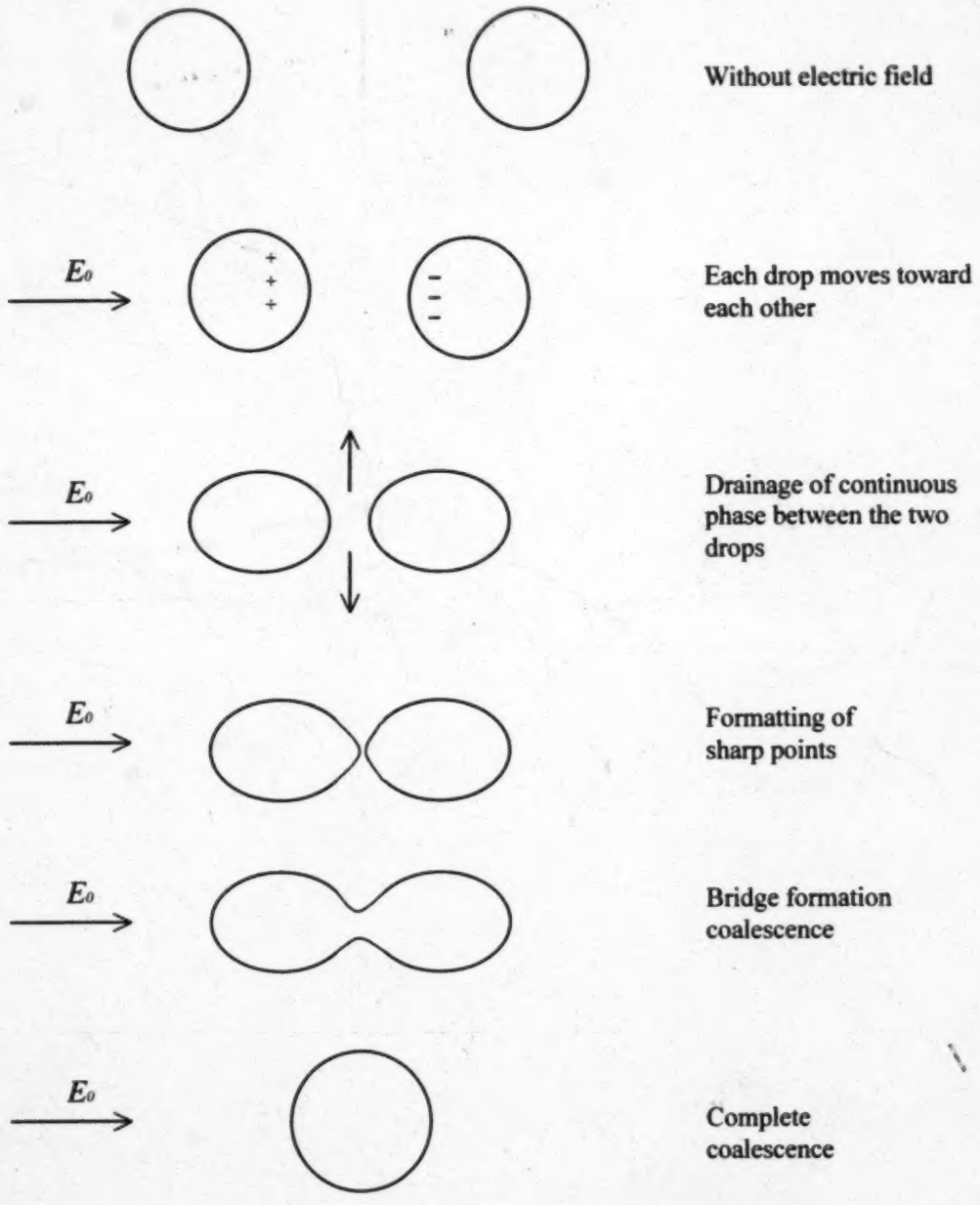

Figure 5.27. Depiction of water drops coalescence in hydrocarbon medium under an electric field

Chapter 6

Summary, Conclusions and Recommendations

6.1 Review of Problem and Objectives

Petroleum is currently one of the most important and common source of energy. As the conventional crude oil resources diminish, oil sands are playing an increasingly important role as an alternative energy source. One of the common problems in oil sands processing is the formation of very stable water-in-diluted bitumen emulsions.

Centrifuge is commonly used in the oil sands industry to eliminate the water droplets in the emulsions. However, because of the high operational and maintenance costs, it is desirable to have an alternative method of demulsification. Electrical method is considered in breaking the water-in-oil emulsions during bitumen extraction. An effective design of electrical coalescer could only be realized if the mechanism of drop coalescence is understood. This study was carried out with that objective in mind.

The first step in studying the electrical demulsification method is to examine the deformation behavior of single water drops and water drop pairs in an electric field. Model oils and diluted bitumen were chosen as the continuous phases. First, the relationship between the degree of deformation and the applied electric field strength was investigated for single water drops as well as water drop pairs. The effects of aging on deformation were also studied. As there are natural surfactants present in bitumen, the effects of surfactants on deformation was also studied. Finally, sequences of video images showing the coalescence of water drops in oil were recorded.

6.2 Conclusions/Summary of Experimental Results

The conclusions obtained for each objective are as follows:

6.2.1 Study of Deformation Behavior of Single Water Drops

The deformation of a water drop in a hydrocarbon medium was investigated by measuring its degree of deformation at different electric field strengths. Since the conductivity of water is much higher than that of the continuous phase, the water drop can be considered a conducting drop. When the conductivity ratio is very large (roughly $R > 100$), the electrohydrostatic assumption is valid. The reader is referred to section 2.1.1 for an explanation of the electrohydrostatic assumption. The induced fluid flow is very weak. Viscosity ratio and dielectric constant ratio are not important parameters within the small deformation limit.

Within the limit of small deformations, the degree of deformation is proportional to the Weber number [Taylor, 1966]. As the electric field strength increases, deviations from Taylor's theoretical prediction become more pronounced. This is reasonable as Taylor assumed that the drop shape deviated only slightly from a sphere in his original derivation. Feng & Scott's numerical results predicted the experimental data better than Taylor's theory, especially in the range of high electric field strengths [Feng and Scott, 1996]. Their analysis was not limited to creeping flow or small deformation. Through numerical techniques, Feng and Scott were able to account for finite inertial effects and large deformations.

Four diluted bitumen systems were used as the continuous phase by adding different amounts of bitumen to toluene. Different aging times (either zero or 30 minutes) were applied to the system for comparison. After 30 minutes, it is assumed that

more surfactants in the bitumen are adsorbed onto the water drop, thus aged water drops deform less when compared with fresh water drops at the same Weber number.

The roles of surfactants in drop deformation were also investigated. The water drop with SDS added in decyl alcohol system tended to deform less at the same Weber number when compared with the case with no surfactants. The experimental results suggest that Marangoni flow is not appreciable in the system of a water drop in decyl alcohol. However, for the other systems (a water drop in toluene with sodium naphthenate added to the aqueous phase & a water drop in diluted bitumen), the experimental data suggested that the surfactants may also induce Marangoni flow. With more bitumen added to the continuous phase, we may assume more surfactants are adsorbed onto the water drop and the protective layer will therefore become thicker. The protective layer may behave as a viscoelastic film. That might explain why the water drop deformed less at the same Weber number while more bitumen were added.

6.2.2 Study of Deformation Behavior of Water Drop Pairs

In this study, the deformation of a water drop pair in decyl alcohol and diluted bitumen is investigated. Qualitative conclusions are obtained from the experimental results, namely, the drop deformation behavior will deviate noticeably from the single drop's behavior when the separation distance is less than one radius of the undeformed drop. If two drops are far apart from each other (separation distance greater than several times the drop radius), the drops could be considered as independent entities.

6.2.3 Study of the Coalescence of Water Drops

When no electric field is applied between two water drops in diluted bitumen, the drops will not coalesce even if one drop was pushed very hard against the other.

However, in an electric field of 1 kV/cm, the water drops coalesced in 0.1s. The polarization charges induced by the electric field on the water drops moved the two drops toward each other. This could be clearly seen from the photographs taken during the coalescence of water drops in an electric field. The much-enhanced electric field between the water drops may help to break the surfactant protective layer at the tip of the water drops.

6.3 Recommendations for Future Work

This study provided some information on the conditions that might affect the coalescence of water drops in bitumen. However, many questions are also raised:

- Will the deformation behavior be different for μm sized water drops under the same electric field?

The water drops being tested were millimeters in size, as were those tested by Allan & Mason(1962), Torza, Cox & Mason (1971), Vizika & Saville(1992) and Ha & Yang(1998). Feng & Scott(1996) also used 1mm as the drop radius in their numerical study. In all of these studies, the diffuse charges could be considered present only at the interface, as the drop radius is very large compared to the Debye length. For emulsion drops that are μm size, the distribution of diffuse charges across the interface needs to be considered. The deformation behavior of such small drops need to be tested in the model system and in the diluted bitumen system to make comparison with the results obtained here.

- What are the effects of the electric field on the coalescence of water drops in W/O emulsions? What happens when W/O emulsions are in bulk flow?

Future experiments to elucidate what happens in the situation of W/O emulsions will be a necessary complement to understanding the mechanism of electrical

coalescence. Moreover, experimental research is needed in the future to understand the effects of electric fields on water drop coalescence when W/O emulsions are in bulk flow.

- How are ionic surfactants distributed at the surfaces of the water drops in the presence of an electric field? What are their effects on the deformation and coalescence of water drops?

It is clear that surfactants play an important role in the coalescence process. Therefore, it is essential to obtain a better understanding of the distribution of ionic surfactants at the surface of the drops and its effects on deformation and coalescence. Experiments under different conditions could be performed to further investigate the effects of ionic surfactants.

References

1. Adamson, A. W. 1990 *Physical Chemistry of Surfaces*, 5th ed. John Wiley. New York
2. Ajayi, O. O. 1978 A note on Taylor's electrohydrodynamic theory. *Proc. R. Soc. Lond. A* **364**, 499-507
3. Allan, R. S. & Mason, S. G. 1962 Particle behavior in shear and electric fields. I. Deformation and burst of fluid drops. *Proc. Roy. Soc. Lond. A* **267**, 45-61
4. Baygents, J. C. & Saville, D. A. 1989 The circulation produced in a drop by an electric field: a high field strength electrokinetic model. *AIP Conf. Proc., Third Intl. Colloquium on Drops and Bubbles* **197**, 7-17
5. Baygents, J. C., Rivette, N. J. & Stone, H. A. 1998 Electrohydrodynamic deformation and interaction of drop pairs. *J. Fluid Mech.* **368**, 359-375
6. Bradley, H. B. 1987 *Petroleum Engineering Handbook*, Society of Petroleum Engineers. Richardson. Chapter 19
7. Brazier-Smith, P. R., Jennings, S. G. & Latham, J. 1971 An investigation of the behavior of drops and drop-pairs subjected to strong electrical forces. *Proc. R. Soc. Lond. A.* **325**, 363-376
8. Davis, W. H. 1964 Two charged spherical conductors in a uniform electric field: forces and field strength. *Quart. J. Mech. Appl. Math.* **17**, 499
9. Feng, J. Q. & Scott, T. C. 1996 Á computational analysis of electrohydrodynamics of a leaky dielectric drop in an electric field. *J. Fluid Mech.* **311**, 298-326
10. Ha, J. & Yang, S. 1995 Effects of surfactant on the deformation and stability of a drop in a viscous fluid in an electric field. *J. Colloid* and *Interface Sci.* **175**, 369-385
11. Ha, J. & Yang, S. 1998 Effect of nonionic surfactant on the deformation and breakup of a drop in an electric field. *J. Colloid and Interface Sci.* **206**, 195-204
12. Harkins, W. D. & Jordan H. F. 1930 A method for the determination of surface and interfacial tension from the maximum pull on a ring, *J. Amer. Chem. Soc.* **52**, 1751

13. Hartland, S. & Hartley R. W. 1976 *Axisymmetric Fluid-liquid Interfaces*. Elsevier. Amsterdam

14. Kwok, D. Y., Vollhardt, D., Miller, R., Li, D. & Neumann, A. W. 1994 Axisymmetric drop shape analysis as a film balance. *Colloids and Surfaces, A.* **88**, 51-58

15. Latham, J. & Roxburgh, I. W. 1966 Disintegration of pairs of water drops in an electric field. *Proc. R. Soc. Lond. A* **295**, 84-97

16. Li, D. & Neumann, A. W. 1992 Contact angle measurement by axisymmetric drop shape analysis (ADSA). *Advances in Colloid and Interface Science.* **39**, 347-382

17. Masliyah, J. H. 2000 *Extraction of Oil Sands Bitumen*, short course material, Edmonton, Alberta

18. Melcher, J. R. & Taylor, G. I. 1969 Electrohydrodynamics: a review of the role of interfacial shear stresses. *Ann. Rev. Fluid Mech.* **1**, 111-146

19. McLean, J. D., Spikecker, P. M., Sullivan, A. P. & Kilpatrick, P. K. 1998 *Structures and Dynamics of Asphaltenes*. Editor Mullins, C. O. & Sheu, Y. E. Plenum Press. New York. Chapter XII

20. Outrim, C. P. & Evans, R. G. 1977 *Alberta's Oil Sands Reserves and Their Evaluation*. Oil Sands of Canada-Venezuela, CIM Special Issue, Volume 17

21. Ptasinski, K. J. & Kerkhof, P. 1992 Electric field driven separations: phenomena and applications. *Separation Sci. and Tech.* **27**, 995-1021

22. Shaw, D. J. 1980 *Introduction to Colloid and Surface Chemistry*. 3rd ed. Butterworths

23. Sozou, C. 1975 Electrohydrodynamics of a pair of liquid drops. *J. Fluid Mech.* **67**, 339-348

24. Strausz, O. P. 1989 *AOSTRA Technical Handbook of Oil Sands, Bitumen and Heavy Oil*. AOSTRA Technical Publications Series #6, Edmonton

25. Taylor, G. 1966 Studies in electrohydrodynamics. I. The circulation produced in a drop by an electric field. *Proc. R. Soc. Lond. A* **291**, 159-166

26. Taylor, G. 1968 The coalescence of closely spaced drops when they are at different electric potentials. *Proc. Roy. Soc. A.* **306**, 423-434

27. Tipman, R. N. & Shaw, R. C. 1993 *Recent Advances in the Treatment of Oil Sands Froth*. AOSTRA. Edmonton. Alberta

28. Torza, S., Cox, R. G. & Mason, S. G. 1971 Electrohydrodynamic deformation and burst of liquid drops. *Phil. Trans. R. Soc. Lond. A* **269**, 295-319

29. Tsukada, T., Sato, M., Imaishi, N., Hozawa, M. & FujiNawa, K. 1986 Static drop formation in an electrostatic field. *J. Chem. Eng. Jpn.* **19**, 537-542

30. Tsukada, T., Yamamoto, Y., Katayama, T. & Hozawa, M. 1994 Effect of an electric field on the behavior of a drop moving in a quiescent liquid. *J. Chem. Eng. Jpn.* **27**, 662-666

31. Tsukada, T., Mayama, J., Sato, M. & Hozawa, M. 1997 Theoretical and experimental studies on the behavior of a compound drop under a uniform DC electric field. *J. Chem. Eg. Jpn.* **30**, 215-222

32. Vizika, O. & Saville, D. A. 1992 The electrohydrodynamic deformation of drops suspended in liquids in steady and oscillatory electric fields. *J. Fluid Mech.* **239**, 1-21

33. Waterman, L. C. 1965 Electrical coalescers. *Chem. Eng. Prog.* **61**(10), 51-57

34. Yan, Z. L. 1999 *Interfacial Behavior of De-asphalted Bitumen*, MSc thesis, University of Alberta

35. Yarranton, H. W. 1997 *Asphaltene Solubility and Asphaltene Stabilized Water-in-Oil Emulsions*, PhD thesis, University of Alberta

36. Yeung, A., Dabros, T., Czarnecki, J. & Masliyah, J. 1999 On the interfacial properties of micro-sized water droplets in crude oil, *Proc. Royal Soc. Lond. A*, **455**, 3709-3723

37. Zhang, X. & Basaran, O. A. 1995 Electric field-enhanced coalescence of liquid drops. *Separation Sci. & Tech.* **30**, 1169-1187

38. Zhou, J, 2000 Private communication

Appendix I

Raw Data for the Figures Included in the Thesis

Figure 3.6. Time dependence of the interfacial tension of diluted bitumen solution over water

Solvent	Time (minute)	Interfacial tension (mN/m)
2.0% vol. bitumen in toluene	4.00	23.32
	6.50	23.18
	8.50	23.10
	11.50	22.97
	16.50	22.86
	26.50	22.59
	41.50	22.35
	56.50	22.16
1.5% vol. bitumen in toluene	4.00	24.39
	6.75	24.20
	9.50	24.03
	13.50	23.82
	16.50	23.70
	21.50	23.53
	31.50	23.18
	50.00	22.70
	62.50	22.50
1.0% vol. bitumen in toluene	4.00	25.15
	6.25	24.83
	8.75	24.61
	11.00	24.45
	15.00	24.23
	20.00	24.02
	30.00	23.69
	45.00	23.39
	60.00	23.18

Figure 3.6. (continued)

Solvent	Time (minute)	Interfacial tension (mN/m)
0.5% vol. bitumen in toluene	4.50	25.54
	7.00	25.39
	9.50	25.25
	14.00	25.06
	20.00	24.83
	30.00	24.54
	45.00	24.26
	60.00	24.05
1.0% vol. bitumen in toluene and hexane (1:1)	3.50	26.75
	5.50	26.66
	7.50	26.56
	9.75	26.48
	15.25	26.34
	20.00	26.23
	30.00	26.06
	45.00	25.87
	60.00	25.75
	70.00	25.69
Toluene	4.00	35.74
	6.50	35.55
	10.75	35.28
	15.25	35.01
	20.00	34.76
	30.00	34.39
	45.00	33.99
	60.00	33.71

Figure 3.7. Equilibrium interfacial tension of toluene over water with different concentration of sodium naphthenate (aqueous) added to water

1 ml surfactant added to different amount of water (ml)	Volume concentration (ml/ml)	Interfacial tension (mN/m)
750	1.33e-3	27.43
500	2.00e-3	26.05
250	4.00e-3	20.90
100	0.01	11.77

Figure 5.1. Degree of deformation as a function of Weber number for a single water drop in decyl alcohol

Drop length along parallel axis, a (mm)	Drop length along perpendicular axis, b (mm)	Degree of deformation, D	Applied voltage (kV)	Weber number
Experiment 1				
Undeformed radius r_0 = 0.628 mm				
1.273	1.233	0.016	0.500	0.014
1.285	1.230	0.022	0.800	0.035
1.303	1.212	0.036	1.000	0.055
1.321	1.191	0.052	1.200	0.080
1.339	1.174	0.066	1.300	0.094
1.370	1.155	0.085	1.400	0.109
1.394	1.131	0.104	1.500	0.125
1.406	1.134	0.107	1.600	0.142
1.430	1.115	0.124	1.700	0.160
1.455	1.088	0.144	1.800	0.180
Undeformed radius r_0 = 0.721 mm				
1.473	1.409	0.022	0.500	0.016
1.497	1.385	0.039	1.000	0.064
1.527	1.365	0.056	1.200	0.092
1.558	1.338	0.076	1.400	0.125
1.618	1.295	0.111	1.500	0.143
Undeformed radius r_0 = 0.794 mm				
1.624	1.551	0.023	0.500	0.018
1.685	1.494	0.060	0.999	0.070
1.715	1.461	0.080	1.199	0.101
1.770	1.430	0.106	1.398	0.137
Experiment 2				
Undeformed radius r_0 = 0.774 mm				
1.569	1.537	0.010	0.500	0.017
1.606	1.512	0.030	0.800	0.044
1.648	1.487	0.051	1.000	0.068
1.678	1.481	0.062	1.100	0.082
1.703	1.475	0.072	1.200	0.098

Figure 5.1 (continued)

Drop length along parallel axis, a (mm)	Drop length along perpendicular axis, b (mm)	Degree of deformation, D	Applied voltage (kV)	Weber number
Undeformed radius r_0 = 1.011 mm				
2.066	2.012	0.013	0.500	0.022
2.139	1.987	0.037	0.800	0.057
2.206	1.937	0.065	1.000	0.089
2.254	1.925	0.079	1.100	0.108
2.321	1.894	0.101	1.200	0.128
2.400	1.862	0.126	1.300	0.150
Undeformed radius r_0 = 0.742 mm				
1.503	1.481	0.007	0.500	0.016
1.545	1.469	0.025	0.800	0.042
1.576	1.425	0.050	1.000	0.065
1.606	1.419	0.062	1.100	0.079
1.636	1.412	0.073	1.200	0.094
1.654	1.394	0.085	1.300	0.110
1.673	1.387	0.093	1.400	0.128
1.721	1.362	0.116	1.500	0.147
1.775	1.344	0.138	1.600	0.167
Undeformed radius r_0 = 0.884 mm				
1.806	1.743	0.017	0.500	0.012
1.860	1.731	0.036	0.800	0.050
1.909	1.712	0.054	1.000	0.078
1.945	1.693	0.069	1.100	0.094
1.975	1.681	0.080	1.200	0.112
2.036	1.675	0.097	1.300	0.131

Note: Electrode distance for the single drop is 0.954 cm

Figure 5.2. Degree of deformation as a function of Weber number for a single water drop in diethyl phthalate

Drop length along parallel axis, a (mm)	Drop length along perpendicular axis, b (mm)	Degree of deformation, D	Applied voltage (kV)	Weber number
Experiment 1				
Undeformed radius r_0 = 0.854 mm				
1.764	1.688	0.022	1.000	0.045
1.776	1.656	0.035	1.200	0.065
1.806	1.650	0.045	1.300	0.076
1.824	1.644	0.052	1.400	0.088
1.836	1.638	0.057	1.500	0.101
1.867	1.631	0.067	1.600	0.115
1.879	1.625	0.072	1.700	0.130
Undeformed radius r_0 = 0.900 mm				
1.855	1.763	0.025	1.000	0.047
1.861	1.738	0.034	1.200	0.068
1.915	1.725	0.052	1.400	0.093
1.952	1.688	0.073	1.600	0.122
2.006	1.656	0.096	1.800	0.154
Undeformed radius r_0 = 0.668 mm				
1.370	1.319	0.019	1.000	0.035
1.376	1.306	0.026	1.300	0.060
1.412	1.275	0.051	1.600	0.090
1.436	1.256	0.067	1.800	0.114
1.485	1.231	0.093	2.000	0.141
Undeformed radius r_0 = 0.838 mm				
1.721	1.644	0.023	1.000	0.044
1.770	1.625	0.043	1.300	0.075
1.818	1.588	0.068	1.600	0.113
1.867	1.569	0.087	1.800	0.143

Figure 5.2. (continued)

Drop length along parallel axis, a (mm)	Drop length along perpendicular axis, b (mm)	Degree of deformation, D	Applied voltage (kV)	Weber number
Experiment 2				
Undeformed radius r_0 = 0.768 mm				
1.552	1.506	0.015	0.800	0.026
1.564	1.500	0.021	1.000	0.040
1.570	1.488	0.027	1.100	0.049
1.576	1.481	0.031	1.200	0.058
1.588	1.463	0.041	1.300	0.068
1.600	1.456	0.047	1.400	0.079
1.612	1.450	0.053	1.500	0.091
1.630	1.444	0.061	1.600	0.104
Undeformed radius r_0 = 0.803 mm				
1.667	1.613	0.017	0.800	0.027
1.685	1.606	0.024	1.000	0.042
1.709	1.600	0.033	1.100	0.051
1.721	1.594	0.038	1.200	0.061
1.733	1.588	0.044	1.300	0.072
1.745	1.575	0.051	1.400	0.083
1.770	1.569	0.060	1.500	0.095
1.788	1.556	0.069	1.600	0.108
Undeformed radius r_0 = 0.982 mm				
1.988	1.944	0.011	0.700	0.025
2.018	1.938	0.020	0.900	0.042
2.036	1.919	0.030	1.000	0.052
2.042	1.913	0.033	1.100	0.063
2.091	1.906	0.046	1.200	0.075
2.109	1.900	0.052	1.300	0.087
2.121	1.894	0.057	1.400	0.101
2.152	1.881	0.067	1.500	0.116
Undeformed radius r_0 = 0.722 mm				
1.461	1.425	0.012	0.800	0.024
1.485	1.419	0.023	1.000	0.038
1.497	1.406	0.031	1.200	0.055
1.509	1.394	0.040	1.300	0.064
1.515	1.381	0.046	1.400	0.075

Figure 5.2. (continued)

Drop length along parallel axis, a (mm)	Drop length along perpendicular axis, b (mm)	Degree of deformation, D	Applied voltage (kV)	Weber number
Undeformed radius r_0 = 0.791 mm				
1.618	1.569	0.016	0.800	0.027
1.630	1.556	0.023	1.000	0.042
1.679	1.575	0.032	1.100	0.050
1.733	1.588	0.044	1.200	0.060
1.733	1.588	0.044	1.300	0.070
Undeformed radius r_0 = 0.860 mm				
1.733	1.681	0.015	0.800	0.029
1.739	1.650	0.026	1.000	0.045
1.752	1.644	0.032	1.100	0.055
1.758	1.638	0.035	1.200	0.065
1.776	1.631	0.042	1.300	0.077
1.788	1.625	0.048	1.400	0.089
1.800	1.613	0.055	1.500	0.102

Note: Electrode distance for the single drop is 0.954 cm

Figure 5.3. Degree of deformation as a function of Weber number for a single water drop in cycloheptanone

Drop length along parallel axis, a (mm)	Drop length along perpendicular axis, b (mm)	Degree of deformation, D	Applied voltage (kV)	Weber number
Experiment 1				
Undeformed radius		$r_0 = 0.920$ mm		
1.903	1.812	0.024	0.400	0.027
1.921	1.787	0.036	0.500	0.043
1.981	1.756	0.060	0.600	0.061
2.072	1.725	0.091	0.700	0.083
Undeformed radius		$r_0 = 0.732$ mm		
1.503	1.431	0.024	0.400	0.022
1.503	1.412	0.031	0.500	0.034
1.533	1.406	0.043	0.600	0.048
1.575	1.387	0.063	0.700	0.066
1.636	1.343	0.098	0.800	0.087
Undeformed radius		$r_0 = 0.812$ mm		
1.660	1.612	0.015	0.400	0.024
1.678	1.593	0.026	0.500	0.034
1.763	1.581	0.054	0.600	0.054
1.812	1.556	0.076	0.700	0.074
1.878	1.512	0.108	0.800	0.096
Undeformed radius		$r_0 = 0.800$ mm		
1.648	1.568	0.025	0.400	0.024
1.678	1.556	0.038	0.500	0.037
1.703	1.531	0.053	0.600	0.053
1.763	1.512	0.076	0.700	0.073
1.872	1.462	0.123	0.800	0.095
Undeformed radius		$r_0 = 0.798$ mm		
1.648	1.575	0.023	0.400	0.024
1.672	1.568	0.032	0.500	0.037
1.733	1.556	0.054	0.600	0.053
1.775	1.550	0.068	0.700	0.072
1.866	1.512	0.105	0.800	0.095

Figure 5.3 (continued)

Drop length along parallel axis, a (mm)	Drop length along perpendicular axis, b (mm)	Degree of deformation, D	Applied voltage (kV)	Weber number
Experiment 2				
Undeformed radius r_0 = 0.786 mm				
1.612	1.562	0.016	0.400	0.023
1.618	1.543	0.023	0.500	0.036
1.660	1.512	0.047	0.600	0.052
1.690	1.487	0.064	0.700	0.071
1.751	1.437	0.098	0.800	0.093
Undeformed radius r_0 = 0.818 mm				
1.660	1.618	0.013	0.200	0.006
1.684	1.606	0.024	0.400	0.024
1.709	1.587	0.037	0.500	0.038
1.727	1.562	0.050	0.600	0.054
1.751	1.531	0.067	0.700	0.074
1.824	1.487	0.102	0.800	0.097
Undeformed radius r_0 = 0.768 mm				
1.563	1.506	0.019	0.300	0.013
1.569	1.493	0.025	0.400	0.023
1.587	1.462	0.041	0.500	0.035
1.600	1.450	0.049	0.600	0.051
1.624	1.406	0.072	0.700	0.067
1.672	1.375	0.098	0.800	0.091
Undeformed radius r_0 = 0.765 mm				
1.539	1.506	0.011	0.300	0.013
1.551	1.493	0.019	0.400	0.023
1.575	1.468	0.035	0.500	0.035
1.593	1.443	0.049	0.600	0.051
1.618	1.418	0.066	0.700	0.069
1.660	1.381	0.092	0.800	0.091
Undeformed radius r_0 = 0.766 mm				
1.551	1.518	0.011	0.200	0.006
1.557	1.518	0.013	0.300	0.013
1.575	1.500	0.024	0.400	0.023
1.587	1.475	0.037	0.500	0.035
1.600	1.443	0.051	0.600	0.051
1.648	1.418	0.075	0.700	0.070
1.678	1.387	0.095	0.800	0.091

Figure 5.3 (continued)

Drop length along parallel axis, a (mm)	Drop length along perpendicular axis, b (mm)	Degree of deformation, D	Applied voltage (kV)	Weber number
Undeformed radius $r_0 = 0.786$ mm				
1.575	1.537	0.012	0.300	0.013
1.593	1.518	0.024	0.400	0.023
1.612	1.512	0.032	0.500	0.036
1.630	1.481	0.048	0.600	0.052
1.648	1.456	0.062	0.700	0.070
1.697	1.418	0.089	0.800	0.092

Note: Electrode distance for the single drop is 0.954 cm

Figure 5.4. Degree of deformation as a function of Weber number for a single water drop in alpha-ionone

Drop length along parallel axis, a (mm)	Drop length along perpendicular axis, b (mm)	Degree of deformation, D	Applied voltage (kV)	Weber number
Experiment 1				
Undeformed radius $r_0 = 0.771$ mm				
1.557	1.525	0.011	0.600	0.017
1.551	1.506	0.015	0.800	0.030
1.575	1.487	0.029	1.000	0.046
1.600	1.468	0.043	1.100	0.056
1.612	1.456	0.051	1.200	0.067
1.630	1.437	0.063	1.300	0.079
1.684	1.406	0.090	1.400	0.091
Undeformed radius $r_0 = 0.779$ mm				
1.600	1.556	0.014	0.600	0.017
1.612	1.543	0.022	0.800	0.030
1.648	1.537	0.035	1.000	0.047
1.666	1.525	0.044	1.100	0.057
1.684	1.512	0.054	1.200	0.068
1.709	1.487	0.069	1.300	0.079
1.721	1.481	0.075	1.400	0.092
1.757	1.462	0.092	1.500	0.105
Experiment 2				
Undeformed radius $r_0 = 0.762$ mm				
1.551	1.512	0.013	0.600	0.016
1.557	1.493	0.021	0.800	0.029
1.563	1.481	0.027	1.000	0.046
1.569	1.462	0.035	1.100	0.055
1.593	1.443	0.049	1.200	0.066
1.606	1.437	0.055	1.300	0.078
1.618	1.406	0.070	1.400	0.090
1.642	1.381	0.086	1.500	0.103
Undeformed radius $r_0 = 0.802$ mm				
1.636	1.587	0.015	0.600	0.017
1.642	1.581	0.019	0.800	0.031
1.672	1.575	0.030	1.000	0.048
1.684	1.568	0.036	1.100	0.058
1.709	1.543	0.051	1.200	0.070
1.745	1.537	0.063	1.300	0.082
1.757	1.506	0.077	1.400	0.095

Note: Electrode distance for the single drop is 0.954 cm

Figure 5.5. Degree of deformation as a function of Weber number for a single water drop in cyclohexyl acétate

Drop length along parallel axis, a (mm)	Drop length along perpendicular axis, b (mm)	Degree of deformation, D	Applied voltage (kV)	Weber number
Experiment 1				
Undeformed radius r_0 = 0.996 mm				
2.023	1.962	0.015	0.800	0.022
2.049	1.949	0.025	1.000	0.034
2.062	1.938	0.031	1.100	0.042
2.080	1.927	0.038	1.200	0.050
Undeformed radius r_0 = 0.999 mm				
2.023	1.962	0.015	0.800	0.022
2.049	1.949	0.025	1.000	0.035
2.062	1.938	0.031	1.100	0.042
2.080	1.927	0.038	1.200	0.050
Undeformed radius r_0 = 0.964 mm				
1.955	1.901	0.014	0.700	0.016
1.966	1.890	0.020	0.900	0.027
1.979	1.885	0.024	1.000	0.033
1.994	1.874	0.031	1.100	0.040
2.010	1.858	0.039	1.200	0.048
2.020	1.852	0.043	1.300	0.056
2.041	1.842	0.051	1.400	0.065
Experiment 2				
Undeformed radius r_0 = 0.972 mm				
1.974	1.911	0.016	0.700	0.016
1.989	1.903	0.022	0.900	0.027
2.007	1.898	0.028	1.000	0.034
2.018	1.890	0.033	1.100	0.041
2.036	1.874	0.041	1.200	0.048
2.049	1.866	0.047	1.300	0.057
2.070	1.861	0.053	1.400	0.066

Figure 5.5 (continued)

Drop length along parallel axis, a (mm)	Drop length along perpendicular axis, b (mm)	Degree of deformation, D	Applied voltage (kV)	Weber number
Undeformed radius $r_0 = 0.971$ mm				
1.966	1.925	0.011	0.500	0.008
1.974	1.919	0.014	0.700	0.017
1.992	1.909	0.021	0.900	0.027
2.007	1.901	0.027	1.000	0.034
2.018	1.885	0.034	1.100	0.041
2.028	1.879	0.038	1.200	0.048
2.044	1.855	0.048	1.300	0.057
Undeformed radius $r_0 = 0.980$ mm				
1.979	1.933	0.012	0.500	0.008
1.992	1.927	0.016	0.700	0.017
2.010	1.914	0.024	0.900	0.028
2.015	1.906	0.028	1.000	0.034
2.036	1.901	0.034	1.100	0.041
2.046	1.890	0.040	1.200	0.049
2.065	1.885	0.045	1.300	0.057
2.078	1.869	0.053	1.400	0.066

Note: Electrode distance for the single drop is 0.954 cm

Figure 5.6. Degree of deformation as a function of Weber number for a single water drop in ethyl benzoate

Drop length along parallel axis, a (mm)	Drop length along perpendicular axis, b (mm)	Degree of deformation, D	Applied voltage (kV)	Weber number
Experiment 1				
Undeformed radius r_0 = 0.955 mm				
1.947	1.869	0.021	1.000	0.032
1.984	1.842	0.037	1.200	0.047
2.013	1.820	0.050	1.400	0.063
2.062	1.791	0.070	1.600	0.083
2.153	1.732	0.108	1.800	0.105
Undeformed radius r_0 = 0.999 mm				
1.854	1.815	0.011	0.700	0.015
1.872	1.796	0.021	1.000	0.031
1.901	1.788	0.030	1.200	0.045
1.932	1.746	0.051	1.400	0.061
1.994	1.735	0.070	1.600	0.079
2.062	1.705	0.095	1.800	0.100
Undeformed radius r_0 = 0.953 mm				
1.927	1.890	0.010	0.700	0.016
1.947	1.877	0.019	1.000	0.032
1.981	1.858	0.032	1.200	0.047
2.013	1.823	0.049	1.400	0.063
2.072	1.799	0.071	1.600	0.083
2.164	1.756	0.104	1.800	0.105
Experiment 2				
Undeformed radius r_0 = 0.951 mm				
1.953	1.866	0.023	1.000	0.032
1.971	1.852	0.031	1.200	0.046
2.008	1.842	0.043	1.400	0.063
2.070	1.791	0.072	1.600	0.083
2.166	1.754	0.105	1.800	0.104

Figure 5.6. (continued)

Drop length along parallel axis, a (mm)	Drop length along perpendicular axis, b (mm)	Degree of deformation, D	Applied voltage (kV)	Weber number
Undeformed radius r_0 = 0.956 mm				
1.941	1.883	0.015	0.700	0.016
1.953	1.871	0.021	1.000	0.032
1.972	1.852	0.031	1.200	0.047
1.996	1.828	0.044	1.400	0.064
2.043	1.781	0.069	1.600	0.083
2.095	1.729	0.096	1.800	0.105
Undeformed radius r_0 = 0.950 mm				
1.921	1.879	0.011	0.700	0.016
1.941	1.859	0.022	1.000	0.032
1.960	1.840	0.032	1.200	0.046
1.985	1.815	0.045	1.400	0.063
2.028	1.772	0.068	1.600	0.082
2.079	1.721	0.094	1.800	0.104

Note: Electrode distance for the single drop is 0.954 cm

Figure 5.7. Degree of deformation as a function of Weber number for a single water drop in 2-ethyl-1,3-hexanediol

Drop length along parallel axis, a (mm)	Drop length along perpendicular axis, b (mm)	Degree of deformation, D	Applied voltage (kV)	Weber number
Experiment 1				
Undeformed radius r_0 = 0.951 mm				
1.929	1.842	0.023	0.300	0.047
1.979	1.812	0.044	0.400	0.084
2.036	1.775	0.068	0.500	0.131
2.179	1.711	0.120	0.600	0.189
Undeformed radius r_0 = 0.656 mm				
1.351	1.302	0.018	0.300	0.033
1.377	1.286	0.034	0.400	0.058
1.406	1.267	0.052	0.500	0.090
1.447	1.240	0.077	0.600	0.130
1.562	1.208	0.128	0.700	0.177
Experiment 2				
Undeformed radius r_0 = 0.761 mm				
1.544	1.486	0.019	0.300	0.038
1.575	1.465	0.036	0.400	0.067
1.645	1.441	0.066	0.500	0.105
1.744	1.414	0.104	0.600	0.151
Undeformed radius r_0 = 0.624 mm				
1.265	1.216	0.012	0.300	0.031
1.283	1.187	0.039	0.400	0.055
1.299	1.165	0.054	0.500	0.086
1.330	1.139	0.078	0.600	0.124
1.388	1.107	0.113	0.700	0.168
Undeformed radius r_0 = 0.705 mm				
1.411	1.326	0.031	0.300	0.035
1.455	1.307	0.054	0.400	0.062
1.559	1.264	0.104	0.600	0.140
1.632	1.213	0.147	0.700	0.190

Note: Electrode distance for the single drop is 0.954 cm

Figure 5.9. Degree of deformation as a function of Weber number for a single water drop in toluene with surfactants added

Drop length along parallel axis, a (mm)	Drop length along perpendicular axis, b (mm)	Degree of deformation, D	Applied voltage (kV)	Weber number
Water drop in toluene (with surfactant added to aqueous phase)				
Undeformed radius $r_0 = 0.889$ mm				
1.821	1.764	0.016	3.700	0.028
1.821	1.764	0.016	4.000	0.033
1.833	1.752	0.023	4.290	0.038
1.833	1.748	0.024	4.290	0.038
1.837	1.748	0.025	4.600	0.043
1.845	1.752	0.026	4.600	0.043
1.853	1.743	0.030	4.800	0.047
1.853	1.748	0.029	4.800	0.047
1.861	1.748	0.031	5.000	0.051
1.857	1.748	0.030	5.000	0.051
1.861	1.743	0.032	5.200	0.055
1.869	1.739	0.036	5.200	0.055
1.884	1.723	0.045	5.400	0.060
1.884	1.723	0.045	5.400	0.060
1.884	1.723	0.045	5.600	0.064
1.884	1.723	0.045	5.600	0.064
1.940	1.719	0.060	5.800	0.069

Figure 5.9 (continued)

Drop length along parallel axis, a (mm)	Drop length along perpendicular axis, b (mm)	Degree of deformation, D	Applied voltage (kV)	Weber number
Undeformed radius $r_0 = 0.882$ mm				
1.809	1.743	0.019	4.000	0.033
1.825	1.731	0.026	4.200	0.036
1.817	1.731	0.024	4.200	0.036
1.825	1.723	0.029	4.400	0.040
1.813	1.739	0.021	4.400	0.040
1.825	1.719	0.030	4.600	0.043
1.821	1.723	0.028	4.600	0.043
1.837	1.727	0.031	4.800	0.047
1.861	1.711	0.042	4.800	0.047
1.853	1.715	0.039	5.000	0.051
1.853	1.715	0.039	5.000	0.051
1.881	1.703	0.050	5.200	0.055
1.841	1.707	0.038	5.200	0.055
1.877	1.699	0.050	5.400	0.059
1.881	1.711	0.047	5.400	0.059
1.928	1.695	0.064	5.600	0.064
1.936	1.674	0.072	5.600	0.064
2.000	1.678	0.087	6.000	0.073

Figure 5.9 (continued)

Drop length along parallel axis, a (mm)	Drop length along perpendicular axis, b (mm)	Degree of deformation, D	Applied voltage (kV)	Weber number
Undeformed radius $r_0 = 0.832$ mm				
1.658	1.609	0.015	4.000	0.031
1.674	1.593	0.025	4.400	0.037
1.686	1.577	0.034	4.700	0.042
1.682	1.589	0.029	4.700	0.042
1.678	1.573	0.032	4.990	0.048
1.682	1.573	0.034	4.990	0.048
1.682	1.561	0.037	5.200	0.052
1.694	1.565	0.040	5.200	0.052
1.702	1.556	0.045	5.400	0.056
1.718	1.561	0.048	5.400	0.056
1.710	1.548	0.050	5.600	0.060
1.706	1.548	0.048	5.600	0.060
1.718	1.544	0.053	5.800	0.065
1.750	1.540	0.063	5.800	0.065
1.730	1.544	0.056	6.000	0.069
1.761	1.524	0.072	6.000	0.069
1.761	1.520	0.074	6.200	0.074
1.746	1.520	0.069	6.200	0.074
1.813	1.512	0.091	6.200	0.074
1.777	1.512	0.081	6.400	0.079
1.845	1.500	0.103	6.400	0.079

Figure 5.9 (continued)

Drop length along parallel axis, a (mm)	Drop length along perpendicular axis, b (mm)	Degree of deformation, D	Applied voltage (kV)	Weber number
Water drop in toluene				
Undeformed radius r_0 = 0.843 mm				
1.738	1.674	0.019	4.200	0.021
1.750	1.662	0.026	4.500	0.024
1.754	1.666	0.025	4.500	0.024
1.781	1.662	0.035	4.800	0.027
1.765	1.658	0.031	4.800	0.027
1.817	1.642	0.051	5.000	0.030
Undeformed radius r_0 = 0.878 mm				
1.793	1.723	0.020	4.000	0.020
1.809	1.743	0.018	4.200	0.022
1.817	1.735	0.023	4.200	0.022
1.841	1.727	0.032	4.400	0.024
1.833	1.731	0.028	4.400	0.024
Undeformed radius r_0 = 0.906 mm				
1.857	1.800	0.015	4.300	0.024
1.857	1.792	0.018	4.300	0.024
1.881	1.792	0.024	4.500	0.026
1.893	1.796	0.026	4.500	0.026

Note: Electrode distance for the double drops is 1.940 cm

Figure 5.10 Degree of deformation as a function of Weber number for a single water drop in decyl alcohol with surfactant added

Drop length along parallel axis, a (mm)	Drop length along perpendicular axis, b (mm)	Degree of deformation, D	Applied voltage (kV)	Weber number
A water drop in decyl alcohol with 0.7 mM SDS added				
Undeformed radius r_0 = 0.741 mm				
1.574	1.538	0.012	1.000	0.017
1.574	1.514	0.020	1.200	0.024
1.586	1.510	0.025	1.400	0.033
1.586	1.502	0.027	1.600	0.043
1.594	1.494	0.033	1.800	0.054
1.590	1.469	0.039	2.000	0.067
1.602	1.457	0.047	2.200	0.081
1.602	1.413	0.063	2.410	0.097
1.622	1.393	0.076	2.600	0.113
1.662	1.345	0.105	2.800	0.131
1.666	1.265	0.137	3.000	0.150
Undeformed radius r_0 = 0.859 mm				
1.807	1.674	0.038	1.500	0.044
1.835	1.654	0.052	1.800	0.063
1.847	1.634	0.061	2.000	0.077
1.867	1.626	0.069	2.200	0.094
1.931	1.594	0.096	2.410	0.112
1.931	1.574	0.102	2.600	0.131
1.975	1.550	0.121	2.800	0.152
Undeformed radius r_0 = 0.817 mm				
1.747	1.638	0.032	1.500	0.041
1.775	1.606	0.050	1.800	0.060
1.783	1.578	0.061	2.000	0.074
1.799	1.578	0.065	2.200	0.089
1.815	1.546	0.080	2.410	0.107
1.859	1.534	0.096	2.600	0.124
1.899	1.494	0.120	2.800	0.144
2.032	1.441	0.170	3.000	0.165

Figure 5.10 (continued)

Drop length along parallel axis, a (mm)	Drop length along perpendicular axis, b (mm)	Degree of deformation, D	Applied voltage (kV)	Weber number
Undeformed radius $r_0 = 0.806$ mm				
1.734	1.622	0.034	1.500	0.041
1.755	1.602	0.046	1.800	0.059
1.767	1.578	0.056	2.000	0.073
1.783	1.538	0.074	2.200	0.088
1.799	1.506	0.089	2.410	0.105
1.819	1.477	0.104	2.600	0.123
1.883	1.449	0.130	2.800	0.142
1.939	1.421	0.154	3.000	0.163

Note: Electrode distance for the double drops is 1.940 cm

Figure 5.11. Deformation of a single water drop in toluene solution (0.5% vol. bitumen added) at two different aging times

Drop length along parallel axis, a (mm)	Drop length along perpendicular axis, b (mm)	Degree of deformation, D	Applied voltage (kV)	Weber number
Aging time t = 0				
Undeformed radius r_0 = 0.855 mm				
1.706	1.690	0.005	3.010	0.015
1.710	1.670	0.012	3.500	0.020
1.714	1.658	0.017	4.000	0.026
Undeformed radius r_0 = 0.861 mm				
1.730	1.710	0.006	3.000	0.015
1.734	1.698	0.011	3.500	0.020
1.739	1.690	0.014	4.000	0.026
Undeformed radius r_0 = 0.872 mm				
1.739	1.722	0.005	3.000	0.015
1.755	1.710	0.013	3.500	0.020
1.734	1.674	0.018	4.000	0.026
Undeformed radius r_0 = 0.859 mm				
1.730	1.718	0.004	2.500	0.010
1.739	1.714	0.007	3.000	0.015
1.734	1.694	0.012	3.400	0.019
1.747	1.702	0.013	3.800	0.023
1.743	1.682	0.018	4.000	0.026
Undeformed radius r_0 = 0.864 mm				
1.730	1.710	0.006	2.500	0.010
1.734	1.710	0.007	3.000	0.015
1.743	1.706	0.010	3.200	0.017
1.743	1.698	0.013	3.400	0.019
1.747	1.694	0.015	3.600	0.021
1.751	1.682	0.020	3.800	0.024

Figure 5.11 (continued)

Drop length along parallel axis, a (mm)	Drop length along perpendicular axis, b (mm)	Degree of deformation, D	Applied voltage (kV)	Weber number
Undeformed radius r_0 = 0.856 mm				
1.730	1.718	0.004	2.500	0.010
1.739	1.710	0.008	3.000	0.014
1.739	1.702	0.011	3.200	0.016
1.743	1.694	0.014	3.400	0.019
1.751	1.694	0.016	3.600	0.021
1.751	1.690	0.018	3.800	0.023
1.747	1.682	0.019	4.000	0.026
Aging time t = 30 mins				
Undeformed radius r_0 = 0.858 mm				
1.742	1.714	0.008	2.500	0.010
1.742	1.706	0.011	3.000	0.015
1.751	1.694	0.016	3.200	0.017
1.746	1.694	0.015	3.390	0.019
1.755	1.682	0.021	3.600	0.022
1.759	1.678	0.023	3.800	0.024
1.763	1.674	0.025	4.000	0.027
1.779	1.670	0.031	4.200	0.030
1.787	1.670	0.034	4.400	0.033
1.807	1.662	0.042	4.600	0.036
1.811	1.646	0.047	4.800	0.039
1.819	1.646	0.050	5.000	0.042
1.847	1.622	0.065	5.200	0.046
Undeformed radius r_0 = 0.817 mm				
1.658	1.618	0.012	3.000	0.014
1.670	1.606	0.020	3.400	0.018
1.670	1.594	0.023	3.700	0.022
1.666	1.582	0.026	4.000	0.026
1.670	1.546	0.039	4.300	0.030
1.674	1.538	0.042	4.600	0.034
1.674	1.510	0.052	4.800	0.037
1.678	1.510	0.053	5.000	0.040
1.686	1.493	0.061	5.200	0.043

Figure 5.11 (continued)

Drop length along parallel axis, a (mm)	Drop length along perpendicular axis, b (mm)	Degree of deformation, D	Applied voltage (kV)	Weber number
Undeformed radius		$r_0 = 0.849$ mm		
1.722	1.670	0.015	3.010	0.015
1.726	1.662	0.019	3.400	0.019
1.726	1.654	0.021	3.700	0.023
1.734	1.650	0.025	4.000	0.027
1.755	1.630	0.037	4.300	0.031
1.767	1.622	0.043	4.600	0.035
1.771	1.610	0.048	4.800	0.038
1.779	1.602	0.052	5.000	0.042
1.799	1.594	0.060	5.200	0.045
Undeformed radius		$r_0 = 0.845$ mm		
1.730	1.698	0.009	3.010	0.015
1.751	1.678	0.021	3.400	0.019
1.759	1.674	0.025	3.700	0.023
1.763	1.670	0.027	4.000	0.027
1.787	1.650	0.040	4.300	0.031
1.803	1.642	0.047	4.600	0.035
1.815	1.638	0.051	4.800	0.038
1.827	1.634	0.056	5.000	0.042
1.855	1.622	0.067	5.200	0.045
1.867	1.606	0.075	5.400	0.048
1.899	1.590	0.089	5.600	0.052
1.915	1.562	0.102	5.800	0.056
1.955	1.558	0.113	6.000	0.060

Note: Electrode distance for the single drop is 1.940 cm

Figure 5.12. Deformation of a single water drop in toluene solution (1.0% vol. bitumen added) at two different aging times

Drop length along parallel axis, a (mm)	Drop length along perpendicular axis, b (mm)	Degree of deformation, D	Applied voltage (kV)	Weber number
Aging time t = 0				
Undeformed radius r_0 = 0.855 mm				
1.759	1.726	0.009	3.000	0.014
1.763	1.710	0.015	3.500	0.020
1.779	1.710	0.020	4.000	0.026
1.779	1.698	0.023	4.400	0.031
1.807	1.682	0.036	4.800	0.037
1.803	1.666	0.039	5.000	0.041
1.815	1.646	0.049	5.200	0.044
1.815	1.646	0.049	5.400	0.047
1.823	1.614	0.061	5.600	0.051
1.859	1.630	0.066	5.800	0.055
1.879	1.610	0.077	6.000	0.058
Undeformed radius r_0 = 0.857 mm				
1.763	1.714	0.014	3.000	0.015
1.779	1.702	0.022	3.500	0.020
1.795	1.698	0.028	4.000	0.026
1.803	1.682	0.035	4.400	0.032
1.815	1.666	0.043	4.800	0.038
1.811	1.650	0.046	4.900	0.039
1.831	1.646	0.053	5.000	0.041
1.831	1.646	0.053	5.200	0.044
1.839	1.622	0.063	5.400	0.048
1.863	1.606	0.074	5.600	0.051
1.879	1.618	0.075	5.800	0.055

Figure 5.12 (continued)

Drop length along parallel axis, a (mm)	Drop length along perpendicular axis, b (mm)	Degree of deformation, D	Applied voltage (kV)	Weber number
Undeformed radius $r_0 = 0.852$ mm				
1.730	1.694	0.011	3.000	0.015
1.751	1.694	0.016	3.500	0.020
1.751	1.678	0.021	4.000	0.026
1.779	1.658	0.035	4.400	0.031
1.779	1.654	0.036	4.800	0.037
1.783	1.646	0.040	5.000	0.040
1.783	1.630	0.045	5.200	0.044
1.799	1.618	0.053	5.400	0.047
1.827	1.606	0.064	5.600	0.051
Undeformed radius $r_0 = 0.866$ mm				
1.743	1.718	0.007	3.000	0.015
1.767	1.706	0.017	3.500	0.020
1.779	1.698	0.023	4.000	0.026
1.795	1.690	0.030	4.500	0.033
1.815	1.686	0.037	5.000	0.041
1.819	1.666	0.044	5.200	0.044
1.851	1.654	0.056	5.400	0.048
Undeformed radius $r_0 = 0.862$ mm				
1.763	1.718	0.013	3.000	0.015
1.783	1.722	0.017	3.500	0.020
1.799	1.710	0.025	4.000	0.026
1.811	1.702	0.031	4.500	0.033
1.835	1.698	0.039	5.000	0.041
1.847	1.670	0.050	5.200	0.044
1.883	1.666	0.061	5.400	0.048
Undeformed radius $r_0 = 0.852$ mm				
1.747	1.710	0.011	3.000	0.015
1.759	1.706	0.015	3.500	0.020
1.771	1.706	0.019	4.000	0.026
1.799	1.682	0.033	4.500	0.033
1.807	1.654	0.044	5.000	0.040
1.851	1.650	0.057	5.200	0.044

Figure 5.12 (continued)

Drop length along parallel axis, a (mm)	Drop length along perpendicular axis, b (mm)	Degree of deformation, D	Applied voltage (kV)	Weber number
Aging time t = 30 mins				
Undeformed radius r_0 = 0.874 mm				
1.787	1.726	0.017	3.000	0.016
1.791	1.722	0.019	3.500	0.022
1.815	1.710	0.030	4.000	0.028
1.843	1.706	0.039	4.500	0.036
1.871	1.690	0.051	5.000	0.044
Undeformed radius r_0 = 0.820 mm				
1.714	1.654	0.018	3.500	0.020
1.702	1.634	0.021	4.000	0.026
1.734	1.622	0.034	4.500	0.033
1.739	1.610	0.038	5.000	0.041
1.775	1.594	0.054	5.400	0.048
1.783	1.586	0.058	5.700	0.054
1.823	1.570	0.075	6.000	0.059
1.839	1.566	0.080	6.200	0.064
1.859	1.542	0.093	6.400	0.068
1.883	1.530	0.104	6.600	0.072
1.919	1.510	0.119	6.800	0.076
1.943	1.498	0.130	7.000	0.081
Undeformed radius r_0 = 0.855 mm				
1.747	1.706	0.012	3.000	0.015
1.783	1.682	0.029	4.000	0.028
1.839	1.662	0.051	5.000	0.043
1.863	1.634	0.065	5.500	0.052
1.915	1.614	0.085	6.000	0.062
Undeformed radius r_0 = 0.845 mm				
1.747	1.694	0.015	3.010	0.015
1.763	1.694	0.020	3.500	0.021
1.767	1.678	0.026	4.000	0.027
1.791	1.662	0.037	4.500	0.034
1.819	1.642	0.051	5.000	0.043
1.863	1.618	0.070	5.500	0.052
1.919	1.586	0.095	6.000	0.061

Note: Electrode distance for the single drop is 1.950 cm

Figure 5.13. Deformation of a single water drop in toluene solution (1.5% vol. bitumen added) at two different aging times

Drop length along parallel axis, a (mm)	Drop length along perpendicular axis, b (mm)	Degree of deformation, D	Applied voltage (kV)	Weber number
Aging time t = 0				
Undeformed radius r_0 = 0.839 mm				
1.751	1.714	0.010	3.000	0.015
1.747	1.690	0.016	3.500	0.020
1.747	1.654	0.027	4.800	0.038
1.767	1.610	0.046	5.500	0.050
1.811	1.582	0.067	6.000	0.060
1.823	1.562	0.077	6.200	0.064
1.839	1.530	0.092	6.400	0.068
1.835	1.506	0.099	6.600	0.072
1.887	1.481	0.120	6.800	0.077
1.935	1.461	0.140	7.000	0.081
Undeformed radius r_0 = 0.857 mm				
1.759	1.710	0.014	3.510	0.021
1.783	1.686	0.028	4.500	0.034
1.811	1.670	0.040	5.000	0.042
1.827	1.654	0.050	5.500	0.051
1.843	1.634	0.060	6.000	0.061
1.892	1.606	0.082	6.400	0.069
1.968	1.578	0.110	6.800	0.078
2.056	1.514	0.152	7.000	0.083
Undeformed radius r_0 = 0.860 mm				
1.767	1.714	0.015	3.500	0.021
1.791	1.686	0.030	4.500	0.034
1.815	1.694	0.034	5.000	0.043
1.843	1.654	0.054	5.500	0.051
1.879	1.634	0.070	6.000	0.061
1.927	1.622	0.086	6.400	0.070
1.959	1.578	0.108	6.800	0.079
2.024	1.562	0.129	7.000	0.083

Figure 5.13 (continued)

Drop length along parallel axis, a (mm)	Drop length along perpendicular axis, b (mm)	Degree of deformation, D	Applied voltage (kV)	Weber number
Undeformed radius r_0 = 0.847 mm				
1.775	1.710	0.018	3.510	0.021
1.787	1.690	0.028	4.500	0.034
1.811	1.678	0.038	5.000	0.042
1.839	1.650	0.054	5.500	0.051
1.851	1.610	0.070	6.010	0.061
1.899	1.582	0.091	6.400	0.069
1.939	1.554	0.110	6.700	0.075
1.996	1.534	0.131	7.000	0.082
2.028	1.473	0.158	7.200	0.087
Undeformed radius r_0 = 0.843 mm				
1.743	1.686	0.016	3.500	0.020
1.775	1.670	0.030	4.500	0.034
1.803	1.662	0.041	5.000	0.042
1.807	1.646	0.047	5.500	0.050
1.859	1.602	0.074	6.000	0.060
1.863	1.578	0.083	6.400	0.068
1.915	1.566	0.100	6.700	0.075
1.992	1.530	0.131	7.000	0.082
2.036	1.510	0.148	7.200	0.086
Undeformed radius r_0 = 0.8384 mm				
1.734	1.678	0.017	3.500	0.020
1.743	1.638	0.031	4.500	0.034
1.751	1.618	0.039	5.000	0.041
1.775	1.606	0.050	5.500	0.050
1.819	1.574	0.072	6.000	0.060
1.851	1.558	0.086	6.400	0.068
1.899	1.542	0.104	6.700	0.074
1.975	1.518	0.131	7.000	0.081
2.020	1.490	0.151	7.200	0.086

Figure 5.13 (continued)

Drop length along parallel axis, a (mm)	Drop length along perpendicular axis, b (mm)	Degree of deformation, D	Applied voltage (kV)	Weber number
Aging time t = 30 mins				
Undeformed radius r_0 = 0.816 mm				
1.706	1.650	0.017	3.500	0.021
1.722	1.614	0.033	4.500	0.034
1.759	1.574	0.055	5.500	0.051
1.799	1.534	0.080	6.500	0.072
1.859	1.494	0.109	7.000	0.083
1.911	1.490	0.124	7.200	0.088
1.895	1.457	0.131	7.400	0.093
1.919	1.437	0.144	7.600	0.098
1.996	1.409	0.172	7.800	0.103
Undeformed radius r_0 = 0.841 mm				
1.722	1.682	0.012	3.000	0.016
1.743	1.678	0.019	4.000	0.028
1.779	1.658	0.035	5.000	0.044
1.835	1.578	0.075	6.000	0.063
1.939	1.562	0.108	7.000	0.086
1.911	1.534	0.110	7.200	0.091
1.951	1.538	0.119	7.400	0.096
2.012	1.485	0.150	7.600	0.101
2.100	1.457	0.181	7.800	0.106
Undeformed radius r_0 = 0.804 mm				
1.698	1.642	0.017	3.000	0.015
1.690	1.638	0.016	4.000	0.027
1.722	1.582	0.043	5.000	0.042
1.743	1.550	0.059	6.000	0.060
1.799	1.502	0.090	7.000	0.082
1.835	1.469	0.111	7.200	0.087
1.839	1.449	0.118	7.400	0.092
1.843	1.409	0.133	7.600	0.097
1.891	1.369	0.160	7.800	0.102

Note: Electrode distance for the single drop is 1.940 cm

Figure 5.14. Deformation of a single water drop in toluene solution (2.0% vol. bitumen added) at two different aging times

Drop length along parallel axis, a (mm)	Drop length along perpendicular axis, b (mm)	Degree of deformation, D	Applied voltage (kV)	Weber number
Aging time t = 0				
Undeformed radius r_0 = 0.859 mm				
1.783	1.710	0.021	4.000	0.028
1.771	1.662	0.032	5.000	0.044
1.823	1.642	0.052	6.000	0.063
1.843	1.622	0.064	6.500	0.074
1.915	1.546	0.107	7.000	0.086
2.016	1.566	0.126	7.400	0.096
Undeformed radius r_0 = 0.856 mm				
1.771	1.666	0.030	4.500	0.036
1.783	1.650	0.039	5.500	0.053
1.803	1.626	0.052	6.000	0.063
1.875	1.630	0.070	6.400	0.072
1.895	1.622	0.078	6.800	0.081
1.895	1.602	0.084	7.000	0.086
1.983	1.550	0.123	7.200	0.091
Undeformed radius r_0 = 0.888 mm				
1.823	1.726	0.027	4.500	0.037
1.867	1.698	0.047	5.500	0.055
1.879	1.670	0.059	6.000	0.065
1.915	1.666	0.069	6.400	0.074
1.939	1.638	0.084	6.800	0.084
2.008	1.654	0.096	7.000	0.089
2.028	1.594	0.120	7.200	0.094

Figure 5.14 (continued)

Drop length along parallel axis, a (mm)	Drop length along perpendicular axis, b (mm)	Degree of deformation, D	Applied voltage (kV)	Weber number
Undeformed radius r_0 = 0.861 mm				
1.799	1.698	0.029	4.500	0.036
1.823	1.674	0.043	5.500	0.053
1.847	1.650	0.056	6.000	0.064
1.895	1.626	0.076	6.400	0.072
1.927	1.610	0.090	6.800	0.082
1.919	1.606	0.089	7.000	0.086
Undeformed radius r_0 = 0.862 mm				
1.803	1.710	0.026	4.500	0.036
1.847	1.690	0.044	5.500	0.053
1.871	1.682	0.053	6.000	0.064
1.903	1.646	0.072	6.400	0.072
1.935	1.626	0.087	6.700	0.079
1.975	1.638	0.093	7.000	0.087
1.992	1.594	0.111	7.200	0.092
Undeformed radius r_0 = 0.880 mm				
1.799	1.718	0.023	4.500	0.037
1.839	1.698	0.040	5.500	0.055
1.863	1.686	0.050	6.000	0.065
1.911	1.674	0.066	6.400	0.074
1.939	1.670	0.075	6.700	0.081
2.000	1.662	0.092	7.000	0.088
2.104	1.642	0.123	7.200	0.093
Aging time t = 30 mins				
Undeformed radius r_0 = 0.885 mm				
1.791	1.722	0.019	3.000	0.017
1.795	1.706	0.025	4.000	0.030
1.815	1.698	0.033	5.000	0.047
1.871	1.670	0.057	6.000	0.068
1.907	1.630	0.078	7.000	0.092
1.939	1.622	0.089	7.200	0.097
1.988	1.618	0.102	7.400	0.103

Note: Electrode distance for the single drop is 1.950 cm

Figure 5.17. Degree of deformation as a function of distance for a water drop pair in decyl alcohol with no aging time

Drop length along parallel axis, a (mm)	Drop length along perpendicular axis, b (mm)	Degree of deformation, D	Relative edge-to-edge separation distance (x/r_0)
Applied electric field E = 0.515 kV/cm			
Undeformed radius r_0 = 0.868 mm			
1.755	1.730	0.006	2.10
1.750	1.714	0.011	1.66
1.743	1.698	0.012	1.45
1.751	1.706	0.012	1.31
1.755	1.690	0.018	1.19
1.755	1.694	0.017	1.02
1.751	1.686	0.018	0.89
1.771	1.690	0.023	0.58
Undeformed radius r_0 = 0.842 mm			
1.751	1.710	0.011	2.13
1.730	1.690	0.011	1.68
1.739	1.690	0.014	1.47
1.726	1.678	0.014	1.32
1.739	1.686	0.015	1.20
1.722	1.678	0.012	1.03
1.734	1.662	0.021	0.89
1.751	1.670	0.023	0.58
Undeformed radius r_0 = 0.909 mm			
1.807	1.767	0.011	1.94
1.803	1.759	0.012	1.61
1.831	1.767	0.017	1.27
1.799	1.743	0.015	1.27
1.803	1.739	0.018	1.00
1.791	1.722	0.019	0.87
1.795	1.730	0.018	0.62

Figure 5.17 (continued)

Drop length along parallel axis, a (mm)	Drop length along perpendicular axis, b (mm)	Degree of deformation, D	Relative edge-to-edge separation distance (x/r_0)
Undeformed radius $r_0 = 0.879$ mm			
1.831	1.787	0.012	1.92
1.827	1.767	0.016	1.59
1.847	1.779	0.018	1.25
1.819	1.759	0.016	1.26
1.803	1.743	0.016	1.00
1.799	1.743	0.015	0.86
1.799	1.722	0.021	0.62
Applied electric field E = 0.773 kV/cm			
Undeformed radius $r_0 = 0.860$ mm			
1.787	1.682	0.030	1.52
1.787	1.678	0.031	1.30
1.787	1.674	0.032	1.24
1.795	1.678	0.033	1.00
1.807	1.678	0.036	0.80
1.819	1.674	0.041	0.64
1.907	1.650	0.072	0.26
1.935	1.630	0.085	0.09
Undeformed radius $r_0 = 0.851$ mm			
1.787	1.682	0.030	1.53
1.791	1.698	0.026	1.30
1.771	1.662	0.031	1.26
1.775	1.658	0.033	1.02
1.779	1.650	0.037	0.82
1.795	1.654	0.040	0.65
1.847	1.626	0.063	0.27
1.899	1.578	0.092	0.09

Figure 5.17 (continued)

Drop length along parallel axis, a (mm)	Drop length along perpendicular axis, b (mm)	Degree of deformation, D	Relative edge-to-edge separation distance (x/r_0)
Undeformed radius $r_0 = 0.866$ mm			
1.789	1.793	0.026	1.80
1.763	1.732	0.031	1.55
1.805	1.769	0.036	1.29
1.710	1.739	0.021	1.99
1.700	1.743	0.027	1.56
1.694	1.734	0.030	1.30
1.692	1.734	0.030	1.14
1.692	1.739	0.038	0.80
Undeformed radius $r_0 = 0.874$ mm			
1.859	1.763	0.026	1.80
1.831	1.718	0.029	1.58
1.887	1.755	0.035	1.32
1.751	1.678	0.024	1.96
1.751	1.658	0.026	1.52
1.763	1.658	0.029	1.27
1.767	1.662	0.029	1.11
1.787	1.654	0.038	0.78
Applied electric field E = 0.928 kV/cm			
Undeformed radius $r_0 = 0.828$ mm			
1.775	1.626	0.043	1.99
1.775	1.614	0.047	1.50
1.775	1.614	0.047	1.30
1.783	1.606	0.052	0.83
1.823	1.582	0.070	0.57
Undeformed radius $r_0 = 0.850$ mm			
1.823	1.662	0.046	1.94
1.811	1.650	0.046	1.47
1.811	1.638	0.050	1.27
1.823	1.634	0.054	0.80
1.859	1.614	0.070	0.55

Figure 5.17 (continued)

Drop length along parallel axis, a (mm)	Drop length along perpendicular axis, b (mm)	Degree of deformation, D	Relative edge-to-edge separation distance (x/r_0)
Undeformed radius		$r_0 = 0.850$ mm	
1.706	1.734	0.042	1.87
1.704	1.739	0.048	1.55
1.706	1.734	0.040	1.93
1.710	1.730	0.045	1.66
1.692	1.716	0.045	1.44
1.688	1.712	0.051	1.19
1.690	1.710	0.053	0.98
Undeformed radius		$r_0 = 0.863$ mm	
1.803	1.654	0.046	1.84
1.815	1.646	0.046	1.52
1.803	1.662	0.043	1.90
1.811	1.654	0.044	1.64
1.807	1.650	0.044	1.42
1.807	1.630	0.049	1.17
1.807	1.622	0.055	0.97
Applied electric field E = 1.031 kV/cm			
Undeformed radius		$r_0 = 0.852$ mm	
1.847	1.666	0.051	1.77
1.851	1.654	0.056	1.49
Undeformed radius		$r_0 = 0.852$ mm	
1.899	1.698	0.055	1.73
1.787	1.594	0.057	1.53
Undeformed radius		$r_0 = 0.862$ mm	
1.883	1.666	0.061	1.76
1.899	1.654	0.068	1.36
1.887	1.638	0.070	1.13
2.196	1.606	0.155	0.18
Undeformed radius		$r_0 = 0.858$ mm	
1.883	1.658	0.063	1.76
1.895	1.658	0.066	1.37
1.895	1.642	0.071	1.14
2.100	1.550	0.150	0.18

Figure 5.17 (continued)

Drop length along parallel axis, a (mm)	Drop length along perpendicular axis, b (mm)	Degree of deformation, D	Relative edge-to-edge separation distance (x/r_0)
Undeformed radius		$r_0 = 0.829$ mm	
1.807	1.590	0.063	1.77
1.795	1.582	0.063	1.52
1.807	1.582	0.066	1.26
Undeformed radius		$r_0 = 0.844$ mm	
1.827	1.618	0.060	1.75
1.839	1.622	0.062	1.48
1.851	1.606	0.070	1.23
Undeformed radius		$r_0 = 0.831$ mm	
1.827	1.618	0.060	1.86
1.815	1.598	0.063	1.43
1.803	1.594	0.061	1.08
1.767	1.570	0.058	1.28
Undeformed radius		$r_0 = 0.864$ mm	
1.875	1.667	0.060	1.80
1.883	1.656	0.064	1.37
1.895	1.656	0.067	1.04
1.871	1.646	0.063	1.22

Note: (1) Electrode distance for the drop pair is 1.940 cm.

(2) Zero aging time.

Figure 5.19. Degree of deformation as a function of distance with different Weber numbers for a water drop pair aged 30 mins in toluene solution (0.5% vol. bitumen added)

Drop length along parallel axis, a (mm)	Drop length along perpendicular axis, b (mm)	Degree of deformation, D	Relative edge-to-edge separation distance (x/r_0)
Applied electric field E = 1.804 kV/cm			
Undeformed radius r_0 = 0.834 mm			
1.674	1.618	0.017	1.48
1.630	1.566	0.020	1.32
1.843	1.763	0.022	1.01
Undeformed radius r_0 = 0.847 mm			
1.730	1.666	0.018	1.45
1.718	1.642	0.022	1.30
1.710	1.630	0.024	1.00
Undeformed radius r_0 = 0.870 mm			
1.791	1.726	0.018	1.64
1.851	1.783	0.018	1.25
1.759	1.698	0.017	1.24
1.799	1.739	0.017	1.12
1.775	1.702	0.020	0.95
1.779	1.650	0.037	0.33
Undeformed radius r_0 = 0.865 mm			
1.839	1.775	0.017	1.60
1.827	1.759	0.019	1.27
1.851	1.787	0.017	1.19
1.734	1.670	0.018	1.18
1.722	1.654	0.020	0.98
1.767	1.630	0.040	0.34
Undeformed radius r_0 = 0.872 mm			
1.779	1.718	0.017	1.64
1.799	1.734	0.018	1.34
1.803	1.734	0.019	1.22
1.787	1.726	0.017	1.12
1.799	1.722	0.021	0.93
1.807	1.718	0.025	0.85
1.807	1.706	0.028	0.37

Figure 5.19 (continued)

Drop length along parallel axis, a (mm)	Drop length along perpendicular axis, b (mm)	Degree of deformation, D	Relative edge-to-edge separation distance (x/r_0)
Undeformed radius	$r_0 = 0.860$ mm		
1.775	1.718	0.018	1.65
1.775	1.718	0.016	1.34
1.775	1.714	0.017	1.24
1.767	1.706	0.017	1.13
1.759	1.678	0.023	0.95
1.751	1.682	0.019	0.86
1.767	1.666	0.029	0.38
Undeformed radius	$r_0 = 0.851$ mm		
1.753	1.700	0.015	1.60
1.747	1.678	0.019	1.38
1.739	1.668	0.020	1.34
1.753	1.682	0.020	1.23
1.734	1.662	0.021	1.10
Undeformed radius	$r_0 = 0.850$ mm		
1.740	1.686	0.016	1.62
1.740	1.680	0.019	1.38
1.740	1.676	0.019	1.34
1.739	1.664	0.021	1.23
1.739	1.662	0.021	1.09
Applied electric field $E = 2.062$ kV/cm			
Undeformed radius	$r_0 = 0.842$ mm		
1.690	1.614	0.023	1.79
1.759	1.666	0.026	1.38
1.743	1.654	0.026	1.34
1.787	1.678	0.031	1.14
1.759	1.646	0.033	0.89
1.714	1.610	0.031	1.13
1.815	1.650	0.047	0.45
Undeformed radius	$r_0 = 0.837$ mm		
1.734	1.654	0.023	1.75
1.743	1.654	0.026	1.41
1.734	1.642	0.027	1.35
1.739	1.638	0.029	1.17
1.747	1.638	0.032	0.90
1.714	1.630	0.025	1.13
1.811	1.650	0.046	0.45

Figure 5.19 (continued)

Drop length along parallel axis, a (mm)	Drop length along perpendicular axis, b (mm)	Degree of deformation, D	Relative edge-to-edge separation distance (x/r_0)
Undeformed radius		$r_0 = 0.853$ mm	
1.779	1.686	0.026	1.69
1.751	1.666	0.024	1.44
1.747	1.658	0.025	1.28
1.747	1.646	0.029	1.17
1.755	1.658	0.028	1.04
Undeformed radius		$r_0 = 0.850$ mm	
1.767	1.682	0.024	1.74
1.747	1.658	0.025	1.44
1.751	1.666	0.024	1.27
1.759	1.658	0.029	1.17
1.771	1.658	0.032	1.04
Undeformed radius		$r_0 = 0.883$ mm	
1.867	1.783	0.023	1.44
1.847	1.747	0.027	1.10
1.743	1.638	0.030	1.39
Undeformed radius		$r_0 = 0.852$ mm	
1.763	1.666	0.028	1.53
1.819	1.706	0.031	1.12
1.662	1.574	0.027	1.45
Undeformed radius		$r_0 = 0.866$ mm	
1.779	1.710	0.019	1.59
1.801	1.710	0.025	1.29
1.801	1.690	0.031	1.12
1.793	1.700	0.026	1.09
1.783	1.698	0.024	0.91
1.783	1.678	0.030	0.75
1.793	1.670	0.035	0.66
1.779	1.654	0.036	0.51
Undeformed radius		$r_0 = 0.865$ mm	
1.795	1.706	0.025	1.58
1.805	1.702	0.029	1.29
1.815	1.696	0.033	1.13
1.793	1.698	0.027	1.09
1.787	1.678	0.031	0.91
1.795	1.682	0.032	0.75
1.789	1.662	0.036	0.66
1.795	1.650	0.041	0.51

Figure 5.19 (continued)

Drop length along parallel axis, a (mm)	Drop length along perpendicular axis, b (mm)	Degree of deformation, D	Relative edge-to-edge separation distance (x/r_0)
Applied electric field E = 2.216 kV/cm			
Undeformed radius r_0 = 0.868 mm			
1.867	1.722	0.040	0.93
1.807	1.642	0.047	0.81
Undeformed radius r_0 = 0.843 mm			
1.787	1.654	0.038	0.96
1.759	1.618	0.041	0.83
Undeformed radius r_0 = 0.863 mm			
1.823	1.730	0.025	1.57
1.771	1.670	0.029	1.41
1.803	1.670	0.038	1.13
1.791	1.666	0.036	1.11
1.811	1.646	0.047	0.81
1.831	1.638	0.055	0.55
1.819	1.726	0.026	1.53
1.847	1.718	0.036	1.22
Undeformed radius r_0 = 0.856 mm			
1.799	1.690	0.031	1.58
1.787	1.662	0.036	1.43
1.787	1.658	0.037	1.13
1.791	1.654	0.039	1.12
1.799	1.658	0.040	0.82
1.811	1.646	0.047	0.55
1.803	1.694	0.031	1.56
1.815	1.674	0.040	1.23

Figure 5.19 (continued)

Drop length along parallel axis, a (mm)	Drop length along perpendicular axis, b (mm)	Degree of deformation, D	Relative edge-to-edge separation distance (x/r_0)
Applied electric field E = 2.320 kV/cm			
Undeformed radius r_0 = 0.895 mm			
1.755	1.630	0.036	1.72
1.891	1.722	0.046	1.23
Undeformed radius r_0 = 0.879 mm			
1.718	1.602	0.035	1.74
1.847	1.690	0.044	1.26
Undeformed radius r_0 = 0.865 mm			
1.831	1.670	0.045	1.38
1.855	1.670	0.052	1.12
1.843	1.646	0.056	0.99
Undeformed radius r_0 = 0.863 mm			
1.831	1.666	0.047	1.37
1.859	1.662	0.055	1.13
1.843	1.654	0.053	1.00
Undeformed radius r_0 = 0.847 mm			
1.779	1.628	0.044	1.56
1.759	1.616	0.042	1.42
1.761	1.604	0.046	1.34
Undeformed radius r_0 = 0.838 mm			
1.791	1.656	0.039	1.55
1.785	1.624	0.047	1.40
1.781	1.624	0.045	1.32

Note: (1) Electrode distance for the drop pair is 1.940 cm

(2) Aging time is 30 minutes.

Figure 5.21. Degree of deformation as a function of distance with different Weber numbers for a water drop pair aged 30 mins in toluene solution (1.5% vol. bitumen added)

Drop length along parallel axis, a (mm)	Drop length along perpendicular axis, b (mm)	Degree of deformation, D	Relative edge-to-edge separation distance (x/r_0)
Applied electric field E = 1.546 kV/cm			
Undeformed radius r_0 = 0.834 mm			
1.718	1.662	0.016	2.13
1.722	1.662	0.017	1.56
1.698	1.630	0.020	1.60
1.710	1.650	0.017	1.33
1.710	1.630	0.024	1.07
1.698	1.618	0.024	0.75
1.702	1.618	0.025	0.43
1.690	1.586	0.031	0.27
Undeformed radius r_0 = 0.831 mm			
1.658	1.610	0.014	2.18
1.610	1.554	0.017	1.65
1.743	1.666	0.022	1.55
1.751	1.674	0.022	1.30
1.730	1.654	0.022	1.05
1.714	1.638	0.022	0.75
1.658	1.566	0.028	0.44
1.634	1.550	0.026	0.27
Undeformed radius r_0 = 0.842 mm			
1.714	1.642	0.021	1.96
1.702	1.650	0.015	1.56
1.714	1.646	0.020	1.27
1.726	1.638	0.026	1.04
1.710	1.626	0.025	0.79
1.726	1.622	0.031	0.53

Figure 5.21 (continued)

Drop length along parallel axis, a (mm)	Drop length along perpendicular axis, b (mm)	Degree of deformation, D	Relative edge-to-edge separation distance (x/r_0)
Undeformed radius $r_0 = 0.8449$ mm			
1.638	1.594	0.013	2.02
1.739	1.674	0.018	1.54
1.743	1.670	0.021	1.26
1.747	1.650	0.028	1.03
1.743	1.654	0.026	0.78
1.755	1.650	0.030	0.52
Applied electric field E = 2.067 kV/cm			
Undeformed radius $r_0 = 0.850$ mm			
1.767	1.634	0.038	2.15
1.755	1.622	0.039	1.67
1.763	1.618	0.042	1.12
Undeformed radius $r_0 = 0.880$ mm			
1.847	1.722	0.034	2.09
1.847	1.698	0.041	1.62
1.843	1.706	0.038	1.08
Undeformed radius $r_0 = 0.817$ mm			
1.686	1.578	0.033	2.36
1.706	1.590	0.035	1.92
1.730	1.598	0.039	1.55
1.747	1.602	0.043	1.28
1.722	1.578	0.043	1.41
1.718	1.594	0.037	1.33
1.718	1.574	0.043	1.24
1.714	1.570	0.044	1.04
1.706	1.542	0.050	1.00
1.702	1.546	0.048	0.96
1.734	1.546	0.057	0.40
1.747	1.542	0.062	0.28

Figure 5.21 (continued)

Drop length along parallel axis, a (mm)	Drop length along perpendicular axis, b (mm)	Degree of deformation, D	Relative edge-to-edge separation distance (x/r_0)
Undeformed radius		$r_0 = 0.848$ mm	
1.843	1.726	0.032	2.28
1.831	1.714	0.032	1.80
1.843	1.698	0.040	1.46
1.843	1.682	0.045	1.20
1.586	1.457	0.042	1.51
1.799	1.662	0.039	1.26
1.779	1.642	0.039	1.17
1.791	1.642	0.043	1.01
1.791	1.646	0.042	0.96
1.775	1.626	0.043	0.91
1.751	1.574	0.053	0.39
1.734	1.538	0.060	0.28
Applied electric field E = 2.320 kV/cm			
Undeformed radius		$r_0 = 0.830$ mm	
1.783	1.614	0.049	2.43
1.779	1.602	0.052	2.34
1.783	1.606	0.052	1.97
1.779	1.590	0.056	1.90
1.755	1.574	0.054	1.59
1.767	1.582	0.055	1.66
1.763	1.574	0.056	1.52
1.771	1.566	0.061	1.39
Undeformed radius		$r_0 = 0.832$ mm	
1.751	1.566	0.055	2.38
1.739	1.562	0.053	2.29
1.642	1.485	0.050	2.07
1.618	1.473	0.046	2.00
1.863	1.670	0.054	1.51
1.859	1.686	0.048	1.58
1.694	1.506	0.058	1.54
1.666	1.494	0.054	1.41

Figure 5.21 (continued)

Drop length along parallel axis, a (mm)	Drop length along perpendicular axis, b (mm)	Degree of deformation, D	Relative edge-to-edge separation distance (x/r_0)
Undeformed radius		$r_0 = 0.741$ mm	
1.590	1.401	0.063	1.65
1.582	1.401	0.060	1.75
1.610	1.393	0.072	1.24
1.598	1.389	0.069	1.34
1.594	1.397	0.065	1.27
1.598	1.385	0.071	1.18
Undeformed radius		$r_0 = 0.748$ mm	
1.614	1.453	0.052	1.63
1.614	1.457	0.050	1.73
1.650	1.445	0.066	1.22
1.626	1.437	0.061	1.33
1.646	1.445	0.064	1.26
1.626	1.437	0.061	1.17
Undeformed radius		$r_0 = 0.819$ mm	
1.747	1.574	0.052	1.97
1.743	1.566	0.053	1.70
1.739	1.538	0.061	1.71
1.726	1.526	0.061	1.73
1.743	1.530	0.065	1.05
1.706	1.510	0.061	1.25
Applied electric field E = 2.474 kV/cm			
Undeformed radius		$r_0 = 0.789$ mm	
1.747	1.518	0.070	1.95
1.722	1.522	0.061	2.04
1.714	1.518	0.060	1.93
1.718	1.510	0.064	1.87
1.743	1.510	0.071	1.34
1.739	1.514	0.069	1.47
1.730	1.518	0.065	1.48

Figure 5.21 (continued)

Drop length along parallel axis, a (mm)	Drop length along perpendicular axis, b (mm)	Degree of deformation, D	Relative edge-to-edge separation distance (x/r_0)
Undeformed radius		$r_0 = 0.784$ mm	
1.698	1.514	0.057	2.54
1.698	1.502	0.061	2.51
1.739	1.494	0.075	1.60
1.706	1.498	0.065	2.50
1.722	1.485	0.073	1.63
1.747	1.498	0.076	1.40
1.831	1.465	0.110	0.64
1.747	1.481	0.082	1.42
Undeformed radius		$r_0 = 0.771$ mm	
1.678	1.502	0.055	2.58
1.670	1.494	0.055	2.55
1.722	1.502	0.068	1.63
1.678	1.490	0.059	2.55
1.686	1.498	0.059	1.66
1.690	1.494	0.061	1.42
1.783	1.457	0.100	0.65
1.698	1.477	0.069	1.44
Undeformed radius		$r_0 = 0.773$ mm	
1.666	1.490	0.055	2.69
1.650	1.494	0.049	2.75
1.642	1.485	0.050	2.38
1.650	1.465	0.059	2.36
1.666	1.465	0.064	1.98
1.650	1.465	0.059	1.78
1.650	1.457	0.062	1.56
1.666	1.473	0.061	1.58
1.682	1.465	0.068	1.40
1.658	1.457	0.064	1.60
1.666	1.441	0.072	1.70
1.666	1.461	0.065	1.36
1.730	1.453	0.087	0.88
1.682	1.445	0.075	1.27
1.678	1.433	0.078	1.05
1.767	1.409	0.112	0.44

Figure 5.21 (continued)

Drop length along parallel axis, a (mm)	Drop length along perpendicular axis, b (mm)	Degree of deformation, D	Relative edge-to-edge separation distance (x/r_0)
Undeformed radius		$r_0 = 0.783$ mm	
1.694	1.518	0.055	2.65
1.698	1.514	0.057	2.71
1.690	1.514	0.055	2.35
1.678	1.510	0.052	2.33
1.698	1.510	0.058	1.96
1.682	1.498	0.058	1.76
1.706	1.490	0.067	1.54
1.678	1.490	0.059	1.56
1.710	1.494	0.067	1.38
1.702	1.494	0.065	1.57
1.702	1.490	0.066	1.68
1.718	1.498	0.068	1.34
1.759	1.429	0.103	0.87
1.702	1.490	0.066	1.26
1.698	1.473	0.070	1.04
1.843	1.465	0.114	0.44

Note: (1) Electrode distance for the drop pair is 1.940 cm.

(2) Aging time is 30 minutes.

Appendix II

Calculation of Maxwell Stress Tensor

A-II.1 Maxwell Stress Tensor of a Perfect Dielectric Drop in a Perfect Dielectric

For a system of a perfect dielectric drop suspended in a perfect dielectric medium in a uniform electric field, the electric field of the system could be described with the following equations (as shown in Figure A-II.1),

Governing equations:

$$\nabla^2 \phi_i = 0 \qquad \text{internal phase} \qquad \text{(A-II.1 a)}$$

$$\nabla^2 \phi_e = 0 \qquad \text{external phase} \qquad \text{(A-II.1 b)}$$

Boundary conditions:

$$\phi_e = \phi_i \qquad \text{at} \quad \eta = r_0 \qquad \text{(A-II.1 c)}$$

$$\varepsilon_e \frac{\partial \phi_e}{\partial n} = \varepsilon_i \frac{\partial \phi_i}{\partial n} \qquad \text{at} \quad \eta = r_0 \qquad \text{(A-II.1 d)}$$

$$\phi_e = -\eta E_\infty \cos\theta \qquad \text{as} \quad \eta \to \infty \qquad \text{(A-II.1 e)}$$

$$\phi_i \to \text{finite} \qquad \text{at} \quad \eta = 0 \qquad \text{(A-II.1 f)}$$

where "i" denotes internal drop phase, "e" denotes external continuous phase, ϕ is the electric potential, ε is the dielectric constant, $\vec{E}$ is the applied electric field strength vector at (η,θ), E_∞ is the uniform field far from the drop. Equation (A-II.1 a) assumes that there is no free charge at the interface.

For slight drop deformation, one can still consider the drop as a sphere. As the electric field is considered to be axi-symmetric in spherical polar coordinates, using separation of variable method, the electrical potential inside and outside the drop can be

expressed as

$$\phi_i = -\frac{3E_\infty \eta \cos\theta}{S+2} \qquad \text{(A-II.2 a)}$$

$$\phi_e = -E_\infty \eta \cos\theta + \frac{S-1}{S+2}\frac{E_\infty r_0^{\,3}\cos\theta}{\eta^2} \qquad \text{(A-II.2 b)}$$

where $S = \frac{\varepsilon_i}{\varepsilon_e}$, S is the dielectric constant ratio of the internal phase to the external phase.

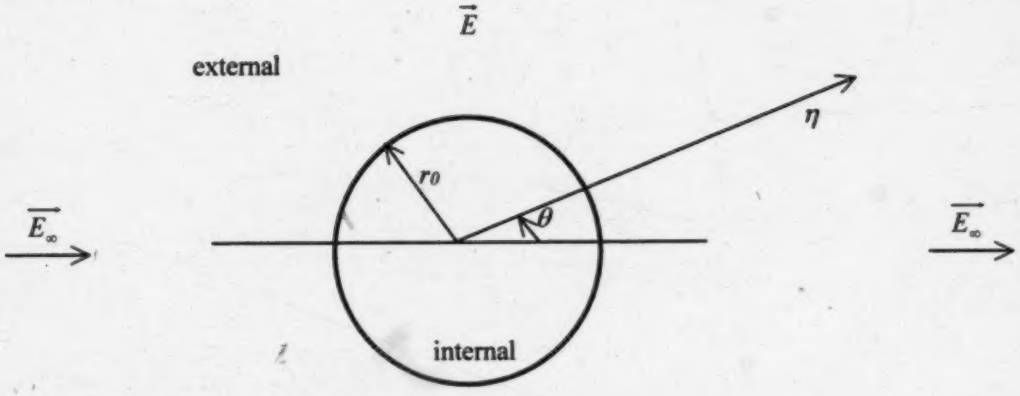

Figure A-II.1 Schematic diagram of a perfect dielectric drop in another perfect dielectric in an electric field

Noting that $\vec{\nabla}\phi = -\vec{E}$, using equation (A-II.2 a) and (A-II.2 b), one can show that the normal and tangential components of the electric field at the surface can be obtained as:

Normal component of the electric field in the internal phase E_{ni}

$$E_{ni} = \frac{3E_\infty \cos\theta}{S+2} \qquad \text{(A-II.2 c)}$$

Normal component of the electric field in the external phase E_{ne}

$$E_{ne} = \frac{3SE_{\infty}\cos\theta}{S+2} \qquad \text{(A-II.2 d)}$$

Tangential component of the electric field in the internal phase E_{ti}

$$E_{ti} = -\frac{3E_{\infty}\sin\theta}{S+2} \qquad \text{(A-II.2 e)}$$

Tangential component of the electric field in the external phase E_{te}

$$E_{te} = -\frac{3E_{\infty}\sin\theta}{S+2} \qquad \text{(A-II.2 f)}$$

Maxwell stress tensor can be expressed as [Wangsness, 1979]

$$\underline{\underline{T}} = \varepsilon_0\varepsilon\vec{E}\vec{E} - \varepsilon_0\varepsilon\frac{E^2}{2}\underline{\underline{I}} \qquad \text{(A-II.3 a)}$$

$$\underline{\underline{T}} = \begin{bmatrix} T_{nn} & T_{nt} \\ T_{nt} & T_{tt} \end{bmatrix} = \varepsilon_0\varepsilon\begin{bmatrix} E_n^2 - \frac{E^2}{2} & E_nE_t \\ E_nE_t & E_t^2 - \frac{E^2}{2} \end{bmatrix} \qquad \text{(A-II.3 b)}$$

where $\underline{\underline{I}}$ is identity tensor, ε is the dielectric constant, E is the local magnitude of electric field strength, E_n and E_t are the normal and tangential component of electric field, respectively. Here,

$$E^2 = E_n^2 + E_t^2 \qquad \text{(A-II.3 c)}$$

where $E_n = -\frac{\partial\phi}{\partial\eta}$ and $E_t = -\frac{1}{\eta}\frac{\partial\phi}{\partial\theta}$.

The normal and tangential components of Maxwell stress tensor for the internal and external phases can be obtained using expression (A-II.3),

Normal component of Maxwell stress tensor for the external phase T_{nn}^{e}

$$T_{nn}^{e} = \frac{9E_{\infty}^{2}\varepsilon_{0}\varepsilon_{e}}{2(S+2)^{2}}\left(S^{2}\cos^{2}\theta - \sin^{2}\theta\right) \qquad \text{(A-II.4 a)}$$

Tangential component of Maxwell stress tensor for the external phase T_{nt}^{e}

$$T_{nt}^{e} = -\frac{9E_{\infty}^{2}\varepsilon_{0}\varepsilon_{e}S}{(S+2)^{2}}\sin\theta\cos\theta \qquad \text{(A-II.4 b)}$$

Normal component of Maxwell stress tensor for the internal phase T_{nn}^{i}

$$T_{nn}^{i} = \frac{9E_{\infty}^{2}\varepsilon_{0}\varepsilon_{i}}{2(S+2)^{2}}\left(2\cos^{2}\theta - 1\right) \qquad \text{(A-II.4 c)}$$

Tangential component of Maxwell stress tensor for the internal phase T_{nt}^{i}

$$T_{nt}^{i} = -\frac{9E_{\infty}^{2}\varepsilon_{0}\varepsilon_{i}}{(S+2)^{2}}\sin\theta\cos\theta \qquad \text{(A-II.4 d)}$$

Thus, the local net tangential component of Maxwell stress tensor, T_{nt}, at the interface is

$$T_{nt} = T_{nt}^{e} - T_{nt}^{i} = 0 \qquad \text{(A-II.5)}$$

There is no tangential electrical stress and thus no flow will be induced. The local normal component of Maxwell stress tensor, T_{nn}, at the interface is then

$$T_{nn} = T_{nn}^{e} - T_{nn}^{i} = \frac{9\varepsilon_{0}\varepsilon_{e}E_{\infty}^{2}}{2(S+2)^{2}}(S-1)\left[1 + (S-1)\cos^{2}\theta\right] \qquad \text{(A-II.6 a)}$$

Alternatively, expression (A-II.6 a) can be expressed as the addition of two terms,

$$T_{nn} = \frac{9\varepsilon_{0}\varepsilon_{e}E_{\infty}^{2}}{2(S+2)^{2}}(S-1) + \frac{9\varepsilon_{0}\varepsilon_{e}E_{\infty}^{2}}{2(S+2)^{2}}(S-1)^{2}\cos^{2}\theta \qquad \text{(A-II.6 b)}$$

The normal electrical stress is composed of two terms: the first term is constant and does not dependent on θ, the second term is θ dependent. The first term might be positive or negative that is dependent on the relative magnitude of the dielectric constants of the liquids. Irrespective of the sign of (S-1), the first term implies a constant radial force on the drop and does not contribute to the drop's deformation. The second term is always

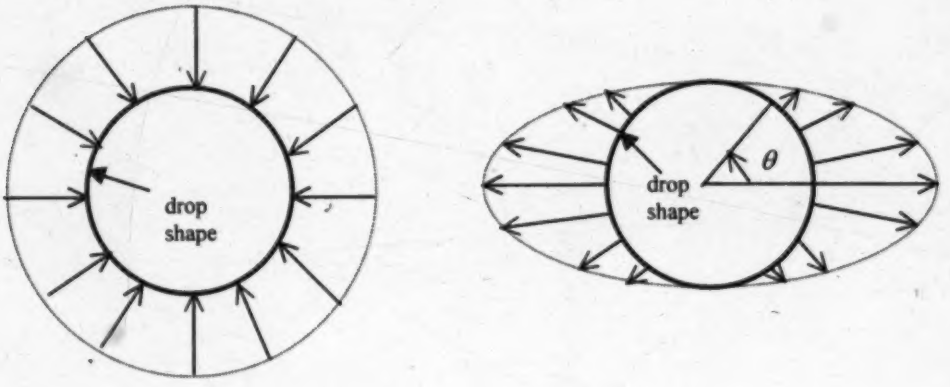

First term: Spherical-symmetric force from equation (A-II.6 b)

Second term: Deforming force from equation (A-II.6 b)

Figure A-II.2 Distribution of Maxwell electrical forces applied at the drop interface

positive and it implies that the normal force is dependent on the angle, as shown in Figure A-II.2. Thus, the drop will always elongate to a prolate spheroid for a perfect dielectric drop in another perfect dielectric.

It should be recognized for the case of two perfect dielectrics, there is no free surface charge. Only polarization charge is developed due to the external electric field.

A-II.2 Maxwell Stress Tensor of a Leaky Dielectric Drop in a Leaky Dielectric

For the system of a leaky dielectric drop suspended in a leaky dielectric fluid under a uniform electric field E_∞, the electric field of the system can be described with the following equations,

Governing equations:

$$\nabla^2 \phi_i = 0 \qquad \text{internal phase} \qquad \text{(A-II.7 a)}$$

$$\nabla^2 \phi_e = 0 \qquad \text{external phase} \qquad \text{(A-II.7 b)}$$

Boundary conditions:

$$\phi_e = \phi_i \qquad \text{at} \quad \eta = r_0 \qquad \text{(A-II.7 c)}$$

$$\sigma_e \frac{\partial \phi_e}{\partial n} = \sigma_i \frac{\partial \phi_i}{\partial n} \qquad \text{at} \quad \eta = r_0 \qquad \text{(A-II.7 d)}$$

$$\phi_e = -\eta E_\infty \cos\theta \qquad \text{as} \quad \eta \to \infty \qquad \text{(A-II.7 e)}$$

$$\phi_i \to \text{finite} \qquad \text{at} \quad \eta = 0 \qquad \text{(A-II.7 f)}$$

where "i" denotes the internal drop phase, "e" denotes the external continuous phase, ϕ is the electric potential, σ is the electrical conductivity, E_∞ is the applied electric field strength far from the drop. In this analysis, no a prior assumption is made regarding free surface charge. Only zero accumulation of current is assumed in equation (A-II.7 e).

For slight deformation, the deformed drop can still be considered as a sphere. Using separation of variables method in spherical polar coordinates with axi-symmetry, the electrical potential inside and outside the drop can be expressed as

$$\phi_i = -\frac{3E_\infty \eta \cos\theta}{R+2} \qquad \text{(A-II.8 a)}$$

$$\phi_e = -E_\infty \eta \cos\theta + \frac{R-1}{R+2}\frac{E_\infty r_0^{\,3} \cos\theta}{\eta^2} \qquad \text{(A-II.8 b)}$$

where $R = \frac{\sigma_i}{\sigma_e}$, R is the electrical conductivity ratio of the internal phase to the external phase.

Noting that $\vec{\nabla}\phi = -\vec{E}$, using equation (A-II.8 a) and (A-II.8 b), one can show that the normal and tangential components of the electric field at the surface can be obtained as

Normal component of the electric field in the internal phase E_{ni}

$$E_{ni} = \frac{3E_\infty \cos\theta}{R+2} \qquad \text{(A-II.9 a)}$$

Normal component of the electric field in the external phase E_{ne}

$$E_{ne} = \frac{3RE_\infty \cos\theta}{R+2} \qquad \text{(A-II.9 b)}$$

Tangential component of the electric field in the internal phase E_{ti}

$$E_{ti} = -\frac{3E_\infty \sin\theta}{R+2} \qquad \text{(A-II.9 c)}$$

Tangential component of the electric field in the external phase E_{te}

$$E_{te} = -\frac{3E_\infty \sin\theta}{R+2} \qquad \text{(A-II.9 d)}$$

Making use of equation (A-II.3) and (A-II.9), one can show that

Normal component of Maxwell stress tensor for the external phase T^e_{nn}

$$T^e_{nn} = \frac{9E_\infty^2 \varepsilon_0 \varepsilon_e}{2(R+2)^2}\left(R^2\cos^2\theta - \sin^2\theta\right) \qquad \text{(A-II.10 a)}$$

Tangential component of Maxwell stress tensor for the external phase T^e_{nt}

$$T^e_{nt} = -\frac{9E_\infty^2 \varepsilon_0 \varepsilon_e R}{(R+2)^2}\sin\theta\cos\theta \qquad \text{(A-II.10 b)}$$

Normal component of Maxwell stress tensor for the internal phase T_{nn}^{i}

$$T_{nn}^{i} = \frac{9E_{\infty}^{2}\varepsilon_{0}\varepsilon_{i}}{2(R+2)^{2}}\left(2\cos^{2}\theta - 1\right) \qquad \text{(A-II.10 c)}$$

Tangential component of Maxwell stress tensor for the internal phase T_{nt}^{i}

$$T_{nt}^{i} = -\frac{9E_{\infty}^{2}\varepsilon_{0}\varepsilon_{i}}{(R+2)^{2}}\sin\theta\cos\theta \qquad \text{(A-II.10 d)}$$

Thus, the net tangential component of Maxwell stress tensor, T_{nt}, at the interface is given by

$$T_{nt} = 9\varepsilon_{0}\varepsilon_{e}E_{\infty}^{2}\frac{S-R}{(R+2)^{2}}\sin\theta\cos\theta \qquad \text{(A-II.11)}$$

The tangential electrical stress is not zero and is not continuous along the interface. A flow will be induced inside and outside the drop. The normal component of the Maxwell stress tensor, T_{nn}, at the interface is given by

$$T_{nn} = \frac{9\varepsilon_{0}\varepsilon_{e}E_{\infty}^{2}}{2(R+2)^{2}}(S-1) + \frac{9\varepsilon_{0}\varepsilon_{e}E_{\infty}^{2}}{2(R+2)^{2}}\left(R^{2}-2S+1\right)\cos^{2}\theta \qquad \text{(A-II.12)}$$

The normal electrical stress can also be decomposed to two terms: The first term is constant and does not contribute to the deformation of the drop; the second term is angle dependent and results in the drop's deformation. It is interesting to note that the term $\left(R^{2}-2S+1\right)$ is also present in Taylor's discriminating function, as shown in the following expression,

$$\beta = \left(R^{2}-2S+1\right) + 3(R-S)\left(\frac{2+3M}{5+5M}\right) \qquad \text{(A-II.13)}$$

where $M = \frac{\mu_i}{\mu_e}$, the dynamic viscosity ratio of the internal phase to the external phase. The first term $\left(R^2 - 2S + 1\right)$ in the discriminating function represents the contribution of the electric field part to the discriminating function while the second term represents the contribution of the flow field part.

From the expression of the discriminating function, it can also be noted that when α is greater than zero, the drop will elongate to a prolate spheroid, in the following two cases: (1) $R>>1$, i.e., the electrical conductivity of drop phase is far greater than that of the continuous phase. For example, water drop in an oil phase will always elongate in the direction of the electric field. (2) $R = S$, i.e., the conductivity ratio of the drop phase to the continuous phase equals to the dielectric constant ratio of the drop phase to the continuous phase. In this case, there is no free charge accumulated at the interface, thus no tangential electrical stress. The system behaves as perfect dielectric materials. The fluids are motionless at steady state in spite of the presence of the electric field.

References

Wangsness, R. K., 1979 *Electromagnetic Fields*, Wiley, New York.

Appendix III

Attractive Force Between Two Equal Sized Water Drops in a Uniform Electric Field

A-III.1 Dipole Moment for a Water Drop in an Electric Field

For a leaky dielectric drop in another leaky dielectric, as shown in Figure A-III.1, the electrical potential outside the drop can be given as (axi-symmetry in spherical polar coordinate)

$$\phi_e = -E_\infty \eta \cos\theta + \frac{R-1}{R+2}\frac{E_\infty r_0^{\,3}\cos\theta}{\eta^2} \qquad \text{(A-III.1)}$$

where E_∞ is the applied electric field strength far away from the drop, R is the electrical conductivity ratio of internal drop phase to external continuous phase and r_0 is the undeformed radius.

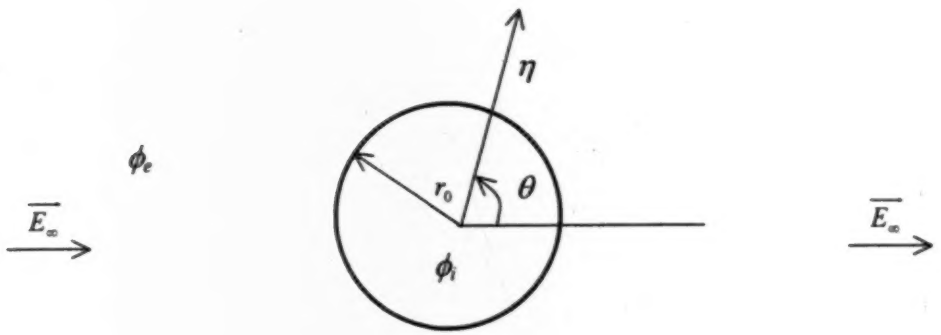

Figure A-III.1 Schematic representation of a single drop in an electric field

For a water drop, $R>>1$ and equation (A-III.1) can be simplified to

$$\phi_e = -E_\infty \eta \cos\theta + \frac{E_\infty r_0^{\,3} \cos\theta}{\eta^2} \qquad \text{(A-III.2)}$$

Let us consider a dipole of moment P located in a uniform electric field E_∞. The dipole moment P is equal to qL, where q is the charge and L is the distance between the negative and positive charges. Superposition of the uniform electric field and the field produced by a dipole yields

$$(\phi_e)_{dipole} = -E_\infty \eta \cos\theta + \frac{P \cos\theta}{4\pi\varepsilon_0 \varepsilon_e \eta^2} \qquad \text{(A-III.3)}$$

The structure of the expressions for the electric potential for a leaky drop in a leaky medium and that for a dipole in a uniform electric field is the same.

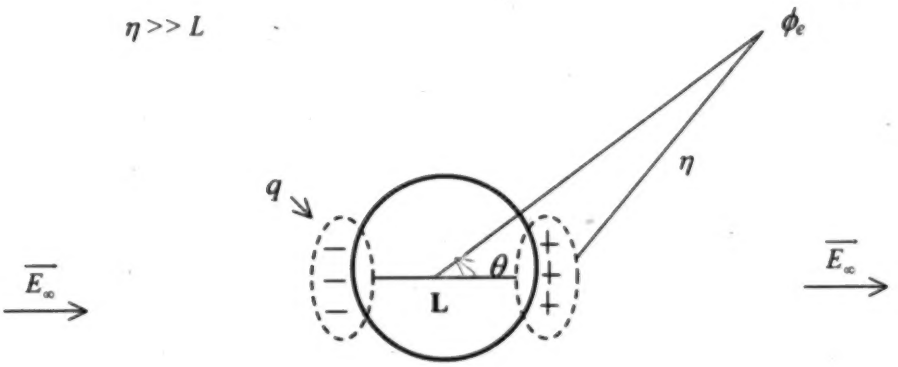

Figure A-III.2 A dipole of moment located in a uniform electric field

If one is to assume that the water drop can be represented as a dipole in an electric field, then by comparing equation (A-III.2) with (A-III.3), the dipole moment P for a water drop in an electric field can be expressed as

$$P = 4\pi\varepsilon_0\varepsilon_e E_\infty r_0^3 \qquad \text{(A-III.4)}$$

For the sake of simplicity, let us assume that a water drop in an electric field would have the same potential as a dipole in an electric field provided that the dipole moment is given by equation (A.III.4). In order to estimate the force between two water droplets, one can make use of two dipoles in an electric field to estimate the force between the two dipoles. In following two sections we will explore this approach.

A-III.2 Attraction Force Between Two Far-away Dipoles

When two dipoles are aligned, as shown in Figure A-III.3, the net attraction force

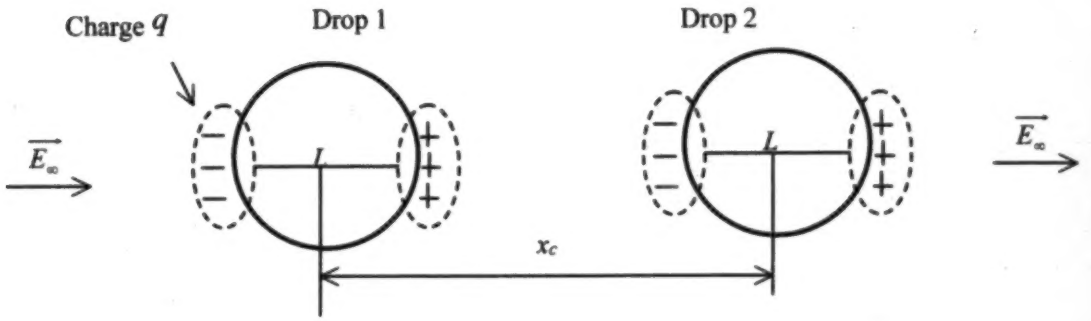

Figure A-III.3 Schematic representation of two water drops as two dipoles in an electric field

between the two dipoles will be the attraction force between the opposite charges minus the repulsion forces between the same charges. It can be expressed as

$$F_a = \frac{1}{4\pi\varepsilon_0\varepsilon_e}\frac{q^2}{(x_c - L)^2} + \frac{1}{4\pi\varepsilon_0\varepsilon_e}\frac{q^2}{(x_c + L)^2} - 2\frac{1}{4\pi\varepsilon_0\varepsilon_e}\frac{q^2}{x_c^2} \qquad \text{(A-III.5)}$$

Equation (A-III.5) can be simplified to

$$F_a = \frac{1}{2\pi\varepsilon_0\varepsilon_e}\frac{q^2}{x_c^2}\left[\frac{1+\frac{L^2}{x_c^2}}{\left(1-\frac{L^2}{x_c^2}\right)^2} - 1\right] \qquad \text{(A-III.6)}$$

Using Taylor series expansions in terms of small parameter L / x_c and retaining only leading terms, equation (A-III.6) can be expressed as

$$F_a = \frac{1}{2\pi\varepsilon_0\varepsilon_e}\frac{3(qL)^2}{x_c^4} = \frac{1}{2\pi\varepsilon_0\varepsilon_e}\frac{3P^2}{x_c^4} \qquad \text{(A-III.7)}$$

under the condition of $L << x_c$, where P is the dipole moment.

A-III.3 Attraction Force Between Two Water Drops in a Uniform Electric Field

When two water drops are sufficiently far from each other in an electric field, the presence of one water drop will not affect the induced dipole moment of the other. Thus, two water drops can be considered as two independent induced dipoles. Substituting (A-III.4) into (A-III.7), the attraction force between two water drops can be expressed as

$$F_a = 24\pi\varepsilon_0\varepsilon_e \frac{E_\infty^{\,2} r_0^6}{x_c^{\,4}} \qquad \text{(A-III.8)}$$

The above equation would indicate that the attractive force is much higher for large droplets and it decays very quickly with distance. Moreover, the attractive force is much reduced for low dielectric constant liquids like oil.

Appendix IV

Physical Properties of Organic Compounds

Chemical Name	Decyl alcohol
Chemical Abstracts Service #	112-30-1
Molecular formula	$C_{10}H_{20}O$
Dielectric constant	8.1 (20∘C) [a]
Density (kg/m^3)	827 [b]
Solubility in water	Insoluble [b]
Viscosity (mPa.s)	8.7[c]
Surface tension (mN/m)	28.60 (20 ∘C) [d]
Interfacial tension (mN/m)	8.93[c]
Electrical conductivity (μS/cm)	2.1×10^{-2} [c] (after saturation with water)

(a) – [CRC Handbook of Chemistry and Physics; Chemical Rubber Company; 1992; 72nd ed.]

(b) – [Material safety data sheet]

(c) – [Measured value]

(d) – [Journal of Chemical Society, Faraday Transactions, I; 1972 (68);10]

Chemical Name	Diethyl phthalate
Chemical Abstracts Service #	84-66-2
Molecular formula	$C_{12}H_{14}O_4$
Dielectric constant	7.86 (20∘C) [a]
Density (kg/m^3)	1116 [b]
Solubility in water	Insoluble [b]
Viscosity (mPa.s)	10.86 (21∘C) [c]
Surface tension (mN/m)	37.3 (25∘C) [d]
Interfacial tension (mN/m)	14.5[e]

(a) – [CRC Handbook of Chemistry and Physics; Chemical Rubber Company; 1992; 72nd ed.]

(b) – [Material safety data sheet]

(c) – [Journal of Chemical and Engineering Data; 1959 (4); 336]

(d) – [Journal of Chemical Society, Faraday Transactions; 1994 (18); 2744]

(e) – [Measured value]

Chemical Name	Cycloheptanone
Chemical Abstracts Service #	502-42-1
Molecular formula	$C_7H_{12}O$
Dielectric constant	13.16 (25°C) [a]
Density (kg/m^3)	949 [b]
Solubility in water	Insoluble [b]
Viscosity (mPa.s)	2.59 (25°C) [c]
Surface tension (mN/m)	35.38 (19.9°C) [d]
Interfacial tension (mN/m)	6.9[e]
Electrical conductivity ($_{\mu}S/cm$)	4.8_X10^{-2} [e] (after saturation with water)

(a) – [CRC Handbook of Chemistry and Physics; Chemical Rubber Company; 1992; 72nd ed.]

(b) – [Material safety data sheet]

(c) – [Journal of Chemical Society; 1914 (105); 2011]

(d) – [Journal of Chemical Society; 1928; 2030]

(e) – [Measured value]

Chemical Name	Alpha-ionone
Chemical Abstracts Service #	127-41-3
Molecular formula	$C_{13}H_{20}O$
Dielectric constant	10.78 (20∘C) [a]
Density (kg/m^3)	928 [b]
Solubility in water	Insoluble [b]
Surface tension (mN/m)	32.21 (20∘C) [c]
Interfacial tension (mN/m)	17.4[d]
Electrical conductivity (μS/cm)	3.2×10^{-2} [e] (after saturation with water)

(a) – [CRC Handbook of Chemistry and Physics; Chemical Rubber Company; 1992; 72nd ed.]

(b) – [Material safety data sheet]

(c) – [Helvetica Chimica Acta; 1943 (26); 2151]

(d) – [Measured value]

Chemical Name	Cyclohexyl acetate
Chemical Abstracts Service #	622-45-7
Molecular formula	$C_8H_{14}O_2$
Dielectric constant	5.08 [a]
Density (kg/m^3)	964 [b]
Solubility in water	Insoluble [b]
Viscosity (mPa.s)	2.57(20∘C) [c]
Surface tension (mN/m)	31.31 (20∘C) [d]
Interfacial tension (mN/m)	14.28[e]

(a) – [CRC Handbook of Chemistry and Physics; Chemical Rubber Company; 1992; 72nd ed.]

(b) – [Material safety data sheet]

(c) – [Journal Fur Praktische Chemie; 1935 (142); 225]

(d) – [Journal of Chemical Society; 1948; 1813]

(e) – [Measured value]

Chemical Name	Ethyl benzoate
Chemical Abstracts Service #	93-89-0
Molecular formula	$C_9H_{10}O_2$
Dielectric constant	5.99 [a]
Density (kg/m^3)	1049 [b]
Solubility in water	Insoluble [b]
Viscosity (mPa.s)	2.22 (20∘C) [c]
Surface tension (mN/m)	35.4 (20∘C) [c]
Interfacial tension (mN/m)	17.19[d]

(a) – [CRC Handbook of Chemistry and Physics; Chemical Rubber Company; 1992; 72nd ed.]

(b) – [Material safety data sheet]

(c) – [Journal of Chemical Society; 1950; 75]

(d) – [Measured value]

Chemical Name	2-ethyl-1,3-hexanediol
Chemical Abstracts Service #	94-96-2
Molecular formula	$C_8H_{18}O_2$
Dielectric constant	18.73 [a]
Density (kg/m^3)	931 [b]
Solubility in water	Very slightly soluble [b]
Viscosity (mPa.s)	67.8 [c]
Surface tension (mN/m)	29.02 (35 ∘C) [c]
Interfacial tension (mN/m)	3.31 [d]

(a) – [CRC Handbook of Chemistry and Physics; Chemical Rubber Company; 1992; 72nd ed.]

(b) – [Material safety data sheet]

(c) – [Journal of American Chemical Society; 1949 (71); 508]

(d) – [Measured value]